

STUDY OF LASER-CLUSTER INTERACTION IN GAS PHASE

By

SOUMITRA DAS

CHEM01201004002

BHABHA ATOMIC RESEARCH CENTRE

*A thesis submitted to the
Board of Studies in Chemical Science*

*In partial fulfillment of requirements
For the degree of*

DOCTOR OF PHILOSOPHY

of

HOMI BHABHA NATIONAL INSTITUTE



March, 2014

Homi Bhabha National Institute

Recommendations of the Viva Voce Board

As members of the Viva Voce board, we certify that we have read the dissertation prepared by **SOUMITRA DAS** entitled “**STUDY OF LASER-CLUSTER INTERACTION IN GAS PHASE**” and recommend that it may be accepted as fulfilling the dissertation requirement for the Degree of Doctor of Philosophy.

Chairman- Dr. D. Das



Date: 16/09/2014

Convener- Dr. R. K. Vatsa



Date: 16/09/2014

External Examiner- Prof. E. Arunan



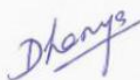
Date: 16/09/2014

Member 1- Dr. P. D. Naik



Date: 16/09/2014

Member 2- Dr. S. Dhanya



Date: 16/09/2014

Final approval and acceptance of this dissertation is contingent upon the candidate's submission of the final copies of the dissertation to HBNI.

I hereby certify that I have read this dissertation prepared under my direction and recommend that it may be accepted as fulfilling the dissertation requirement.

Date: 16/09/2014

Place: Mumbai

Dr. R. K. Vatsa
(Guide)

STATEMENT BY AUTHOR

This dissertation has been submitted in partial fulfillment of requirements for an advanced degree at Homi Bhabha National Institute (HBNI) and is deposited in the Library to be made available to borrowers under rules of the HBNI.

Brief quotations from this dissertation are allowable without special permission, provided that accurate acknowledgement of source is made. Requests for permission for extended quotation from or reproduction of this manuscript in whole or in part may be granted by the Competent Authority of HBNI when in his or her judgment the proposed use of the material is in the interests of scholarship. In all other instances, however, permission must be obtained from the author.

Soumitra Das

Soumitra Das

DECLARATION

I, hereby declare that the investigation presented in the thesis has been carried out by me.

The work is original and has not been submitted earlier as a whole or in part for a degree

/diploma at this or any other Institution / University.

Soumitra Das

Soumitra Das

List of Publications arising from the thesis

1. "Coulomb explosion of methyl iodide clusters using giga watt laser pulses in the visible region: Effect of wavelength, polarisation and doping." **S. Das**, P. Sharma and R. K. Vatsa. *Journal of Chemical Sciences* **2009**, 121 965-972.
2. "A technique for charge density measurement in laser-cluster interaction studies." **S. Das**, P. Sharma, A. Majumder and R. K. Vatsa. *Journal of Indian Chemical Society* **2010**, 87, 165-172.
3. "Multiphoton ionisation and Coulomb explosion of C₂H₅Br clusters: a mass spectrometric and charge density study." **S. Das**, P. M. Badani, P. Sharma, R. K. Vatsa, D. Das, A. Majumder and A. K. Das. *Rapid Communications in Mass Spectrometry* **2011**, 25, 1028-1036.
4. "Size and wavelength dependent photoionisation of Xenon clusters." **S. Das**, P. M. Badani, P. Sharma and R. K. Vatsa. *Chemical Physics Letters* **2012**, 552, 13-19.
5. "Diverse photochemical behavior of dibromodifluoromethane (CF₂Br₂) monomer and cluster under gigawatt intensity laser fields." **S. Das**, P. M. Badani, P. Sharma and R. K. Vatsa. *RSC Advances* **2013**, 3, 12867-12873.
6. "Understanding laser-cluster interaction: A case study of methyl iodide clusters ionized by gigawatt intensity laser pulses." **S. Das**, P. Sharma, P.M. Badani and R. K. Vatsa. (Submitted)

Soumitra Das

Soumitra Das

Dedicated to

My Parents & Amrita

Acknowledgment

I am deeply indebted to Dr. R. K. Vatsa, Head, Structural chemistry section, Chemistry Division, Bhabha Atomic Research Centre, Mumbai for his invaluable guidance, critical comments and constant encouragement during the entire course of this study. I take this opportunity to state that his keen interest and valuable suggestions were of immense help in improving the quality of work as well as enriching my knowledge. It is also my pleasure to express my sincere thanks to him for his constant help and support during planning, execution of the work and interpretation of the results.

This thesis would not have been possible without the guidance, help, support, critical analysis and valuable suggestions from Dr. Pramod Sharma who has been truly invaluable to me both on an academic and a personal level, for which I am extremely grateful. I am also thankful to him for sharing his excellent knowledge and scientific understanding with me. His enthusiasm, deep engagement in research and critical analysis strategy of experimental data has made a deep impression on me.

Special thanks go to my dear friend Purav Badani for his diversified help during the experiments, scientific discussions offered to me from time to time throughout the course of the work. I will definitely miss him for his friendly company in my professional and personal life.

I am also thankful to Dr. A. Majumder and Dr. A. K. Das, Laser & Plasma Division, BARC for modifying the ion optics of time-of-flight mass spectrometer which has been used for charge density measurement.

I sincerely acknowledge the support and encouragement rendered to my research work by Dr. B. N. Jagatap, Director, Chemistry Group, Dr. V. K. Jain, Head, Chemistry

Division, Dr. T. Mukherjee, former Director, Chemistry Group and Dr. S. K. Sarkar, former Director, Chemistry Group.

Chairman (Dr. D. Das) and members (Dr. P. N. Bajaj, Dr. P. D. Naik and Dr. S. Dhanya) of the doctoral committee are gratefully acknowledged for their critical review and suggestions during progress review and pre-synopsis viva-voce examination.

I am also thankful to all the members of Chemistry division particularly members of electronic group- Mrs. K. G. Girija and Shri. R. K. Mishra. I would also like to thank all the workshop staff for their kind cooperation and support from time to time.

I would also like to express my gratitude towards my parents and my wife, Amrita for their selfless love and continued support they have provided me. I couldn't have achieved this without them. I am grateful to their love, encouragement, support and patience that allowed me to finish this work.

BARC, Mumbai
March, 2014

Soumitra Das
Soumitra Das

CONTENTS

	Page number
Synopsis	xiv-xxvii
List of Figures	xxviii-xxxv
List of Tables	xxxvi-xxxvii
Chapter 1: Introduction	
1.1 Laser	2
1.1.1 Principles of laser operation	3
1.2 Clusters	4
1.2.1 Classification of clusters	5
1.2.2 Different methods for generation of clusters	7
1.3 Techniques to study laser-cluster interaction	11
1.3.1 Time-of-flight mass spectrometer (TOFMS)	11
1.3.1.1 Principle of TOFMS	12
1.3.1.2 Resolution of TOFMS	13
1.3.1.3 Dual stage TOFMS	14
1.4 Atomic and molecular process in laser field	18
1.4.1 Multiphoton ionisation	18
1.4.2 Optical field ionisation	20
1.4.3 Keldysh parameter	22
1.4.4 Ponderomotive energy	23
1.4.5 Inner and outer ionisation	23
1.4.6 Inverse bremsstrahlung absorption	24
1.5 Motivation and outline of the thesis	25

Chapter 2: Experimental details	
2.1 Introduction	31
2.2 Vacuum system of time-of-flight mass spectrometer	32
2.3 Molecular and cluster beam source	35
2.4 The laser system	36
2.4.1 Characterization of the laser pulse	38
2.4.2 Pyroelectric laser power meter	39
2.5 Synchronization of laser and molecular beam	40
2.6 The time-of-flight mass spectrometer	41
2.6.1 Ion-optics assembly	41
2.6.2 The detector	44
2.6.3 High voltage DC power supplies	45
2.6.4 Calibration of the TOFMS	45
Chapter 3: Photochemistry of dibromo difluoro methane (CF₂Br₂) monomer and cluster under gigawatt intense laser field	
3.1 Introduction	47
3.2 Experimental details	49
3.3 Results and Discussion	
3.3.1 Multiphoton dissociation/ ionisation of CF ₂ Br ₂ monomer at different wavelengths	49
3.3.2 Ionisation of CF ₂ Br ₂ clusters at different wavelengths	54
3.3. Probable mechanism of multiply charged atomic ion formation in clusters	59
3.4 Conclusions	62

Chapter 4: Coulomb explosion of C₂H₅Br clusters using nanosecond laser pulses: Determination of kinetic energy of multiply charged ions	
4.1 Introduction	64
4.2 Experimental details	66
4.3 Results and Discussion	
4.3.1 Interaction of C ₂ H ₅ Br clusters with 266, 355 and 532 nm laser pulses: Observation of multiphoton dissociation/ionisation and Coulomb explosion	66
4.3.2 Determination of kinetic energy of multiply charged carbon and bromine ions due to interaction of ethyl bromide clusters at 355 and 532 nm	69
4.3.3 Laser power dependency study of ethyl bromide clusters at 266, 355 and 532 nm	74
4.3.4 Different aspects of cluster explosion mechanism	75
4.4 Conclusions	80
Chapter 5: Coulomb explosion phenomenon in methyl iodide clusters irradiated by gigawatt intense laser field: Effect of cluster size, laser polarisation and doping in clusters	
5.1 Introduction	81
5.2 Experimental details	84
5.3 Results and Discussion	
5.3.1 Effect of cluster size on the charge state of atomic ions at different wavelengths	86

5.3.2 Effect of extraction field on kinetic energy of multiply charged ions of carbon and iodine	90
5.3.3 Effect of laser polarisation on ion yield and kinetic energy of multiply charged ions	92
5.3.4 Effect of dopant in cluster ionisation dynamics	95
5.4 Conclusions	98
Chapter 6: Interaction of xenon clusters with nanosecond laser pulses: Determination of minimum cluster size and threshold laser intensity for observation of multiply charged ions	
6.1 Introduction	100
6.2 Experimental details	103
6.3. Results and Discussion	
6.3.1 Effect of laser wavelength on photo ionisation of xenon clusters	104
6.3.2 Determination of threshold cluster size for observation of multiply charged ions	107
6.3.3 Kinetic energy of multiply charged xenon ions as a function of cluster size	109
6.3.4 Threshold laser intensity for observation of Coulomb explosion as a function of cluster size	112
6.3.5 Ionisation of water doped xenon clusters by 532 nm laser pulses	115
6.4 Conclusions	116

Chapter 7: Laser-cluster interaction under gigawatt intense laser

field: Detection of negative ions

7.1 Introduction	118
7.2 Experimental details	120
7.3 Results and Discussion	
7.3.1 Detection of negative ions in photo ionisation CF_2Br_2 clusters under gigawatt intense laser field	121
7.3.2 Detection of negative ions in photo ionisation CH_3I clusters under gigawatt intense laser field	124
7.3.3 Effect of negative ion in cluster ionisation dynamics under gigawatt intense laser field	127
7.4 Conclusions	128

Chapter 8: Charge density measurement in atomic and molecular clusters under gigawatt intense laser field

8.1 Introduction	129
8.2 Experimental details	130
8.3 Results and Discussion	
8.3.1 Charge density measurements of $\text{C}_2\text{H}_2\text{Br}$, CH_3I and Xe clusters ionised at different wavelengths	134
8.3.2 Role of electron ionisation in generating charge density of interaction zone in atomic/molecular clusters	138
8.3.3 Comparative study of charge density measurement in atomic/ molecular clusters	139
8.4 Conclusions	140

Chapter 9: Conclusions and future scope of the present work

9.1 Conclusions	142
9.2 Future scope of the work	148
References	152

SYNOPSIS

Interaction of light with different forms of matter is a topic of interest for researchers' for several decades. Light is an electromagnetic radiation and when the electric field of light interacts with matter, different photo physical/chemical processes can occur. These photo processes can be broadly classified as absorption, emission and scattering. Before the start of laser era, studies were performed using low intensity light sources where optical response of matter was linear with respect to the light intensity. However, the discovery of laser light introduced a new dimension in light-matter interaction studies. Unique properties of laser, such as monochromaticity, coherence, tunability over a wide wavelength range and high intensity make it a powerful pump and probe tool for a number of spectroscopic as well as photochemical studies. Because of high intensity of laser light, more than one photon can be absorbed by the matter which leads to entirely new field of non linear laser chemistry. Different solid and liquid materials qualify for non linear media because their dielectric polarization responds nonlinearly with electric field of light. Moreover, atomic and molecular clusters in gas phase also show similar behaviour under the influence of laser field which attracts the researchers to study laser-cluster interaction in gas phase. A gaseous cluster target produces a unique combination of gas and solid phase components. Their solid like local density and gas like average density causes individual clusters to efficiently absorb laser energy forming highly charged atomic ions, molecular ions, energetic electrons and even neutrons. Moreover, generation of X-ray & higher order harmonic is also accomplished as a result of efficient interaction of cluster with intense laser light. In the present thesis, interaction of atomic and molecular cluster was confined to considerable low intensity

regime with nanosecond long pulse width and the ionic outcome is studied using mass spectrometry technique.

In the present work, a comparative study has been carried out on interaction of monomer and clusters with laser pulses. Clusters act as a nano laboratories and open new reaction channels which are not observed in the monomer case. These new photochemical behaviour is attributed due to solvation of molecules under our experimental conditions. However, the most interesting observation in laser-cluster interaction study is generation of multiply charged atomic ions with high kinetic energy at a laser intensity $\sim 10^9$ W/cm². Earlier, multiply charged energetic ions have been observed as a result of interaction of atomic and molecular clusters with femtosecond laser pulses of intensity $\sim 10^{15}$ W/cm². Violent explosion of matter due to strong repulsive Coulombic forces is known as Coulomb explosion. The explosion leads to particle flying with high kinetic energy. Thus, we have observed Coulomb explosion phenomena in atomic and molecular clusters at a laser intensity $\sim 10^6$ times lower than the earlier reported results. Observation of Coulomb explosion phenomena at high intense laser conditions can be understood based on the field ionisation, however under our laser intensity conditions possibility of field ionisation can be completely ruled out. Thus, systematic study has been carried out on different molecular (CF₂Br₂, C₂H₅Br and CH₃I) and atomic (Xe) clusters system and different experimental parameters have been varied to understand the mechanism of formation of multiply charged ions, under such low laser intensity conditions.

In **chapter 1**, the subject of laser-cluster interaction has been introduced in order to provide necessary background for the thesis. Firstly, laser source has been described along with the basic principle of operation. Secondly, clusters are defined in this chapter along with its classification and methods for generation in gas phase.

Under our experimental conditions, clusters are produced by supersonic expansion of the sample. When these clusters are interacted with laser pulses several photoproducts are produced such as positive ions, negative ions and electrons. In our experiment, positive and negative ions are detected using time-of-flight mass spectrometer. Therefore, the principle of time-of-flight mass spectrometer has been explained in detail, along with its advantages and disadvantages in this chapter. In the subsequent section, few terms are discussed like multiphoton ionisation, field ionisation, Keldysh parameter, ponderomotive energy, inner/ outer ionisation etc which are important to understand the laser-cluster interaction under gigawatt intense laser field. Finally, a brief outline of the thesis is presented at the end of this chapter.

The experimental set-up, which has been used to investigate the laser-cluster interaction, is described in **chapter 2**. As described earlier, the experimental set up is a cluster generation source coupled with a time-of-flight mass spectrometer. For ionisation of atomic/ molecular clusters a port for entry of pulse has been provided. The time-of-flight mass spectrometer instrument consists of three interconnected vacuum chambers i.e. expansion chamber, ionisation chamber and the time-of-flight tube which are differentially pumped to fulfill the necessary condition of collisionless flight of ions in the mass spectrometer. Details of the different types of pumps along with their pumping capacity are described in this chapter. In the expansion chamber, molecular beam arrangement is housed for generation of atomic and molecular clusters. A pulsed valve nozzle is employed for generation of clusters under our experimental conditions. Different parts of the pulsed valve nozzle are described in this chapter along with its control unit. Further, laser systems which are used for ionisation of clusters are described in the subsequent section. Fundamentals, second, third and fourth harmonics of Nd: YAG laser are used for ionisation of different

atomic and molecular clusters. In addition, for generation of 563 nm, Nd: YAG pumped dye laser (Rhodamine 6G dye) is also used. For ionisation of atomic/molecular clusters by means of laser pulse, synchronization of laser pulse and the gas pulse is very important. Using a digital delay generator, laser pulse and the gas pulse are overlapped temporally. As a result of interaction of gas pulse and laser pulse, singly and multiply charged positive ions are produced in the interaction region. In order to analyze the ionic output of laser-cluster interaction, time-of-flight mass spectrometer is used. The spectrometer consists of ion optics and the detector system. The ion optics has three grids, namely repeller, extractor and accelerator which focus the ions on to the detector. In order to guide the ion beam in horizontal and vertical direction two additional deflector plates have also been employed. Moreover, to collimate the ion beam, einzel lens (0-V-0) is incorporated in the ion optics. The ions are detected using channel electron multiplier (CEM) and working principle of the CEM detector is described in this chapter. For guiding the ion beam in the spectrometer five stable power supplies are used. Specifications of these low noise and highly stable regulated DC output voltages are listed in the subsequent section. The performance of this time-of-flight mass spectrometer is tested by ionizing ethyl bromide monomer at 532 nm. The resolution of this time-of-flight mass spectrometer obtained from the experimental time width shows $m/\Delta m \sim 300$.

As the title of the thesis suggests, our focus is to study interaction of clusters with gigawatt intense laser field. However, studies were carried out for monomer system and the experimental results are compared with cluster system. For monomer studies difluorodibromo methane system (CF_2Br_2) has been chosen and experimental results are presented in **chapter 3**. CF_2Br_2 monomers were ionised with 266 nm, 355 nm and 532 nm laser pulses and the ions were detected using time-of-flight mass

spectrometer. Based on the mass spectra it has been concluded that CF_2Br_2 molecule exhibits ladder switching mechanism i.e. undergoes dissociation followed by ionisation at all wavelengths. Primary photo dissociation of CF_2Br_2 molecule leads to generation of CF_2Br and Br radical. At 266 nm, CF_2Br radical undergoes further dissociation to CF_2 and Br thus no CF_2Br^+ ion was observed in mass spectra. At 355 and 532 nm, CF_2Br_2 molecule leads to generation of CF_2Br and Br radical which subsequently ionises via multi-photon ionisation. However, when CF_2Br_2 clusters are ionised with nanosecond laser pulses, altogether new photochemistry and exotic species were observed in the mass spectra which were absent in monomer spectra. At 266 nm, new ion signals of CF_2Br^+ and Br_2^+ are observed in the cluster spectra and their ion intensity varies with clustering probability of the CF_2Br_2 molecule. Generation of these ion peaks has been attributed to stabilization of the ion as a result of cluster solvation. At 355 nm and 532 nm, multiply charged atomic ions of carbon, fluorine and bromine were observed in the mass spectra of clusters. Highest observed charge state of carbon, fluorine and bromine was +2 at 355 nm. While at 532 nm, charge state of carbon, fluorine and bromine extends up to +4, +4 and +5 respectively. Thus, charge state of multiply charged ions was found to increase with laser wavelength. Observation of multiply charged ions could not be explained based solely on multiphoton ionisation process. In order to understand the ionisation process under our experimental conditions, a three stage cluster ionisation model as proposed by H. Li and co-workers has been utilised. According to this mechanism, Coulomb explosion in clusters is initiated via multiphoton ionisation of neutral cluster constituents. During this process, the electrons generated due to the ionisation of atoms/molecules present on the surface leave the cluster immediately. These are referred as outer ionized electrons. Removal of these outer ionized electrons leaves

behind a net positive charge on the cluster. On the other hand, electrons generated due to ionisation of atoms/molecules present in the bulk are caged within the cluster. These are known as inner ionized electrons. These inner ionized electrons which are quasi free, under the influence of Coulombic field of positive ions, extract energy from laser pulse via inverse bremsstrahlung process. Once the inner ionized electrons gain enough energy, further ionisation takes place via electron ionisation resulting in generation of doubly ionized species within clusters. The ionisation process repeats to generate multiply charged atomic ions which are in close proximity. The cohesive energy of cluster tries to hold the cluster, whereas the electrostatic repulsion arising from positive charges, forces the cluster to expand. Finally, at a stage when repulsion energy overcomes total cohesive energy, cluster undergoes Coulomb explosion.

In order to get a better understanding of generation of multiply charged ions under gigawatt intense laser conditions, further studies have been carried out on similar type of cluster system i.e. in C_2H_5Br clusters and results are presented in **chapter 4**. When C_2H_5Br clusters were ionized with nanosecond laser pulses, only singly charged fragment ions were observed at 266 nm. Moreover, Br_2^+ ions were observed in the mass spectra at this wavelength because of concerted photodissociation of the ionized ethyl bromide clusters. At 355 nm, multiply charged ions of carbon and bromine were observed up to +2 state, while the charge state of carbon and bromine increased up to +4 and +5 respectively at 532 nm. Thus, ethyl bromide cluster system showed similar trend as observed in CF_2Br_2 clusters and charge state of atomic ions increased with increasing wavelength. In order to characterize the multiply charged ions produced as a result of Coulomb explosion of ethyl bromide clusters, kinetic energies of multiply charged ions of carbon and bromine were measured. For kinetic energy determination of carbon ions, peak

splitting method has been employed. Split peak arises for energetic multiply charged ions in the time-of-flight mass spectra because of disintegration of clusters in all direction. The ion bunch moving towards the detector forms the forward component which constitutes the broad peak. On the other hand, the ion bunch moving away from the detector reaches later to the detector and constitutes the focused part of the split peak. Using the difference in time of arrival of the forward and backward peak, kinetic energy of multiply charged ions of carbon is determined. Kinetic energy of multiply charged carbon was found to increase with charge state. For kinetic energy determination of bromine, peak splitting method was not suitable because bromine has two isotopes at m/z 79 and 81 which complicated the assignment of split peak. Thus, kinetic energy of multiply charged bromine ion was determined using retarding potential method. Using peak splitting method, most probable kinetic energy of the multiply charged ions can be determined while retarding potential method determines the highest kinetic energy of the ions. Thus, Coulomb explosion of ethyl bromide clusters has been presented in this chapter along with the kinetic energy of the multiply charged ions of carbon and bromine. In order to understand the mechanism of multiply charged ions at different wavelength, laser power dependency study has been carried out. Based on the experimental results, it has been found that (2+1), (2+1) and (4+1) multiphoton ionisation is the primary step of ionisation in ethyl bromide clusters at 266, 355 and 532 nm respectively. Subsequently, the inner ionized electrons extract energy from the laser field via inverse bremsstrahlung mechanism and cause further ionisation in the cluster. The extent of energy extraction by electrons is calculated for a fixed time interval at different wavelength and time-of-flight mass spectra is compared with the calculation. From the comparison, it has been concluded that cluster survives for different time scales at different wavelengths. At

two lower wavelengths (266 nm and 355 nm) because of high multiphoton ionisation probability cluster disintegrates quickly which leads to lowering of the cluster size. As a result of that extraction of energy by electrons within the ionized cluster is not efficient and lower charge state formation has been observed at these wavelengths. On the contrary, at 532 nm because of initial less facile multiphoton ionisation, cluster survives for longer time and inner ionized electron extract more energy from the laser field and cause higher charge state formation. Thus, cluster size and interaction time of inner ionized electron with laser field plays an important role in governing the cluster ionisation dynamics under gigawatt intense laser field.

In **chapter 5**, results of ionisation of methyl iodide clusters have been presented. As described in earlier chapter, cluster size plays an important role in determining the efficiency of laser cluster interaction, thus studies have been carried out on methyl iodide clusters as a function of cluster size. Clusters of different size were produced using pulsed valve nozzle of different diameter (0.6 mm and 0.8 mm). Clusters produced via 0.6 mm nozzle diameter were ionised with 266, 355, 532 and 563 nm laser pulses. Multiply charged ions of carbon and iodine were observed at 532 nm up to +3 state. Charge state of carbon and iodine increases to +4 and +5 respectively at 563 nm. However, no signal could be observed for methyl iodide clusters at 1064 nm. This could be due to higher number of photon (9 photons) requirement for multiphoton ionisation of methyl iodide clusters at 1064 nm. Clusters produced via 0.8 mm nozzle diameter were ionised with 266, 355, 532 and 1064 nm. Multiply charged ions of carbon and iodine (up to +2 state) starts appearing at 355 nm. At 532 nm, extent of charge state increases up to +4 for both carbon and iodine. Highest observed charge state of iodine at 1064 nm was +11. Thus, these experimental results clearly demonstrate that for observation of Coulomb explosion,

under gigawatt intense laser field, a threshold cluster size is required and charge state increases with cluster size at a fixed wavelength. However, we are unable to determine the threshold cluster size for methyl iodide using Hagena's parameter under our experimental conditions. Hagena's parameter is applicable for noble gas clusters where no carrier gas is used. In the next section, kinetic energy of multiply charged ions of carbon and iodine was determined based on the peak splitting method. During peak splitting method, extraction voltages are applied to these multiply charged ions in time-of-flight mass spectrometer. In order to understand the effect of extraction field on kinetic energy of these multiply charged ions, extraction field is varied in the range of 250 V/cm to 600 V/cm and the kinetic energy of different charge state has been determined. From the experimental results it has been found that kinetic energy of multiply charged ions is more or less similar (with $\pm 10\%$ variation) even though the extraction field has been changed by a factor of 2.4. Thus, the kinetic energy measured by this method is a manifestation of the strong Columbic repulsive forces in the ionized cluster and remains unaffected by the externally applied electric field for ion extraction. In the subsequent section, effect of laser polarization on generation of multiply charged ions of carbon and iodine was studied by varying laser polarization throughout 360° in steps of 45° . From the time-of-flight mass spectra at parallel and perpendicular polarization, ion yield of different charge state of iodine and carbon was found to be similar. Further, kinetic energy of these multiply charged ions determined as a function of laser polarization angle and similar results were obtained at different polarization angle. These results indicate that the Coulomb explosion of clusters under gigawatt intense laser field is isotropic in nature. Finally, water doped methyl iodide clusters were studied in order to understand effect of dopant on cluster ionisation dynamics. In the mass spectra, multiply charged ions of oxygen have been

observed along with higher charge state of iodine and carbon. From the experimental observation, it has been concluded that Coulomb explosion phenomena is a collective property of the cluster as a whole and individual molecular properties do not play any significant role.

In earlier chapters results of interaction of nanosecond laser pulses with different molecular clusters have been described. In **chapter 6**, interaction of gigawatt intense laser pulse with atomic clusters i.e. xenon clusters has been presented as a function of laser wavelength and cluster size. In the first section, studies have been carried out in xenon clusters as a function of laser wavelength and multiply charged ions of xenon are detected using time-of-flight mass spectrometer. At 266 nm, multiply charged ions of xenon are observed up to +3 state. Charge state of xenon ions increased to +6 state at 355 nm while up to Xe^{11+} for 532 nm laser pulses. Thus, charge state of xenon was found to increase with laser wavelength and follows similar trend as observed in case of molecular clusters. Thus, three stage cluster ionisation mechanism can qualitatively explain the wavelength dependent Coulomb explosion phenomena of xenon clusters under our experimental conditions. However, role of cluster size in generation of multiply charged ions is discussed in earlier chapters. Thus, cluster size of xenon has been varied from tens of atoms to thousands of atoms and interaction of nanosecond laser pulses is studied. Using Hagena's empirical formula average cluster size of xenon has been estimated for certain experimental conditions. When clusters of average size $\langle \text{Xe}_{17} \rangle$ were ionized with 532 nm laser pulses of intensity $\sim 10^9 \text{ W/cm}^2$, only singly charged cluster fragments are observed up to Xe_4^+ . With increase in cluster size to $\langle \text{Xe}_{50} \rangle$, time-of-flight mass spectra changes drastically. Multiply charged xenon ions were observed in the mass spectra up to Xe^{11+} . From this observation it has been concluded that there is a threshold

cluster size for gigawatt pulse induced Coulomb explosion which lies in between $17 < N < 50$ for xenon clusters. With further increase in cluster size of xenon, no enhancement in charge state was observed. Earlier in molecular clusters (in methyl iodide clusters) charge state is found to increase with cluster size. However, in case of atomic clusters such a trend was not observed. Kinetic energy of multiply charged ions of xenon was determined using retarding potential method as function of cluster size. Kinetic energy of a particular charge state was found to increase with cluster size. Based on simple calculation, it has been concluded that during cluster explosion, the potential energy of the cluster gets transformed into the kinetic energy of the multiply charged ions. In another set of experiments, threshold laser intensity for occurrence of Coulomb explosion in xenon clusters is determined as a function of cluster size. The intensity threshold was found to decrease exponentially with cluster size. This decrease in the threshold intensity for Coulomb explosion was attributed to higher multiphoton and electron impact ionisation probability in larger xenon clusters. Finally, water doped xenon clusters were irradiated with 532 nm laser pulses to understand the effect of dopant on ionisation dynamics of atomic clusters. Multiply charged ions of oxygen (from H₂O clusters) are observed in the mass spectra along with different charge state of xenon. Earlier similar observation has been reported in water doped methyl iodide clusters. From the observation, it has been concluded that molecular/ atomic property does not play any major role in Coulomb explosion phenomena under gigawatt intense laser field and it's a collective property of the cluster.

Interaction of different atomic and molecular clusters with nanosecond laser pulses leads to generation of singly and multiply charged positive ions with high kinetic energy. As explained above, generation of these multiply charged ions under

gigawatt intense laser field has been explained based on multiphoton ionisation followed by energization of inner ionized electron and finally electron impact ionisation within the cluster. During energization process, these inner ionized electrons are in close proximity of the neutral and other ions in the cluster. There is always a possibility of an electron attaching itself to the neutral atoms/ molecules in the cluster and forming negative ions. Thus in **chapter 7**, results of formation of negative ions in CF_2Br_2 and CH_3I clusters during the interaction of nanosecond laser pulses have been presented. For detection of negative ions, the detector circuit was suitably modified and biasing of the channel electron multiplier detector has been reversed. From the ion intensity as observed in time-of-flight mass spectra, it has been found that the yield of negative ions is much less compared to positive ions. The negative ion formation under our experimental conditions has been explained based on dissociative electron attachment. The electron attachment cross-section of neutral molecules depends on the electron energy which in turn dictates the negative ion yield. Under our experiment conditions, inner ionized electrons are energized via inverse bremsstrahlung process, which lowers the electron attachment cross-section and subsequently leads to less number of negative ions. Thus, generation of negatively charged ions is suggested to be a minor channel and ionisation dynamics remains unaltered in $\text{CF}_2\text{Br}_2/ \text{CH}_3\text{I}$ clusters at 532 nm.

In earlier chapters, we mentioned that the charge state of atomic ions is found to increase with increase in laser wavelength. Though mass spectrometry is a very sensitive method for the detection of ions, it is difficult to comment on the efficiency of laser-cluster interaction at different wavelengths merely on the basis of the observation of multiply charged ions. It is possible that the total yield of ions (including multiply charged ions) generated in the ionisation volume at higher

wavelength might be less than the total yield of singly charged ions generated at lower wavelength. In order to resolve this issue, total number of charges produced in the interaction zone at different wavelength has been measured and the results are presented in **chapter 8**. In order to measure the total number of charges per unit volume i.e. charge density of the interaction zone, slight modification has been done in ion optics of time-of-flight mass spectrometer. In the new configuration, repeller grid has been replaced by a larger area stainless steel plate and positive ions are pushed towards the repeller plate by applying sufficient positive voltage to the extractor grid. The current produced in the circuit due to movement of ions is recorded in the form of voltage by applying appropriate resistor. Charge density of C₂H₅Br, CH₃I and Xe cluster system has been measured at different wavelength. For a particular atomic or molecular cluster system, charge density is found to increase with laser wavelengths. In C₂H₅Br clusters, the charge density at 266, 355 and 532 nm was measured to be 1.5×10^9 charges/cc (charge state observed in mass spectra up to +1), 5.7×10^9 charges/cc (charge state observed in mass spectra up to +2) and 2×10^{11} charges/cc (charge state observed in mass spectra up to +5) respectively. In CH₃I clusters, the charge density at 266, 355, 532 and 1064 nm was measured to be 4×10^9 charges/cc (charge state observed in mass spectra up to +1), 2×10^{10} charges/cc (charge state observed in mass spectra up to +2), 2×10^{11} charges/cc (charge state observed in mass spectra up to +4) and 9×10^{11} charges/cc (charge state up to +11) respectively. In xenon clusters the observed charge density is 5×10^9 charges/cc (charge state observed in mass spectra up to +3), 1.3×10^{10} charges/cc (charge state observed in mass spectra up to +6) and 1.8×10^{10} charges/cc (charge state observed in mass spectra up to +11) at 266, 355 and 532 nm respectively. Thus, the charge density and the observed charge state of multiply charge ions shows similar trend in

atomic and molecular clusters and efficiency of laser-cluster interaction increases with laser wavelength. However, if one compares charge density of atomic and molecular clusters at a particular wavelength than charge density does not correlate with the observed charge state in mass spectra. In xenon clusters, highest observed charge state at 532 nm is +11 with charge density 1.8×10^{10} charges/ cc which is much less than the charge density (2×10^{11} charges/cc) observed in ethyl bromide clusters where charge state is limited up to +5. Thus, using charge density measurement, efficiency of laser-cluster interaction can be measured unambiguously.

Finally, conclusions based on the experimental results upon interaction of atomic and molecular clusters with gigawatt intense laser pulses are discussed in **chapter 9** along with future scope of the present work.

LIST OF FIGURES

	Page Number
Figure 1.1: Schematic diagram of supersonic gas jet	9
Figure 1.2: Schematic diagram of a linear time-of-flight mass spectrometer with dual acceleration stage.	16
Figure 1.3: Different ionisation schemes for a molecule (a) Single photon ionisation (b) Non-resonant multiphoton ionisation - 3 photons are involved (c) Resonant two-photon ionisation via excited state rovibrational levels	19
Figure 1.4: Schematic view of inner and outer ionisation of a cluster based on the effective cluster potential.	24
Figure 2.1: Schematic diagram of the experimental set-up used for laser-cluster interaction studies	33
Figure 2.2: Actual photograph of the experimental set-up used for laser-cluster interaction studies	34
Figure 2.3: Temporal profile of the Nd:YAG laser pulse, measured using a fast photodiode	38
Figure 2.4: Plot of integrated ion signal as a function of delay time for synchronization of laser and gas pulse	41
Figure 2.5: Ion optics of time-of-flight mass spectrometer optimized using SIMION 8.0 where R, E, A, V, H and En represents repeller,	43

extractor, accelerator, vertical, horizontal and einzel lens respectively

Figure 2.6: Photograph of ion optics assembly of the mass spectrometer mounted in ionisation chamber. Different components of the ion-optics assembly are labelled in the diagram. 43

Figure 2.7: An illustration showing secondary electron emission from a continuous dynode when ions strike the semiconducting surface. 44

Figure 2.8: (a) Time-of-flight spectra of ethyl bromide monomer recorded at 532 nm. (b) The expanded portion of the spectra corresponding to $C_2H_5Br^+$ ion (marked portion) is shown along with Gaussian fit for calculating the FWHM of the ion peak. 46

Figure 3.1: Time-of-flight mass spectrum of CF_2Br_2 monomer at 266 nm under laser intensity of $\sim 10^9$ W/cm² 50

Figure 3.2: Time-of-flight mass spectrum of CF_2Br_2 monomer at 355 nm under laser intensity of $\sim 10^9$ W/cm². 50

Figure 3.3: Time-of-flight mass spectrum of CF_2Br_2 monomer at 532 nm under laser intensity of $\sim 10^9$ W/cm². 51

Figure 3.4: Time-of-flight mass spectra of CF_2Br_2 monomer at 355 nm as a function of laser energy. 53

Figure 3.5: Time-of-flight mass spectrum of CF ₂ Br ₂ clusters ionised at 266 nm using laser intensity of ~ 10 ⁹ W/cm ²	55
Figure 3.6: Ion intensity of CF ⁺ , Br ₂ ⁺ and CF ₂ Br ⁺ as a function of delay between laser and gas pulse at 266 nm	55
Figure 3.7: Time-of-flight mass spectrum of CF ₂ Br ₂ clusters at 355 nm under laser intensity of ~ 10 ⁹ W/cm ²	58
Figure 3.8: Time-of-flight mass spectra of CF ₂ Br ₂ clusters at 532 nm under laser intensity of ~ 10 ⁹ W/cm ²	58
Figure 3.9: Laser power dependency study of (a) C ⁺ (b) C ²⁺ (c) F ⁺ and (d) F ²⁺ ions generated by 532 nm photo ionisation of CF ₂ Br ₂ clusters	60
Figure 3.10: Schematic representation of three stage model for the generation of multiply charged ions at an intensity of ~ 10 ⁹ W/cm ²	62
Figure 4.1: Time-of-flight mass spectra of ethyl bromide clusters ionised at 266 nm using laser pulses of intensity ~ 10 ⁹ W/cm ²	67
Figure 4.2: Time-of-flight mass spectra of ethyl bromide clusters ionised at 355 nm using laser pulses of intensity ~ 10 ⁹ W/cm ²	68
Figure 4.3: Time-of-flight mass spectra of ethyl bromide clusters at 532 nm. Inset shows ion signal for cluster fragments of ethyl bromide.	69

Figure 4.4 (a) Direction of motion of energetic multiply charged ions in the ion optics of time-of-flight mass spectrometer showing turn around motion of backward ions and direct motion of forward ions (b) asymmetric peak shape of multiply charged ions in time-of-flight mass spectra	70
Figure 4.5: Ion optics arrangement for determination of kinetic energy of multiply charged bromine ions using retarding potential method	72
Figure 4.6: Representative time-of-flight mass spectra of ethyl bromide clusters at different retardation potential	73
Figure 4.7: ln-ln plot of charge density as a function of laser energy for ionisation at (a) 266 nm (b) 355 nm and (c) 532 nm laser wavelength	75
Figure 5.1: Time-of-flight mass spectra of methyl iodide clusters using 0.6 mm nozzle diameter at (a) 266 nm* (b) 355 nm (c) 532 nm and (d) 563 nm. * Time-of-flight mass spectra of 266 nm have been taken from reference 69.	87
Figure 5.2: Time-of-flight mass spectra of methyl iodide clusters using 0.8 mm nozzle diameter at (a) 266 nm (b) 355 nm (c) 532 nm and (d)1064 nm	88
Figure 5.3: Kinetic energy of multiply charged ions of carbon and iodine as a function of extraction field in time-of-flight mass spectrometer for 532 nm photo ionisation	91

Figure 5.4: Time-of-flight mass spectra of ions produced by photo ionisation of CH ₃ I clusters at 532 nm (a) parallel (0°) and (b) perpendicular (90°) polarization with respect to time-of-flight axis	93
Figure 5.5: Variation in kinetic energy of multiply charged ions (a) C ²⁺ (b) C ³⁺ (c) I ²⁺ and (d) I ³⁺ as a function of plane of polarisation	94
Figure 5.6: Variation in ion yield of multiply charged ions (a) C ²⁺ (b) C ³⁺ (c) I ²⁺ and (d) I ³⁺ as a function of plane of polarisation	95
Figure 5.7: Time-of-flight mass spectra of CH ₃ I–H ₂ O mixed clusters when subjected to 563 nm laser pulses at an intensity of ~ 10 ⁹ W/cm ² .	98
Figure 6.1: Time-of-flight mass spectrum of xenon clusters subjected to photo ionisation by 266 nm laser pulse of intensity ~ 10 ⁹ W/cm ² . (a) depicts multiply charged ions up to +3 while (b) represents the cluster ion fragments up to Xe ₁₄ ⁺ .	105
Figure 6.2: Time-of-flight mass spectrum of xenon clusters subjected to 355 nm photo ionisation by laser pulse of intensity ~10 ⁹ W/cm ² . Inset depicts xenon dimer ions observed in the mass spectrum.	105
Figure 6.3: Time-of-flight mass spectrum of xenon clusters subjected to photo ionisation by 532 nm laser pulse of ~ 10 ⁹ W/cm ² . Singly and doubly charged xenon ions are shown in the inset.	106

Figure 6.4: Time-of-flight mass spectra of xenon clusters photo ionised by 532 nm laser pulses of intensity $\sim 10^9$ W/cm ² ; nozzle diameter: 0.3 mm at (a) 0.5 atm (Xe ₁₇) and (b) 0.8 atm (Xe ₅₀) pressure of xenon	108
Figure 6.5: Time-of-flight mass spectra of xenon clusters as function of cluster size (Ionisation wavelength: 532 nm, Intensity: $\sim 10^9$ W/cm ² , Nozzle diameter: 0.8mm)	109
Figure 6.6: Kinetic energy of multiply charged ions of xenon as a function of cluster size ionised at 532 nm	111
Figure 6.7: Normalized value of N/R and kinetic energy of Xe ⁵⁺ ions plotted as a function of cluster size	112
Figure 6.8: Threshold laser intensity for observation of multiply charged ions of xenon as a function of cluster size	113
Figure 6.8: Time-of-flight mass spectra of water doped xenon clusters irradiated by 532 nm laser pulses of intensity $\sim 10^9$ W/cm ² . Multiply charged ions of oxygen were observed along with multiply charged xenon ions. C ⁺ , C ₂ ⁺ and C ₂ H ₅ ⁺ appear in the mass spectra because of background diffusion pump oil.	116
Figure 7.1: Electrical connections of channel electron multiplier for detection of (a) positive ions and (b) negative ions	121
Figure 7.2: Negative ion time-of-flight mass spectra of CF ₂ Br ₂ clusters photo ionised at 532 nm for a laser intensity of $\sim 10^9$ W/cm ² . Two isotopes of bromine (⁷⁹ Br and ⁸¹ Br) are shown in inset.	122

Figure 7.3: Negative ion time-of-flight mass spectrum of CH ₃ I clusters photo ionised at 532 nm	125
Figure 8.1: Electrical circuit of the ion optics for (a) time-of-flight mass spectrometer and (b) charge density experiment	131
Figure 8.2: Typical oscilloscope trace for ion signal recorded at repeller plate across a 10 K Ω resistance, for a given applied voltage on extraction plate.	131
Figure 8.3: Laser-cluster interaction volume (shaded portion) to determine charge density for atomic/molecular clusters	133
Figure 8.4: Scanning electron microscope image of the laser spot obtained at the interaction zone using 1064 nm laser pulses	134
Figure 8.5: Ion signal at repeller plate as a function of extraction voltage for ethyl bromide clusters as a result of irradiation with laser pulses of 532 nm	135
Figure 8.6: Charge density of ethyl bromide cluster as a function of applied voltage between parallel plates for ionisation at 532, 355 and 266 nm	135
Figure 8.7: Charge density of methyl iodide cluster as a function of applied voltage between parallel plates for ionisation at 1064, 532, 355 and 266 nm	136

Figure 8.8: Charge density of xenon cluster as a function of applied voltage between parallel plates for ionisation at 532, 355 and 266 nm 137

Figure 9.1: Schematic of laser-cluster interaction studies under gigawatt laser field 143

LIST OF TABLES

	Page Number
Table 4. 1: Kinetic energy of multiply charged atomic ions of carbon and bromine measured for ionisation of ethyl bromide clusters at 532 and 355 nm.	73
Table 4.2: Laser wavelength and the corresponding ponderomotive energy for intensity of $\sim 5 \times 10^9$ W/cm ² . Electron-ion collision frequency is assumed to be of the order of laser frequency. The total energy gained by electron is derived by taking product of ponderomotive energy and the average number of collisions experienced by the caged electron in ~ 1 ns.	77
Table 4.3: Ionisation energy of different charge states of carbon and bromine ions	77
Table 5.1: Kinetic energy of multiply charged atomic ions on 532 nm photo ionisation, based on arrival time difference ' Δt (in nanoseconds)' between forward and backward ion peak of mass m (in amu), calculated using formula ' $E_{kin} = 9.65 \times 10^{-7} \Delta t^2 n^2 F^2 / 8m$ ', where F is the static electric field for ion extraction in V cm ⁻¹ and n is the charge of the ion.	91
Table 6.1: Kinetic energy of multiply charged xenon ions as a function of cluster size for ionisation at 532 nm, measured using retarding potential analyzer	110
Table 6.2: Ionisation energy of xenon cluster as a function of size	114

Table 8.1: Charge density of interaction zone for different atomic and molecular clusters at different wavelengths is listed below. Corresponding highest observed charge state in mass spectra is also shown.

140

Chapter 1

Introduction

Interaction of light with different forms of matter is a topic of interest for several decades.¹⁻¹⁴ Light is an electromagnetic radiation and when the electric field of light interacts with matter, different photo physical/chemical process can occur. These photo processes can be broadly classified as absorption, emission and scattering. Before the start of laser era, studies were performed using low intensity light sources where optical response of matter was linear with respect to the light intensity. However, the discovery of laser light introduced a new dimension in light-matter interaction studies. Unique properties of laser, such as monochromaticity, coherence, tunability over a wide wavelength range and high intensity makes it a powerful pump and probe tool for a number of spectroscopic as well as photochemical studies like laser induced fluorescence¹⁵, photo acoustic spectroscopy¹⁶, laser ionisation spectroscopy¹⁷ etc. Therefore, with the development of laser technology, almost every field of science and technology has been revolutionized. Because of high intensity of laser light, more than one photon can be absorbed by the matter which leads to entirely new field of nonlinear optics. Different solid and liquid materials qualify for nonlinear media because their dielectric polarization responds nonlinearly with electric field of light. Moreover, atomic and molecular clusters which are aggregates of atoms/molecules intermediate in size between individual atoms/molecules and bulk, also show nonlinear behaviour under the influence of laser field which attracts the researchers to study laser-cluster interaction in gas phase. A cluster produces a unique combination of gas and solid phase components. Their solid like local density and gas like average density causes

individual clusters to efficiently absorb laser energy forming highly charged atomic ions, molecular ions, energetic electrons and even neutrons. Moreover, generation of x-ray light¹⁸, higher order harmonic¹⁹ was also accomplished as a result of efficient interaction of cluster with intense laser light. However, in the present thesis, interaction of atomic and molecular cluster with laser light was confined to considerable low intensity using nanosecond pulses and the ions formed were studied using mass spectrometry technique. This chapter intends to introduce the subject of laser-cluster interaction in order to provide necessary background for the rest of the thesis. In section 1.1, basics of Laser have been described with working principles of nanosecond laser. Classification and generation techniques of cluster have been explained in section 1.2. As mentioned above, laser-cluster interaction leads to generation of singly and multiply charged ions. In section 1.3, technique related to detection of ions has been described. In order to understand the chemical/physical process of such laser-cluster interaction, few terms are used throughout the thesis. These terms are listed and described in section 1.4. Finally, the motivation and outline of the thesis work is sketched in section 1.5.

1.1 Laser

Laser is an acronym for **L**ight **A**mplification by **S**timulated **E**mission of **R**adiation²⁰. Laser light has three distinct characteristics that distinguish it from ordinary light. These are as follows:

a) Collimation: A laser beam is collimated i.e. it consists of waves travelling parallel to each other in a given direction with very little divergence. This allows laser light to be focused to a spot of very small diameter leading to very high intensity in the focal area.

b) Monochromatic: Laser light is monochromatic which means that it consists of one

colour/ wavelength or a narrow range of colours/wavelengths. This helps to selectively excite an atoms/ molecules to a particular electronic energy state.

c) *Coherence*: Laser light is coherent i.e. all the light waves move in phase together in both time and space.

1.1.1 Principles of laser operation

When an electron is in an excited energy state, it must eventually decay to a lower level, emitting a photon. This event is called “*spontaneous emission*” and the photon is emitted in a random direction, phase.²¹ On the other hand, if an electron is in energy state E_2 , and its decay path is to E_1 , but, before it has a chance to spontaneously decay, a photon happens to pass by whose energy is equal to $E_2 - E_1$, there is a probability that the passing photon will cause the electron to decay in such a manner that a photon is emitted at exactly the same wavelength, in the same direction and with the same phase as the passing photon. This process is called “*stimulated emission*.” During stimulated emission, the incoming photon interacts with one of the excited atoms, causing stimulated emission of a coherent photon; these two photons then interact with the next two atoms in line and the result is four coherent photons. Thus, cascade of photons are generated with identical phases and travelling in the same direction. Since the probability for an individual atom to absorb a photon is the same as the probability for an excited atom to emit a photon via stimulated emission, the collection of atoms will be a net absorber, not a net emitter, and amplification will not be possible. Consequently, in order to make a laser, we have to create a “population inversion” situation.

Population inversion:

A population inversion occurs when an atom or molecule exists in a state with more numbers in an excited state than in lower energy states. This condition is

required for light amplification in a non equilibrium distribution of atoms among the various energy levels. For two level system with equal degeneracy, the probability of stimulated absorption and emission is equal, therefore even with very intense pumping, equality of the population is achieved. Thus, to achieve population inversion, three or four energy level system is required. Three level process involves pumping of population from the lowest energy level to the highest, third energy state. The population can then decay down very fast to the second energy level or back down to the first energy level. The population that makes it to the second energy level is available for stimulated emission. Light matching the energy difference between the second and first energy level will cause a stimulated emission. Ruby laser is an example of three level laser.

Four level systems follow roughly the same process except that population is moved from the lowest state to the highest fourth level. Then it decays to the third level and lasing occurs when the incident light matches the energy between the third and second level. After lasing there is decay to the first level. Nd:YAG laser is an example of four level laser.

1.2 Clusters

Clusters are defined as aggregates of atoms/molecules, commonly intermediate in size between individual atoms/ molecules and bulk matter, which are held by interactions ranging from weak van der Waals forces to strong ionic bonds.²² They are formed by bridging atoms/molecules together in such a way that the force holding them do not saturate, so that the number of constituents in the cluster can be altered, without significantly changing the local structure and properties of the clusters. This characteristic which may be regarded as a primary property of clusters is referred to as stackability.²³ In clusters, number of atoms lying on the surface would

be higher than the number of atoms inside. Due to this surface effect, reactivity of the clusters can be significantly altered with the loss or addition of single atoms/molecules.²⁴ This very fact makes cluster different from their constituents atoms/molecules and the bulk material and recognized as separate class of materials.

Since clusters are intermediate in size between individual atoms/molecules and bulk materials, it is interesting to understand how different physical/chemical properties such as electrical, magnetic, optical, catalytic, reactivity etc. evolve with size of cluster.²⁵ However, it has been difficult to get a unique answer as the size at which bulk behavior manifest depends not only on the constituent atom/molecule but also on the property under consideration. Thus, size dependent studies of a given property have attracted researchers in recent years.

1.2.1 Classification of clusters

Clusters are classified in different ways; it can be done in terms of material they are made up of or in terms of their properties. Clusters can be homogeneous i.e. consisting only one type of atoms/molecules or heterogeneous, with more than one type of atoms/molecules. They may be neutral or charged. Structure, stability, reactivity and properties of clusters strongly depend on the type of interactions, which hold the constituent species within the cluster.²⁶ Classification of clusters based on the chemical bonding or interactions is most significant. According to chemical bonding, clusters are classified as ionic, covalent, metallic, hydrogen bonded, van der Waals cluster etc. These are briefly described below-

i) Ionic clusters

Ionic clusters are hetero-atomic clusters as they are formed from atoms with large difference in the electronegativity. The atoms are bound by ionic bond and generally made up of electropositive and electronegative elements similar to the bulk

ionic materials. The bond between the atoms in the cluster is strong with binding energy ~ 2 to 4 eV. Examples of ionic clusters are $[\text{Na}_x\text{Cl}_y]^{n+}$, $[\text{Mg}_x\text{O}_y]^{m+}$ etc.

ii) Covalent clusters

Covalent clusters are also known as network cluster which are strongly bound by means of covalent bond. The binding energy in network clusters is strong, typically 1 to 4 eV/atom or higher. However, the covalent bonding is modified from what is usually seen in their respective bulk because of the constraint imposed due to finite size. For example, diamond like (sp^3 hybridised) clusters would have surfaces with lots of dangling bond, but this number is greatly reduced if the cluster structures are based on graphite, in which the carbon atoms are sp^2 hybridized. C_{60} , the buckminsterfullerene, may be classified in this type of cluster. Other examples are met-cars which are formed by carbon and Group IV metals like Si, Ge etc.

iii) Metallic clusters

Metal clusters are aggregates of metal atoms bonded together through metallic bonding. The strength of metallic cluster ranges from 0.5 to 3 eV/atom. The inter-atomic forces in metals are not simple and many metals have no close packed structure because of the partially directional character of the inter-atomic forces. One can distinguish between simple metals like Na, Al by the hybridisation character of valence electrons whereas the localised d electrons play important role in transition metals like Fe, Co etc.

iv) Hydrogen bonded clusters

A special type of clusters is formed involving hydrogen atom and some electronegative elements which are known as hydrogen bonded clusters. Typically the bond energy in this type of clusters is in the range of 0.10 - 0.25 eV. Examples of hydrogen bonded clusters are $(\text{HF})_x$, $(\text{NH}_3)_y$, $(\text{ROH})_z$ etc. Clusters of water, methanol,

ethanol etc. show highly interesting structural properties because of partial electrostatic and directional character of hydrogen bonds.

v) van der Waals cluster

Clusters bonded by van der Waals attraction fall in this class and the interaction between atoms/molecules are weak with binding energy ~ 0.04 eV or less. The interaction between atoms/molecules can be described by central pair force. Due to simple central force, the most stable clusters are those with high atomic density i.e. with a close packing of atoms. Inert gases like He, Ne, Ar, Kr, Xe form van der Waals cluster. Moreover, molecular clusters like $(N_2)_x$, $(CO_2)_y$, $(SF_6)_z$ also belong to this class.

1.2.2 Different methods for generation of clusters

Several techniques have been developed for generation of clusters in the laboratory in line with the differing requirements of various experiments. When designing an experimental system, there are fundamental choices to be made, depending on whether the experiment involves free clusters where a pulsed source may be appropriate or deposited clusters where the requirements are likely to be a continuous intense beam with a small energy spread. In all cluster sources irrespective of the type of sources or experimental conditions, cluster generation consist of three consecutive processes viz. *vaporization* i.e. production of atoms or molecules in gas phase, *nucleation* i.e. initial condensation of atoms or molecules to form cluster nucleus and *growth-coalescence* i.e. the addition of more atoms or molecules to the initially formed nucleus and merging of small clusters forming larger cluster. Depending on the nature and conditions of the source, different size distributions of clusters might be generated. Example of cluster sources are Knudsen source,

supersonic nozzle source²⁷⁻²⁹, laser vaporisation source³⁰, ion sputtering source, hybrid magnetron sputtering³¹ etc.

i) Knudsen Cell (Effusive Source)

The Knudsen cell is the primitive effusive source. It is a continuous, low flux, subsonic source which involves heating a solid or liquid in an oven with a small aperture, thereby generating a low vapour pressure. At low vapour pressures, the mean free path of particles in the cell is greater than the diameter of the aperture, so there are very few collisions before leaving the cell. It has broad energy and angular distributions. If the aperture is small enough (though nozzle clogging may be a problem for less volatile solids) then the solid (or liquid)-gas equilibrium is not perturbed, an equilibrium distribution of clusters is generated, with a Maxwell-Boltzmann distribution of energy.

ii) Supersonic Nozzle Source

A supersonic free jet is formed in this type of source where a gas expands from a high-pressure region into a low-pressure background through a small circular aperture (also called nozzle).²⁷⁻²⁹ This technique exploits adiabatic expansion i.e. no heat transfer occurs between system and surroundings. Moreover, the expansion is also isentropic under this condition. As a consequence of isentropic expansion, density and translational temperature decreases within a few nozzle distance defined by the ratio of distance to orifice diameter. Figure 1.1 shows a schematic of supersonic jet expansion. The source gas is at temperature T_0 and pressure P_0 (stagnation condition), while the other side of the nozzle is maintained at a low background pressure P_b . As the gas leaves the source chamber through the nozzle, the pressure gradient across the nozzle causes the gas flow to accelerate. The degree of acceleration depends upon the pressure ratio - P_0/P_b . The flow may reach sonic speed i.e. mean velocity equal to the

local speed of sound (Mach no. ($M=1$) at the exit of the nozzle provided the ratio P_0/P_b exceeds a critical value G given by equation 1.1.

$$G = \left(\frac{\gamma+1}{2}\right)^{\gamma/(\gamma-1)} \quad (\gamma \text{ is the heat capacity ratio}) \quad (1.1)$$

The value of G is less than 2.1 for all the gases. Since the pressure at the exit of the nozzle exceeds P_b , the flow is said to be “under-expanded” and a subsequent expansion occurs as the flow attempts to meet the necessary condition imposed by the ambient pressure P_b .

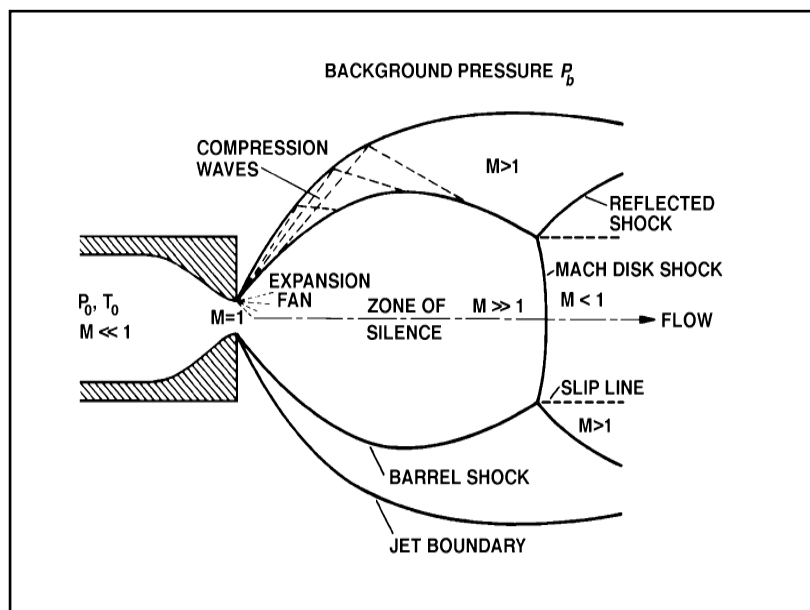


*Figure 1.1: Schematic diagram of supersonic gas jet*²⁷

Under these conditions beyond the nozzle, the flow will become supersonic, that is, the flow velocity exceeds the local speed of sound in the gas (Mach number $M > 1$). In this case, the situation may be complicated by the fact that shock waves are formed around the beam when the cold gas in the supersonic flow collides with the warm background molecules present in the vacuum chamber. The Mach disk perpendicular to the flow occurs at a characteristic distance from the nozzle and marks a transition from supersonic flow back to subsonic flow. An experimentally derived correlation for the distance from the nozzle to the Mach disk in nozzle units is given by -

$$\frac{x_m}{d} = 0.67 \left(\frac{P_0}{P_b} \right)^{1/2} \quad (1.2)$$

Where d is the diameter of the nozzle opening and x_m is the distance to the mach disk from the nozzle.

iii) Laser Vaporization Source

The laser vaporization-flow condensation source was introduced by Smalley and co-workers in the early 1980s.³⁰ This is a pulsed cluster source which is used to produce small and medium-sized (up to several hundreds of atoms) clusters of any metal-including refractory transition metals, carbon and silicon. It combines laser ablation with a supersonic jet expansion. In the laser vaporization source, vapour is produced by pulsed-laser ablation of a rod of the material of interest, using a ($>10^7$ W cm^{-2}) pulsed UV Nd:YAG or excimer laser. Each 10 ns pulse vaporizes 10^{14} – 10^{15} atoms per mm^2 of the target. The vaporized material (plasma with a temperature of around 10^4 K) is introduced into a pulse of cold carrier gas (example- He, Ar etc) which rapidly cools the vapour and induces cluster formation. The adiabatic cooling occurs at a greater rate than for the seeded supersonic nozzle and temperatures of under 100 K can be produced. The use of a laser for cluster generation also leads to some cluster ionisation, so this source generates neutral as well as cationic and anionic clusters.

iv) Ion Sputtering Source

In an ion sputtering source, clusters are produced by bombarding a target with high energy inert gas ions. Clusters of refractory metals and other high-melting materials can be generated. This source typically generates small, singly ionized clusters. Clusters are generated hot and cluster cooling involves evaporation, so that the abundance spectra reflect the thermodynamic stabilities of the clusters, via their binding energies. The heavier inert gases (Kr and Xe) are generally used as sputtering

ions, with bombardment energies in the range 10–30 keV and currents of approximately 10 mA.

1.3 Techniques to study Laser-cluster interaction

When a laser pulse interacts with atomic or molecular cluster, different photo physical/chemical processes can be observed. The outcome of the interaction can be either in the form of singly, multiply charged ions, energetic electrons, neutrons etc. or photons of different wavelength (x-rays, higher order harmonic generation etc.). In particle detection technique, most widely used technique is mass spectrometry for detection of ions. These mass spectrometers have been grouped into different categories on the basis of the ionisation source, mass analysers and detection methods used for analysis. A variety of methods are available for the ionisation of molecules such as electron impact, chemical ionisation, photoionisation etc. and a range of techniques have been used for mass separation of ions such as magnetic/electric fields, quadrupole mass filters and time-of-flight (TOF).³² Out of different types of mass spectrometry, time-of-flight mass spectrometry is most appropriate for cluster study since in principle there is no upper limit for mass detection in this method and it is well adapted for pulsed laser ionisation. Most of the work in the present thesis was done using time-of-flight mass spectrometer. General principles of time-of-flight mass spectrometer and factors affecting the resolution of the spectrometer have been discussed elaborately in section 1.3.1.

1.3.1 Time-of-flight mass spectrometer (TOFMS)

Time-of-flight mass spectrometer (TOFMS) is widely used in cluster studies because of its capability to detect higher masses.³³ TOFMS is a pulsed detection technique because of the need for an initial time reference ($t = 0$) for each recorded mass spectrum. For this reason, with pulsed laser as ionisation source, time-of-flight

is the natural technique for mass analysis as ions can be created in a reasonably small volume in a very short time, thus offering a built in $t = 0$ for the time-of-flight equation.

1.3.1.1 Principle of TOFMS

Mass separation in a TOFMS is achieved by accelerating ions having different m/z values, to identical kinetic energies and allowing them to separate due to their mass dependent velocities in the field free region. This results in arrival of different ions at the detector at different times. Ions with lower mass reach the detector faster than the higher mass ions.³⁴ The spectrometer consists of three basic regions: The ion source (also known as the extraction/acceleration region), the flight tube (also known as the field-free or drift region) and the detector. The ion source is the region where ions are first formed in the tiny source/ionisation region, usually with a pulsed ionisation source and the time recording process is initiated.

The potential applied to the repeller/acceleration grids accelerates the ions out of the source region and into the field-free drift region. In this process, all the ions are imparted with the same kinetic energy, given by equation 1.3-

$$U = zEs_a \quad (1.3)$$

Where U is the kinetic energy of the ion, E is the electric field (V/cm), z represents the charge of the ion and s_a is the initial position of ion formation (in cm). Different ions imparted with same kinetic energy upon acceleration will acquire range of velocities based on the mass-to-charge (m/z) ratio of the ions, since the kinetic energy is related to the velocity (v) of the ion by the equation-

$$U = \frac{1}{2}mv^2 \quad (1.4)$$

Upon substituting above equation in equation 1.3, we get-

$$v = \left(\frac{2zEs_a}{m} \right)^{1/2} = \left(\frac{2Es_a}{m/z} \right)^{1/2} \quad (1.5)$$

From equation 1.5 it is clear that for singly charged ions with same kinetic energy, lighter ions will be imparted more velocity in comparison to heavier ions and hence get separated along the drift tube. This is the governing principle of separation-in-time. Assuming that the ions spend most of the time (t) in the drift region (D) before reaching the detector, the time-of-flight of the ion can be calculated from the relation

$$t = \frac{D}{v} = D \left(\frac{m/z}{2Es_a} \right)^{1/2} \quad (1.6)$$

Rearranging the terms in above equation yields the relation-

$$\frac{m}{z} = 2Es_a \left(\frac{t}{D} \right)^2 \quad (1.7)$$

Thus, by precisely knowing the length of the drift tube (D) and the applied electric field (E), the m/z ratio and hence ion identity can be determined from the time-of-flight data.

In theory, equation 1.7 implies that infinite mass separation can be achieved if time-of-flight of the ions is infinitely long. This is possible if the drift length (D) is extremely long, and/or the applied field (E) is extremely low. However, practical instrumental considerations and compromises eliminate such approaches. Typically, flight tubes are 1-2 meters long. In general, a longer flight tube results in a better separation of adjacent masses (higher mass resolution), but can result in loss of sensitivity due to insufficient ion-beam collimation.

1.3.1.2 Resolution of TOFMS

Resolution (R) of a mass spectrometer is defined as the ability to distinguish two ions of different masses and is usually given by the relation-

$$R = \frac{m}{\Delta m} \quad (1.8)$$

Where Δm is the full width at half maximum (FWHM) of the ion peak of mass m . In TOFMS, it is convenient to work in time domain. Therefore, to obtain the resolution of TOFMS in time domain, we make use of the relation $m \propto t^2$ (equation 1.7) and $\Delta m \propto 2t\Delta t$. On substituting these values of m and Δm in equation 1.8, the resolution of time-of-flight mass spectrometer can be expressed as-

$$R = \frac{t}{2\Delta t} \quad (1.9)$$

Where t represents the flight time of the ion while Δt represents the full width at half maximum (FWHM) of the ion peak. Thus, it is clear from the above equation that an increased time-of-flight (t) (long drift length) and/or low acceleration potential and narrow peak width (Δt) maximizes resolution. This could be done simultaneously, but system parameters usually affect t and Δt in opposite manners.³⁵ In the following section we will discuss about various factors which affect the resolution of the linear time-of-flight mass spectrometer and possible solution for improving the resolution based on Wiley-McLaren principle.³⁶

1.3.1.3 Dual stage TOFMS

For a linear time-of-flight mass spectrometer it is assumed that all the ions were formed within the same ionisation region at the same time with no initial velocity spread. However, this is not true for any given ionisation method and resolution in TOFMS is severely limited by the ions (with the same m/z) not being formed at the same time, in the same place and with the same kinetic energy prior to acceleration. These differences are commonly referred to the initial time, space and energy distributions and they contribute significantly to the broadening (Δt) of the ion peak. The ability to minimize these contributions defines the maximum achievable resolution in TOFMS. In 1955, Wiley and McLaren introduced the dual stage ion

source as a means to improve mass resolution.³⁶ Based on their mathematical derivation, following conclusions can be drawn regarding the contribution from spatial, temporal and energy distribution of ions to the overall resolution of the time-of-flight spectrometer-

- (a) Ions with the same m/z , formed at the same position at the same time but with different initial kinetic energies, will arrive at the detector at different time.
- (b) Ions with the same m/z , formed at the same time, in the same position, with the same initial kinetic energy, but with opposing velocity vectors will contribute to the temporal spread of the ion peak. This condition is also referred as the “turn-around” time of an ion. Though, at the end of the acceleration region both ions will acquire the same kinetic energy, and therefore the same velocity, but the ion which was initially travelling away from the flight tube has to be stopped and turned around by the electric field before being deflected into the drift tube. This turn-around time results in a temporal distribution of ions with the same m/z .
- (c) Ions that are formed at the same time, with the same kinetic energy but at different positions in the source region will have different kinetic energies following acceleration. This difference is because the energy imparted to ion during acceleration (zEs) due to electric field depends on the position of the ion. Since electric field strength is measured in V/cm , an ion closer to the field-free region will be given less kinetic energy. This results in spatial distribution of ions.
- (d) If ions of the same m/z have the same initial kinetic energy and are formed at the same position in the ion source, the final peak width is determined by the initial time distribution of ion formation. This factor leads to temporal distribution of ions.

Thus, to improve the resolution of TOFMS, it is essential to minimise the contributions of spatial, temporal and energy distribution which result in broadening of the ion peak width (Δt). Temporal contribution can be minimised by using a short pulse width ionisation source, which will minimize the initial time distribution of ion formation. For spatial and energy distribution, following measures are taken-

(a) Space focussing: For a single stage time-of-flight mass spectrometer, space focusing can be achieved at a point in the field-free region where the ion with higher kinetic energy catches up with the slower ion that were initially formed closer to the flight tube. Thus, plane of space focus occurs at a distance equal to twice the length of the acceleration region. This distance (1-10 cm) is too small for any meaningful separation of ions. Wiley and McLaren showed that using a dual-stage ion source, the spatial focus plane can be moved to longer distances. They have introduced two new parameters i.e. the length of the second stage (d) and the ratio of acceleration field (E_d/E_e) in case of dual-stage ion source.

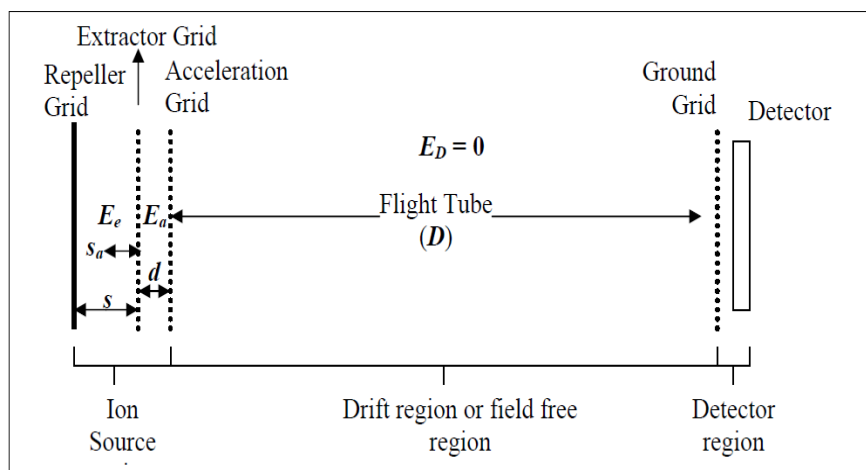


Figure 1.2: Schematic diagram of a linear time-of-flight mass spectrometer with dual acceleration stage.³⁶

Figure 1.2 shows a schematic diagram of dual stage TOFMS. Here the length of the extraction region (s) and the acceleration region (d) are fixed. The space focus

is then empirically optimised by systematically adjusting the ratio E_a/E_e and observing where the maximum resolution is obtained. Typically, E_e is ten to fifteen percent of E_a .

(b) Energy focusing:

Wiley and McLaren also introduced a technique called time-lag focusing to overcome the energy-spread problem. By restricting ionisation within a narrow volume and allowing a delay between ionisation and ion extraction, the velocity dispersion causes the ion packet to spread out. The resultant large spatial distribution (correlated to the initial velocity distribution) is refocused by a spatial focusing technique as discussed in the previous section. Unfortunately this correction is mass dependent and enhanced resolving power is attainable only over a limited mass range.

To increase the resolution of the instrument further, Mamyrin and Shmikk³⁷ formulated reflectron principle for the energy focusing of the ions, this led to the birth of **Reflectron Time-Of-Flight Mass Spectrometer (R-TOFMS)**. The reflectron compensates for the kinetic energy distribution by ensuring that ions with different kinetic energy (but with same mass) reach the detector at the same time. This is achieved by placing a reflectron (an assembly of grids with parabolically increasing retarding potential) at the end of drift region. The faster ions in a given ion packet penetrates deeper into the grid before getting reflected back, thus taking longer time to travel in the reflectron assembly. The slower ions, on the other hand, penetrate less and thus have a shorter trajectory in the grids. This leads to energy focusing as well as an increase in the overall flight length, as the ion packet reaches the detector after getting reflected by the retarding field. Both these factors significantly improve the resolution. Thus, for a RTOFMS a resolution of 5000-10,000 can be easily obtained.³⁸

1.4 Atomic and molecular process in laser field

There are several photo physical and chemical processes such as excitation, dissociation, ionisation, etc. which can occur for an atom or molecule under the influence of the laser field. In the present work, we mainly focus on the ionisation process in atomic and molecular clusters. Few relevant terms for cluster ionisation under nanosecond laser field are described briefly in the subsequent section which would be used frequently in the thesis.

1.4.1 Multiphoton ionisation

Interaction of laser radiation, having photon energy much smaller than the ionisation potential, with atoms, molecules or clusters primarily leads to their excitation by absorption of one photon provided certain optical selection rules are satisfied. These excited atoms or molecules would normally decay back to ground state by emission of radiation or undergo dissociation. However, if the laser intensity is sufficiently high, then these excited atoms/molecules can absorb additional photons from the laser pulse before decaying and reach higher excited states or may even get ionized. This process is called multiphoton ionisation.³⁹⁻⁴¹

A primary advantage of using a multiphoton transition instead of a single photon transition to study photochemistry of molecules arises from the difference in selection rules. Because, for molecule having a center of symmetry, one-photon transitions and multiphoton transitions involving odd number of photons are allowed only between the states of different parity, i.e. *ungerade* \leftrightarrow *gerade*, while multiphoton transitions involving even number of photons are allowed between the states of the same parity, i.e. *gerade* \leftrightarrow *gerade* and *ungerade* \leftrightarrow *ungerade*. Since the ground level of a molecule is usually of *gerade* parity, multiphoton transitions facilitates investigation of excited *gerade* parity levels that are usually very difficult to

access by ordinary linear absorption spectroscopy.⁴²

The transition probability of multiphoton ionisation is given by the expression⁴³-

$$W^{(N)} = \sigma_N I^N \quad (1.10)$$

Where $W^{(N)}$ is the N -photon transition probability (sec^{-1}), σ_N is the N -photon absorption cross-section with units $\text{cm}^{2N} \text{sec}^{N-1}$ and I is the light intensity expressed as photons $\text{cm}^{-2} \text{sec}^{-1}$. Typically, the single photon absorption cross-section is $\sim 10^{-17} \text{cm}^2$ while two and three photon absorption cross-section is much less ($\sigma_2 \sim 10^{-51} \text{cm}^4 \text{sec}^2$ and $\sigma_3 \sim 10^{-82} \text{cm}^6 \text{sec}^3$).⁴⁴ Thus, sufficient high laser intensity is required for a transition having low multiphoton ionisation cross-section.

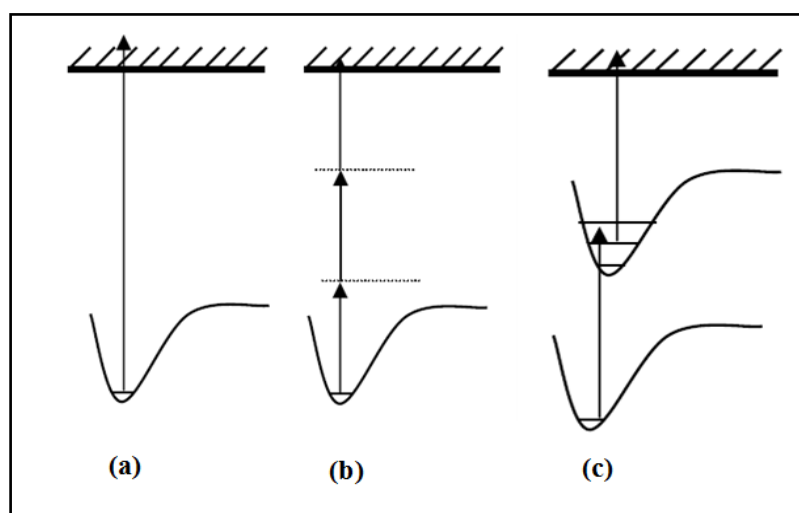


Figure 1.3: *Different ionisation schemes for a molecule (a) Single photon ionisation (b) Non-resonant multiphoton ionisation - 3 photons are involved (c) Resonant two-photon ionisation via excited state rovibrational levels*

If multiphoton process does not involve any real excited state of the molecule, it is termed as non-resonant multiphoton ionisation. However, in case of polyatomic molecules, which have dense manifold of excited states, it is likely that N -photon excitation via intermediate virtual state may take the molecule to a so-called real intermediate excited vibronic state of the neutral molecule which has a longer lifetime and is often (but not always) a readily ionisable Rydberg state. Absorption of one or

more (M -photons) additional photons by this intermediate vibronic state excites the molecule to the ionisation continuum, resulting in formation of parent ion and an electron. Often the latter step i.e. excitation from intermediate vibronic state to ionisation continuum is very efficient and the rate of ionisation is limited by multiphoton excitation of the molecule from the ground electronic state to excited vibronic state of the neutral molecule. This is because the Heisenberg uncertainty principle stipulates that the frequency width of the final state, which lies above the ionisation potential, is very broad and relatively structureless. Since the probability of multiphoton absorption processes, which involve real intermediate states, is greatly enhanced in comparison to those which do not involve the real eigen states, such type of ionisation is termed as **Resonance Enhanced Multi Photon Ionisation (REMPI)**.

1.4.2 Optical field ionisation

At laser intensity above $\sim 10^{14}$ W/cm² where the electric field associated with the laser pulse approaches atomic field, optical field ionisation (OFI) processes take place. OFI is a general term for different types of ionisation mechanisms observed at very high laser intensity namely above threshold ionisation, tunneling ionisation and barrier suppression ionisation which are induced by the electric field of the laser pulse.

(a) Above threshold ionisation

Above threshold ionisation (ATI) was discovered by Agostini *et al.* in 1979.⁴⁵ This ionisation process occurs when an electron is excited to a Rydberg state located above the ionisation potential. The Rydberg state then autoionizes, creating a charged ion. Autoionisation may lead to an ion which may be able to absorb additional photons, resulting in multiple charging of the ion.⁴⁶ Thus, the ATI mechanism primarily results from interaction of newly freed electron with laser field and also

provides a controllable heating mechanism in plasmas.⁴⁷ A typical ATI photoelectron energy spectrum consists of several peaks, separated by the photon energy. As the laser intensity increases, a peak at higher energies appear, whose intensity dependence does not follow the power law, according to lowest order perturbation theory.

(b) Barrier suppression ionisation

When the electronic state of the chromophore interacts with strong electric field of laser pulse, the electronic states are Stark shifted to lower energies. The resulting potential surface allows ionisation to occur more readily. In the case of barrier suppression ionisation, the ionisation potential is lowered so far that multiphoton processes easily ionise the chromophore. If the process were repeated in a stepwise manner, higher charge states of the chromophore would be generated.⁴⁸⁻⁵⁰

The threshold intensity of barrier suppression (I_{BS}) is expressed by the following equation:

$$I_{BS} = cI_p^4 / (128 \pi Z^2 e^6) = 4 \times 10^9 I_p^4 / Z^2 \text{ (Wcm}^{-2}\text{)} \quad (1.11)$$

where Z is the charge state of atomic ion and I_p denotes the ionisation potential of atom or molecule in eV.

(c) Tunneling ionisation

Tunnel ionisation is a process in which electrons in an atom/ molecule pass through the potential barrier and escape from the atom/ molecule. In an intense electric field, the potential barrier of an atom/ molecule is distorted drastically. Therefore, the height of the barrier that electrons have to pass decreases and electrons can escape from the atom/ molecule easily. Tunneling ionization is a quantum mechanical phenomenon; a non-zero probability event for observing a particle escaping from the deformed Coulomb potential barrier, obviously this phenomenon is

forbidden by classical laws, as in the classical picture an electron does not have sufficient energy to escape.⁵¹

1.4.3 Keldysh parameter

Multiphoton ionisation and tunnel ionisation processes can occur in the presence of intense laser field. The characteristic feature of electromagnetic radiation is that it is not a DC field but is an alternating sinusoidal field. This means that the barrier against ionisation in any given direction is lowered only for the duration of a single cycle implying that only levels which can tunnel ionize on a time scale shorter than the inverse frequency of the radiation can undergo tunnel ionisation. Thus, low frequency radiation at high intensities is suited for such processes. Multiphoton ionisation on the other hand requires that individual photons have a large energy so that a given process can take place with a fewer number of photons. The larger the energy, the higher is the frequency of the incident laser radiation. The two processes therefore are efficient in different regimes of the frequency spectrum. A quantitative measure of this division had been proposed by Keldysh⁵², who suggested that the adiabaticity parameter (γ) now known as the Keldysh parameter, might be an indicator of the regime in which the processes might occur. Keldysh parameter can be expressed as-

$$\gamma = \sqrt{\frac{I_p}{2U_p}} \quad (1.12)$$

where I_p is ionisation potential of atom or molecule and U_p is ponderomotive energy given in eV. Ponderomotive energy depends on laser intensity, wavelength and details are explained in subsequent section (Section 1.4.4). In case of $\gamma > 1$, multiphoton ionisation is expected to be dominant ionisation process for an atom/molecule under certain laser conditions. On the contrary, $\gamma < 1$ indicates optical field ionisation of the

atoms/molecules under the specified laser conditions. Thus, multiphoton ionisation process dominates in atoms/molecules at low laser intensity conditions and the electron energy spectra shows structured feature. As the intensity of laser increases, the ejected electron spectra changes from sharp structure to a continuous distribution. Thus, the electron motion in the laser field is sensitive to the laser intensity and frequency which subsequently dictates the ionisation rate of the atoms/molecule.

1.4.4 Ponderomotive energy

Ponderomotive energy refers to the cycle averaged energy gain of a free electron in an electromagnetic field. Ponderomotive energy of an electron is expressed as⁵³ -

$$U_p (eV) = \frac{E_0^2 e^2}{4m_e w^2} \cong 9.33 \times 10^{-14} I (\text{W/cm}^2) (\lambda (\mu\text{m}))^2 \quad (1.13)$$

e , m_e , E_0 , w , I and λ represent electron charge, electron mass, laser electric field, laser frequency, laser intensity, wavelength respectively. It is important to note that the ponderomotive energy is not permanently transferred to the electron during the laser pulse, if no force acts on electron. Therefore, if the electron starts at rest and the laser pulse is turned on slowly over many cycle, electron will return to a state of rest after the laser pulse is passed. Only the presence of another force like inelastic collision between electrons and ions can lead to transfer of the energy to the electron.

1.4.5 Inner and outer ionisation

When an atom/ molecule is ionised by means of an external energy source like laser field or electric field, the electrons are removed from the outermost shell to infinity. However, in case of clusters the situation is different from individual atom or molecule. Clusters composed of large number of atoms/molecules in close proximity with interactions ranging from van der Waals force to strong ionic bonds. Electrons in a cluster which are interacting with a laser pulse may be classified into tightly bound,

quasifree, and continuum electrons (as shown in figure 1.4). Within this picture, inner ionisation describes the excitation of tightly bound electrons to the conduction band, i.e., electrons are removed from their host ion but reside within the cluster. Correspondingly, the final excitation into the continuum is termed outer ionisation, which contributes to the net ionisation of the system.⁵⁴ At moderate laser intensities, systems with initially delocalized electrons, may undergo outer ionisation only. The energy span between the thresholds for inner and outer ionisation grows with cluster charge, indicating the importance of quasifree or delocalised electrons for strong excitations. Moreover, the ionisation barriers are influenced by the fields from the neighbouring ions which give rise to charge resonance enhanced ionisation in strong field excitations. Within this process, an appropriate inter nuclear separation results in a simultaneous lowering of inner and outer barrier and enhances ionisation.⁵⁵

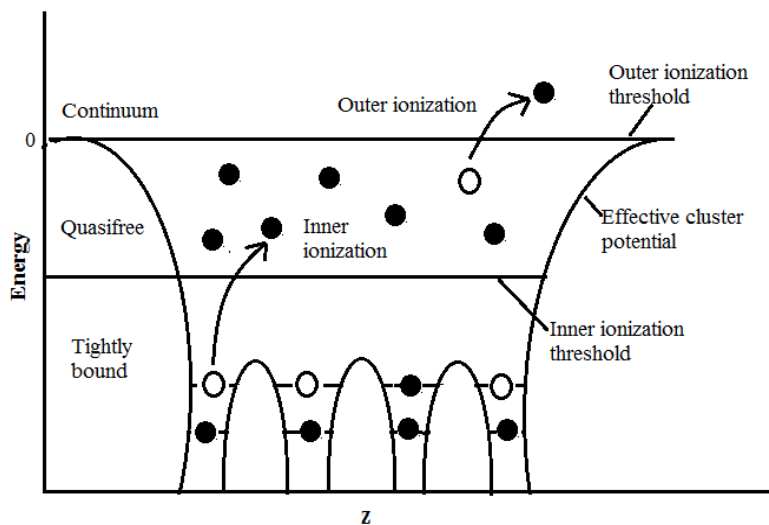


*Figure 1.4: Schematic view of inner and outer ionisation of a cluster based on the effective cluster potential.*⁵⁴

1.4.6 Inverse bremsstrahlung absorption

If a charged particle decelerates due to deflection by another charged particle, it emits bremsstrahlung radiation. The process in which an electron absorbs a photon while colliding with an ion or with an electron is called inverse bremsstrahlung.⁵⁶ At

low laser intensities, inverse bremsstrahlung is the main absorption mechanism, which depends on the electron-ion collision probability, the shape of the density profile, electrical conductivity associated with electron mean-free-path comparable to the interatomic spacing. At low intensities $I < 10^{13} \text{ W/cm}^2$, the absorption was quite high. The high absorption via this mechanism is broadly consistent with collisional absorption theory.^{57, 58} The energy gain on inverse bremsstrahlung absorption of rapid electrons with electron temperature T ($T \gg Z^2$ and $\omega \ll T$) is

$$\left\langle \frac{dE}{dt} \right\rangle = \frac{4\sqrt{2\pi}n_i \varepsilon^2 Z^2}{3 T^{3/2} \omega^2} \ln \Lambda \quad (1.14)$$

Where n_i , ε , ω , Z , T and $\ln\Lambda$ represent concentration of Coulomb scatterers, electric field strength amplitude, electric field frequency, Coulomb charge, temperature and Coulomb logarithm respectively.⁵⁹

1.5 Motivation and outline of the thesis

As the title of the thesis suggests, the main objective of the present work is to understand interaction of nanosecond laser pulses of intensity $\sim 10^9 \text{ W/cm}^2$ with atomic and molecular clusters. Some of the basic questions to which we have tried to seek answer from our studies are listed below-

1. How is the interaction of a cluster different from its monomer constituent under gigawatt intense laser field?

In general, the degree of aggregation in a cluster alters the electronic properties of the system as well as its photoionisation behaviour with respect to its monomer.⁶⁰ As a result, new reaction channels become accessible which lead to generation of several exotic species. Multiply charged atomic ions are one of such exotic species which are produced with large kinetic energy.⁶¹ Generation of energetic multiply charged atomic ions due to cluster disintegration is a signature of Coulomb explosion.⁶² The basic aim

of the thesis is to understand the mechanism of Coulomb explosion of clusters which are exposed to gigawatt intense laser pulses.

Coulomb explosion of clusters has been reported previously using laser pulses over a wide range of electromagnetic spectrum ranging from IR to X-ray region employing intensity in the range of 10^{14} – 10^{20} W/cm².⁶³⁻⁶⁷ Based on Auguste formula⁶⁸ [$I(\text{W/cm}^2) = 4 \times 10^9 E_i^4 / Z^2$, where E_i is ionisation energy of multiply charged ion (eV) and Z is the charge on the ion] the threshold intensity required for generation of multiply charged species via multiphoton ionisation process was calculated to be $\sim 10^{14}$ W/cm². However, our group has observed generation of multiply charged atomic ions using nanosecond laser pulses of intensity $\sim 10^9$ W/cm² in few molecular systems like methyl iodide⁶⁹, carbon disulphide⁷⁰ and acetone⁷¹ clusters. The laser intensity employed in these experiments was at least $\sim 10^5$ times lower than the previously reported value. Though the high intensity Coulomb explosion is reasonably well understood, the understanding of gigawatt induced Coulomb explosion is very poor. Thus, systematic experiments need to be carried out to understand low intensity laser-cluster interactions.

II. What is the effect of laser parameters like wavelength, intensity, polarisation on generation of multiply charged species under gigawatt intense laser field?

Laser parameters play an important role in governing the laser-cluster interaction.^{65,66} Thus, different laser parameters have been varied and formation of multiply charged atomic ions was monitored. These experiments are helpful in understanding the energy absorption mechanism in cluster at an intensity of $\sim 10^9$ W/cm².

III. What are the kinetic energies of multiply charged species that are produced due to Coulomb explosion of clusters?

As discussed earlier, multiply charged ions are produced as a result of cluster ionisation in the laser field and it leads to violent explosion of the cluster.⁶¹ Thus, multiply charged ions are associated with high kinetic energy. In order to quantify the kinetic energy of different multiply charged ions, two different techniques have been used depending on the nature of element. First method is ‘peak splitting method’ which is based on the difference in time of arrival of same mass peaks in time-of-flight mass spectra. Second method is ‘retarding field method’ where the energy analysis of the multiply charged ions was carried out prior to the extraction of the ions in the time-of-flight mass spectrometer.

IV. What is the role of intermediate energy states of the constituent atoms/molecules in laser-cluster interaction?

In our previous report on Coulomb explosion of methyl iodide clusters, role of resonant energy states was emphasized for unusually high energy absorption in the cluster from the laser field.⁶⁹ In order to get better understanding of the role of intermediate electronic state, similar type of halogen containing organic compounds were chosen such as C_2H_5Br and CF_2Br_2 along with CH_3I . The ionisation potential of these molecules are in the range of 9.5-11 eV where multiphoton ionisation can take place via intermediate energy state under gigawatt intensity conditions. Thus, systematic study has been carried out on these molecules by varying different experimental parameters.

V. Does the presence of a dopant play any significant role in altering cluster ionisation dynamics?

Cluster composition plays an important role in governing the nature of interaction in the laser field.⁷² Depending on the ionisation potential of the dopant, ionisation dynamics differs a lot for a given laser intensity. Thus, pure molecular

clusters were doped with a molecule having high ionisation potential and the cluster ionisation processes were probed using time-of-flight mass spectrometer.

VI. Do atomic clusters behave in a similar way as molecular clusters for a given laser intensity?

Molecular clusters have inherent complications such as presence of several dissociation channels, energy dependent electron attachment processes leading to the formation of metastable negative ions etc. which complicate understanding of multiply charged ion formation.⁷³ These complications can be eliminated if studies are carried out using inert gas atomic clusters. Thus, atomic clusters were photo ionised with laser pulses of gigawatt intensity and the difference in charge state and kinetic energy of ions was compared with molecular cluster.

VII. What is the minimum cluster size for generation of multiply charged species under our experimental conditions?

The basic interest in most of the cluster studies has been to trace the evolution of different properties of matter as it grows from its individual constituents to the bulk phase.²⁵ Understanding the variation in the properties of clusters with size provides a new dimension to laser-cluster interaction studies. Thus, cluster size has been varied over a wide range and evolution of multiply charged ion formation was studied systematically.

VIII. What is the fate of photoelectrons during cluster ionisation process? Is there any possibility of generation of negative ions? If yes, what is the effect of negative ions in the cluster ionisation dynamics?

In laser-cluster interaction studies, most of the reports deal with generation of singly or multiply charged positive ions. However, there are very few reports on generation of negative ions in laser-cluster interaction.⁷⁴ Thus, we attempted to detect

negative ions which can be generated by attachment of photoelectrons to the neutral atom in an ionized cluster. Moreover, effect of negative ion formation on cluster ionisation dynamics has also been probed.

IX. What is the total charge produced in the interaction volume of laser-cluster interaction?

Generation of multiply charged ion was studied using time-of-flight mass spectrometer where one can get the qualitative idea of relative ion yield of various charge state formation under certain experimental conditions. However, it is very difficult to comment on the total ion yield of the interaction volume under different experimental conditions based on the time-of-flight mass spectrum. Thus, in order to quantify the absolute ion yield of the interaction zone in laser-cluster ionisation process, a new and simple method was devised which can complement the time-of-flight mass spectrometer results.

A systematic study has been carried out to answer these basic questions in the present thesis. The experimental setup used in these studies is described in **chapter 2**. This includes details about the laser system, vacuum system, molecular beam setup and the mass spectrometer for detection of ions.

In **chapter 3, 4 and 5**, results of interaction of nanosecond laser pulses with CF_2Br_2 , $\text{C}_2\text{H}_5\text{Br}$ and CH_3I clusters are presented respectively. Different laser parameters have been varied in each molecular cluster system and effect of these laser parameters on charge state and kinetic energy of ion was studied. The study is further extended to atomic clusters i.e. xenon cluster which is described in **chapter 6** and the experimental results obtained on atomic clusters were compared with molecular clusters.

Large number of electrons are produced due to severe ionisation of cluster in

the laser field and there is always a possibility of electron attachment to neutral atoms. Electron attachment to neutral atoms/molecules may lead to generation of negative ions within the interaction zone. Thus, an attempt has been made to detect negative ions in different molecular clusters and presented in **chapter 7**.

Based on solely time-of-flight mass spectrometric studies, it is very difficult to comment on the absolute ion yield of laser-cluster interaction. A simple and effective method has been used to determine the charge produced per unit volume i.e., charge density of the interaction zone. Charge density of different atomic and molecular clusters was studied at different wavelengths and the time-of-flight mass spectrometer results were compared which are described in **chapter 8**.

Finally in **chapter 9**, conclusions drawn from all these studies have been summarized and future scope of the present work is discussed.

Experimental Details

2.1 Introduction

As the title of the thesis suggests, laser-cluster interaction study has been carried out in gas phase. However, in equilibrium conditions, atomic/molecular clusters are not available off the shelf and clusters have to be produced in situ in vacuum chamber. For ionisation of atomic/molecular cluster, laser system has been used and the ionic outcome of the laser-cluster interaction has been studied using time-of-flight mass spectrometry technique. In this chapter, the design and implementation of the experimental set up for exploration of different aspects of laser-cluster interaction are described. The details of the experimental parameters are given in individual chapters dealing with separate set of measurements. However, the basic set up used for most of the experiments is depicted here. The instrument consists of three interconnected vacuum chambers which are essential for maintaining molecular beam conditions during gas flow, as well as for providing the collision free paths to the ions during their flight from the ionisation zone to the detector in the mass spectrometer. Thus, vacuum system along with the details of different pumps is described in section 2.2. Within this vacuum chamber, molecular beam arrangement is housed for generation of atomic and molecular clusters. Details of the cluster source are described in section 2.3. For excitation and ionisation of clusters, pulsed Nd:YAG laser was used. Basic principles of laser and its components are discussed in chapter 1 (section 1.1). The relevant information regarding Nd:YAG laser is illustrated in section 2.4. In our experiments, both cluster beam and the laser beam are pulsed. Thus, it is very crucial to overlap (spatially and temporally) these two beams to study

laser-cluster interaction. Synchronization of these two pulsed beams is done by using time delay equipment and details of the procedure are explained in section 2.5. Thus, interaction of cluster beam with laser pulses leads to generation of ionized charged particle. In order to identify and characterize the ions, time-of-flight mass spectrometer was employed. Basic principles of time-of-flight mass spectrometer have been discussed in chapter 1(section 1.3.2). Hence, ion optics and the detector system of time-of-flight mass spectrometer are described in section 2.6.

2.2 Vacuum system of time-of-flight mass spectrometer

The system consists of three interconnected vacuum chambers i.e. expansion chamber, ionisation chamber and the time-of-flight tube, which are differentially pumped to fulfill the necessary condition of collision-less flight of ions in the mass spectrometer.^{75,76} All the chambers have been fabricated out of stainless steel (SS-304). The expansion and ionisation chambers are similar in dimension having a length of 34 *cm* and inside diameter of 34 *cm* with a wall thickness of 12 *mm*. These two chambers are separated by a skimmer (3 *mm* diameter). The third chamber acts as the flight tube (78 *mm* inner diameter, 140 *cm* length) of the time-of-flight mass spectrometer and is attached to the ionisation chamber with the help of a 180 *mm* diameter flange having an opening of 25 *mm* diameter at its center.

The expansion chamber which houses the nozzle (pulsed molecular beam source), is pumped by a 250 *mm* diameter liquid nitrogen cooled oil diffusion pump (pumping speed ~3000 *l/s*) which is backed by a 500 *l/m* rotary pump. This large pump is used to take care of the carrier gas load, which is mostly pumped out in this chamber. A skimmer assembly is mounted on the interconnecting flange of the expansion and ionisation chamber, coaxially with the nozzle orifice, to skim the supersonic jet of molecular vapours seeded in inert carrier gas coming out of the

nozzle. This results in the formation of a molecular beam which passes into the ionisation chamber. The nozzle and skimmer are mounted separately at a distance of 3 cm apart. Nozzle and skimmer apertures were precisely aligned with the help of a He-Ne laser.

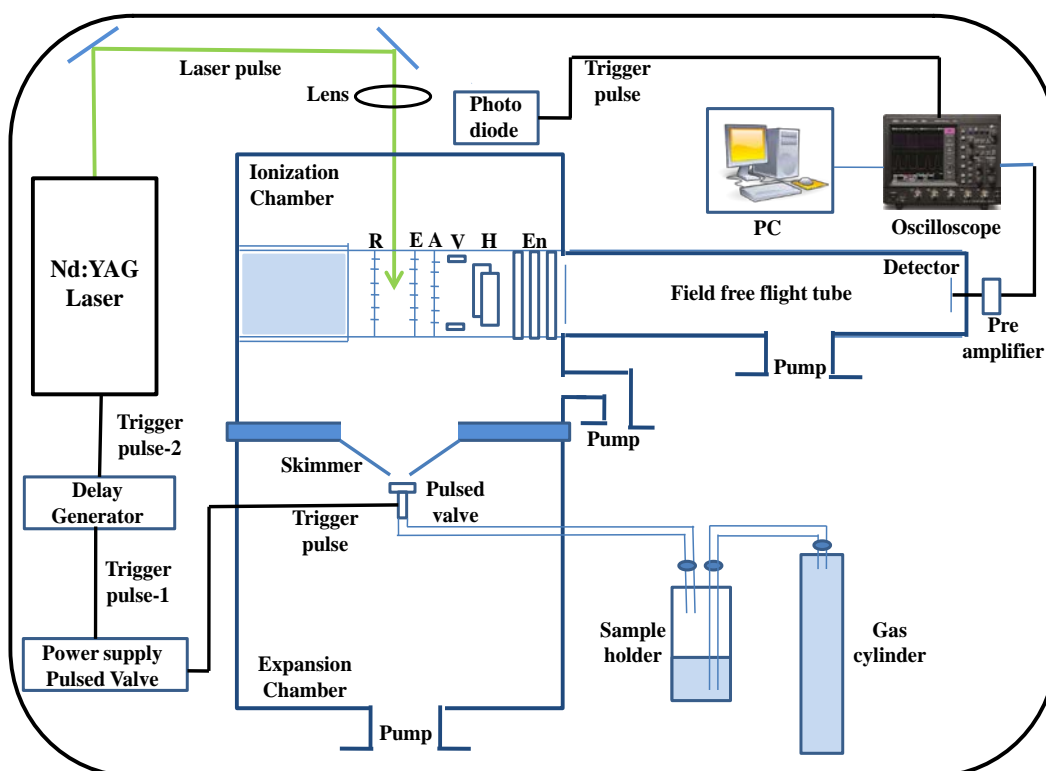


Figure 2.1: Schematic diagram of the experimental set-up used for laser-cluster interaction studies

The ionisation chamber is pumped by a 1000 *l/s* liquid nitrogen cooled oil diffusion pump backed by a 300 *l/m* rotary pump. This chamber is provided with four 25 mm and four 50 mm ports. Out of these, two 50 mm ports are used to mount electrical feed-through for supplying high voltages to different grids of the ion optics assembly in the TOFMS. Pirani and penning gauge heads are mounted on two additional ports for measurement of ultimate vacuum in this chamber. The whole ion-optics assembly of the time-of-flight mass spectrometer is mounted in this chamber coaxially with the flight tube. The ionising laser beam enters this chamber from the

top through a port, fitted with a two-inch quartz window. A quartz lens of 35 cm focal length, mounted vertically above this window, is used to focus the ionisation laser beam at the centre of repeller and extractor grids of the ion optics assembly.

A 140 cm flight tube is placed in the horizontal plane so that all the three beams, namely - molecular beam, laser beam and the repelled ion beams are orthogonal to each other. This flight tube is attached to a 150 mm diameter turbo molecular pump (Alcatel, Model-ATP 900DN) (pumping speed ~900 l/s) and is backed by a suitable rotary pump (pumping speed 300 l/m). At the end of the flight tube, a channel electron multiplier (CEM) detector assembly is mounted for detection of ions. This detector assembly can be isolated from the rest of the chamber by a gate valve. This gate valve arrangement is made to keep the detector always under a vacuum of 10^{-5} Torr or in helium inert gas atmosphere, which is desirable to increase the life-time of the detector. A penning gauge head is mounted in front of the detector to monitor the pressure. The base pressure of the entire system without gas load is $\sim 2 \times 10^{-6}$ Torr. A photograph of the instrument used for laser-cluster interaction is given in figure 2.2.

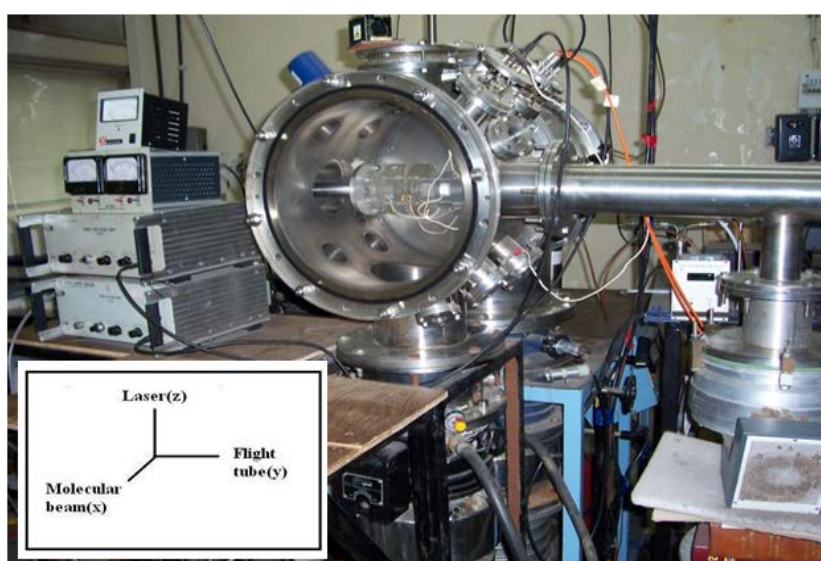


Figure 2.2: Actual photograph of the experimental set-up used for laser-cluster interaction studies

2.3 Molecular and cluster beam source

For carrying out experiments on clusters in gas phase, we have to make use of a conical nozzle. The setup consists of a General valve (series 9 stainless steel body) fitted with o-ring and a Teflon poppet. Different nozzles of 0.3 mm, 0.6 mm and 0.8 mm orifices and 45° half expansion angle are used to produce clusters. The valve is controlled using a controller. There is an actuator called armature within the nozzle, sitting on the main spring and surrounded by the coil of solenoid which is tipped with a Teflon poppet. This armature moves axially as the pulsed current is passed to solenoid coil. The coil draws a current of ~ 500 mA rated at 24 V DC and 12 W power. Current to the valve is supplied from the controller of the pulsed valve through vacuum feed-throughs. The normal temperature range of working the valve is ranging from -40°C to 200°C . However, our experiments are done in gas medium at room temperature. The Teflon poppet at the end of the actuator rod opens and closes the nozzle orifice. The buffer spring supplied with the actuator-poppet assembly properly controls to and fro motion of the actuator. The valve can be pulsed at any frequency up to 120 Hz, though our experiments were carried out at 2 Hz which is the repetition rate of the laser pulses. The intensity and duration of the gas pulse can also be varied by controlling the current to the coils. This is achieved by using pulse driver unit. Pulse duration ranges in microseconds, milliseconds or minutes can be selected in pulse valve driver. However, for our experiments, typical opening time is set to be $350\ \mu\text{s}$ - $400\ \mu\text{s}$ and pulsed at 2 Hz (the repetition rate laser pulse). Moreover, the driver is able to trigger the pulse valve externally as well as internally depending on the experimental conditions. In general, the pulse valve driver is triggered externally and synchronized with the laser pulse. For synchronisation of these two pulses a delay generator is used and the details are described in section 2.5.

The nozzle is connected to the sample holder (placed outside the vacuum system) via ¼ inch copper tubing. The samples in the present experiments were used as such, without further purification, except for few freeze-pump-thaw cycles. The vapours of a room temperature sample placed inside the sample holder were transported to the nozzle by bubbling inert carrier gas through the sample. The nozzle introduces the sample seeded in inert carrier gas via supersonic expansion. The molecular beam so produced is skimmed at a distance of 3 cm from the nozzle, prior to entering the ionisation chamber. The distance between nozzle and ionisation spot is 22 cm.

By varying the supersonic expansion conditions, it is possible to produce atomic and molecular clusters of different average sizes.⁷⁷ Cluster size depends on three body collision and the rate of three body collision (Z_3) is expressed as-

$$Z_3 \propto P_0^2 d / T_0^2 \quad (2.1)$$

Where P_0 is stagnation pressure, d is nozzle diameter and T_0 is stagnation temperature. Thus, cluster formation is facilitated by using large diameter (d) nozzles and high backup pressures (P_0). Stagnation temperature was kept at ~300 K (room temp.) during the experiments.

2.4 The laser system

During the study of laser-cluster interaction, two types of laser are used. First one is a pulsed dye laser (Quantel, TDL-70) which is pumped by another pulsed Nd:YAG laser (Quantel, Model YG 980 E) which operates at 20 Hz repetition rate and provides ~ 9 ns laser pulses with maximum laser energy output of 650 mJ at 1064 nm. The second one is also a Nd:YAG (Quanta system, GIANT G790-10) laser with slightly different specifications. It operates at 10 Hz repetition rate and provides ~ 9 ns laser pulses with maximum laser energy output of ~ 1200 mJ at 1064 nm. In

most of the experiments, second laser system is used with its output ranging from IR to UV region. A brief description of the dye laser and Nd:YAG laser is given below.

The dye laser (Quantel, TDL-70) output has wavelength tunability from 220 nm to 750 nm and is provided with automatic tracking facility for the doubling and mixing crystals. Dye lasers are fundamentally different from the other commonly available lasers because of its tunable facility over a limited wavelength region. The fluorescence emission of the organic dyes is used as a broad band output of the lasers. In our studies, the dye laser is pumped by the second harmonic of the Nd:YAG laser (532 nm). The dye used in our studies is Rhodamine-6G with conversion efficiency of 22%. This dye provides laser output in the wavelength region 552-580 nm ($\lambda_{max}= 564$ nm) regions. Since the fluorescence emission of the organic dye is usually very broad, a high resolution grazing incidence grating coupled with rotating mirror is used to tune the dye laser output over a wide range of wavelengths with narrow linewidth. This grazing incidence grating - rotating mirror assembly forms an integral part of the oscillator system.

The Nd:YAG laser is a four level laser system. Its gain medium consists of Nd^{3+} ions doped at low concentration in Yttrium Aluminum Garnet (YAG). Population inversion results from pumping a majority of the Nd^{3+} ions into an excited state by using intense flash lamp, followed by a radiationless transition to another excited state (${}^4\text{F}_{3/2}$), which acts as the upper laser level. The radiative transition from ${}^4\text{F}_{3/2} \rightarrow {}^4\text{I}_{11/2}$ then leads to laser emission at 1064 nm. Subsequently, the collisional decay from ${}^4\text{I}_{11/2}$ level causes the repopulation of the ground state.⁷⁸

The Nd:YAG laser is provided with frequency doubling, tripling and quadruple options for generation of 532, 355 and 266 nm from the fundamental (1064 nm) of the Nd:YAG laser. The conversion efficiencies for generation of these higher

harmonics from the fundamental wavelength are approximately ~50%, 25% and 10% respectively. The pulse profile of these harmonics is similar to that of the fundamental laser. In most of our studies we have utilised the higher order harmonics of Nd:YAG laser.

2.4.1 Characterization of the laser pulse

The pulse width of the laser beam was measured using a photodiode with fast rise time. The experimentally measured temporal profile of the laser pulse is shown in figure 2.3. The FWHM (Full Width at Half Maxima) of the pulse is ~ 9 ns (τ_{pulse}). The optical power of the laser pulse was measured using a pyroelectric detector. Thus, by knowing the pulse width and the laser power it is possible to calculate the laser intensity at the focal point in the ionisation region provided we know the radius of the focal spot. The radius W_0 of the focal spot can be calculated from the relationship⁷⁹-

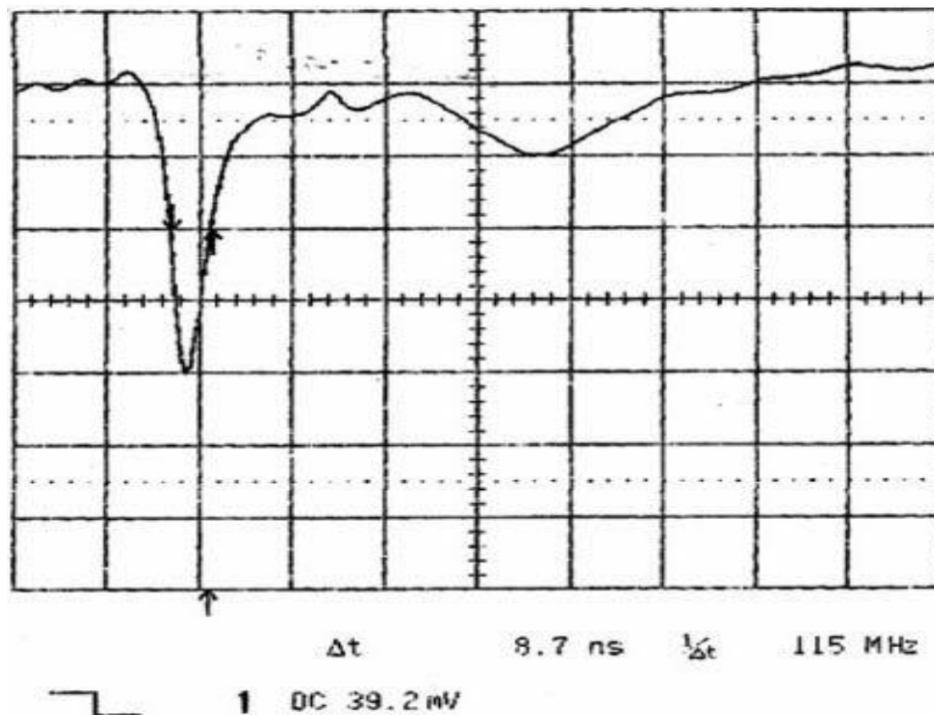


Figure 2.3: Temporal profile of the Nd:YAG laser pulse, measured using a fast photodiode

$$W_0 = \frac{f\lambda}{\pi r} \quad (2.2)$$

Where λ is the wavelength of the laser light, r is the radius of the laser beam on the lens of focal length f . By knowing these three parameters, the peak intensity of the laser pulse can be calculated using the expression-

$$I_{peak} = \frac{E}{\pi W_0^2 \tau_{pulse}} \quad (2.3)$$

Where E is the energy of the laser pulse in Joules. In our studies a plano-convex lens has been used having a focal length 35 cm, while the diameter of the laser beam waist is ~ 9 mm.

2.4.2 Pyroelectric laser power meter

Optical power of the laser pulse is measured using a Gentec make detector (PSV 3103 model) which works based on the pyroelectric property of the material. Pyroelectricity is the ability of materials to generate a temporary voltage when they are heated by external means like laser pulse.⁸⁰ The change in temperature modifies the positions of the atoms slightly within the crystal structure, such that the polarization of the material changes. The polarization change gives rise to a voltage across the crystal. Thus, voltage change is calibrated with the power falling on material and the value is displayed in power meter.

The laser power meter has two components i.e. (a) power meter display and (b) the thermopile probe. The laser power meter display is an analogue meter where 9 V battery is used for power supply. Moreover, it has an option for zero adjustment of the meter which removes the ambient thermal condition. The power range can be adjusted from 1 mW to 10 kW using the range selector. The second component is the thermopile probe which has a spectral range of 0.25-3 μm with maximum power of 10 W. The resolution of the probe is 1 mW and the power can be measured with ± 3 % accuracy.

2.5 Synchronization of laser and molecular beam

As stated earlier, since laser beam and the cluster beam both are pulsed, it is essential to synchronize these two beams spatially as well as temporally at the centre of the repeller and extractor grid before carrying out experiment. Moreover, the exact time of laser-cluster interaction ($t = 0$) is also necessary for precise mass calibration of time-of-flight mass spectra.

In order to achieve the time synchronization, both the beams (laser beam and molecular beam) are triggered by external TTL pulse produced from a digital delay generator. The digital delay generator can provide four precisely timed logic TTL output signals, with selectable time reference. This selectable time reference allows the timing of these channels to be slaved to another channel. Thus, upon internally triggering the delay generator, the time delay between these output signals can be easily varied. In our study, one of the output TTL signal was used to trigger the pulsed valve, while the second output TTL signal was used to trigger the laser system. The synchronization of the molecular beam and the laser pulse is attained by varying the relative delay between the triggering of the pulsed valve and the laser system.

For optimising synchronization of the laser and gas pulse, we monitored signal intensity of ions generated upon photoionisation of C_2H_5Br molecule at 532 nm as a function of delay at 2 atm helium backup pressures. Figure 2.4 shows the total ion signal i.e area under the total time-of-flight mass spectra as a function of delay time. As can be seen from the graph, integrated ion signal of all ions reaches maximum at $\sim 1400 \mu s$ delay. This is the delay time at which laser pulse interacts with the cluster region and two adjacent regions depict the less clustered or the monomer dominated region. Here, it is worth noting that, for 300 μs set value of the electrical opening of pulsed valve, the FWHM of actual gas pulse is $\sim 416 \mu s$.

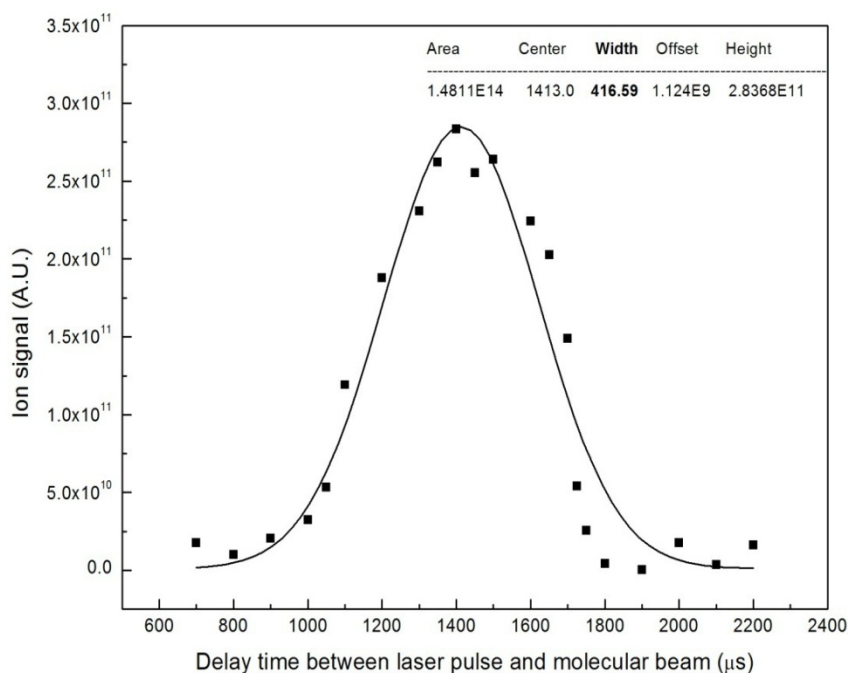


Figure 2.4: Plot of integrated ion signal as a function of delay time for synchronization of laser and gas pulse

2.6 The time-of-flight mass spectrometer

The time-of-flight mass spectrometer consists of ion optics and the detector. The ions produced in the laser-cluster interaction volume are guided to the flight tube using suitable potentials to different components of the ion optics. Details of the ion optics assembly are described in section 2.6.1. The ions are detected using channel electron multiplier detector and the working principle of the detector is explained in section 2.6.2. For detection of ions in the time-of-flight mass spectrometer, stable high voltage power supplies are required and the specifications of power supplies are given in 2.6.3. Calibration of the time-of-flight mass spectrometer is described in section 2.6.4.

2.6.1 Ion-optics assembly

The ion optics assembly is made out of Perspex material and includes repeller, extractor and acceleration grids sandwiched between circular perspex rings having an

opening of 20 *mm*. The repeller, extraction and acceleration grids are made of a stainless steel wire mesh (mesh size was 25 lines per inch and 0.2 *mm* thickness). The distance between the repeller and extractor grids is 20 *mm*, while the distance between the extractor and acceleration grid is 10 *mm*. The perspex ring between the repeller and extractor grids is provided with two additional hollow channels which run orthogonal to each other and intersect at the center of the ionisation region. These two hollow orthogonal openings are used to deliver the molecular beam and the laser pulse to the ionisation region, while the third channel (clear aperture of the Perspex ring) which is coaxial with the time-of-flight axis is used for repelling the ions towards the detector at the end of the flight tube. The ion optics is also provided with two pairs of deflection plates for the horizontal and vertical directions respectively, along with an Einzel lens assembly for guiding the ion beam along the axis of the flight tube so as to reach the detector, thereby increasing the signal intensity. This ion optics unit is assembled outside and then mounted inside the ionisation chamber in such a way that the axis of the ion optics assembly coincides with the axis of the flight tube. While mounting, care was taken to ensure that the ionisation spot (point of interaction of the molecular beam and the laser beam) lies close to the center, between the repeller and the extraction grids. The optimised ion optics of the time-of-flight mass spectrometer is shown in figure 2.5 while the actual photograph is depicted in figure 2.6.

For detection of positive ions, typical DC voltages applied on the grids were +2900 V, +2000 V and ground potential for the repeller, extractor respectively. The acceleration grid is grounded. Two different high voltage DC power supplies (ECIL, Model-HV4800E) having common ground was used for applying the voltages to the grids.

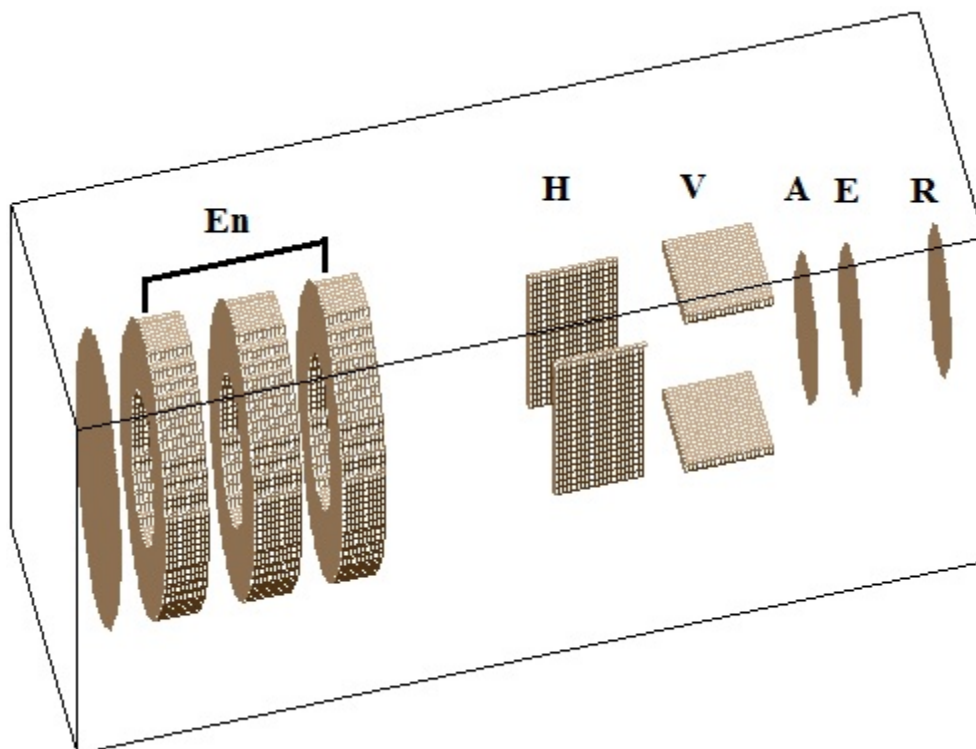


Figure 2.5: Ion optics of time-of-flight mass spectrometer optimized using SIMION 8.0⁸¹ where R, E, A, V, H and En represents repeller, extractor, accelerator, vertical, horizontal and einzel lens respectively

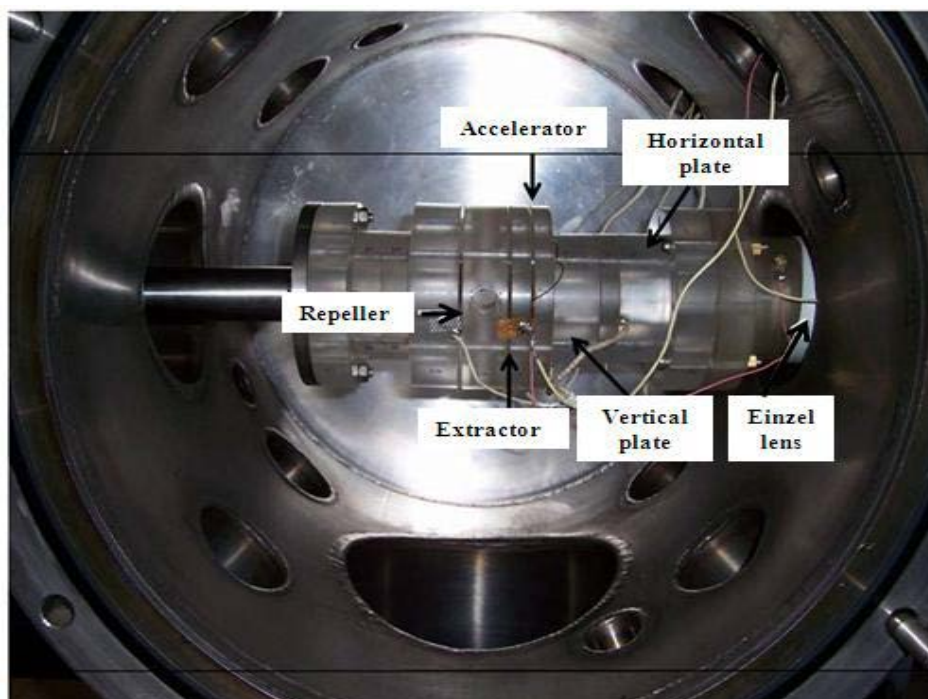


Figure 2.6: Photograph of ion optics assembly of the mass spectrometer mounted in ionisation chamber. Different components of the ion-optics assembly are labelled in the diagram.

An additional stainless steel wire mesh is mounted at the end of the flight tube and just before the detector. The acceleration grid and this mesh are given common ground to ensure that the drift region (flight tube) is free from any electrical field along the ion path. Also it provides the necessary acceleration to the positive ions from the end of the drift region to the detector surface.

2.6.2 The detector

The ions produced as a result of laser ionisation and accelerated along the time-of-flight axis are detected using a channel electron multiplier detector (CEM). This detector is generally fabricated from a lead silicate glass and reduced in a hydrogen furnace to produce semiconducting lead on the inner channel of the detector, which acts as secondary electron emissive surface.⁸² These CEM are durable and efficient detector for ions (positive and negative) as well as electrons and photons. Further, these detectors offer several advantages like, high electron gain, low background noise, small physical size and simplicity of use.

When a potential is applied between the input and output end of the detector, its resistive surface forms a continuous dynode, which has the property of emitting secondary electrons when primary particles are impinged upon it (see figure 2.7). Thus, when an ion strikes the input face of the detector, it typically produces 2-3

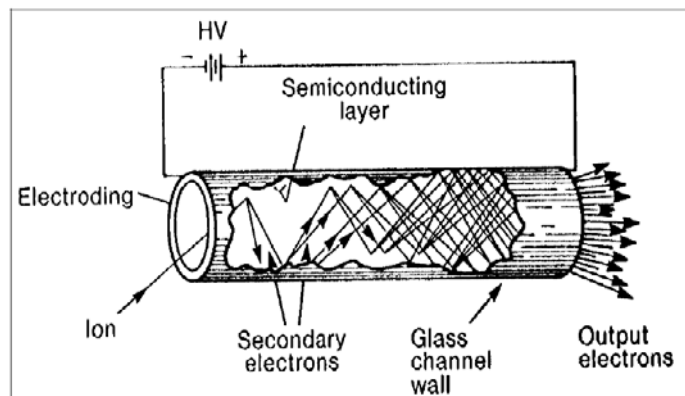


Figure 2.7: An illustration showing secondary electron emission from a continuous dynode when ions strike the semiconducting surface.

secondary electrons. These 2-3 secondary electrons are further accelerated down the channel by a positive bias and in turn strike the channel wall, producing additional electrons (and so on) until, at the output end a pulse of 10^7 to 10^8 electrons emerges. For detection of positive ions, the input is generally at a negative potential of 1900 to 3000 volts and the output is at ground.

2.6.3 High voltage DC power supplies

The performance of time-of-flight mass spectrometer crucially depends on the stability of high voltage power supply units used for applying DC voltages to the ion-optics assembly and detector system of the time-of-flight mass spectrometer. A small ripple in the voltages can significantly reduce the resolution of the mass spectrometer by broadening the peaks. Simultaneously, this can also strongly affect the reproducibility of the TOFMS instrument. To avoid such instrumental errors, we have used five high voltage power supplies, which have low noise and provide highly stable regulated DC output voltages. The power supplies were procured from Electronics Corporation of India Limited (ECIL, Model-HV4800E) with an output stability of ± 2 V (over 1 hour) and an output ripple of 30 mV (peak to peak). Two of these power supplies were used to apply voltages to the repeller and extraction grids while two other power supplies were used for applying voltages to the auxiliary ion-optics i.e. horizontal/vertical deflection plates and Einzel lens. The other high voltage unit is used for the detector.

2.6.4 Calibration of the TOFMS

The mass calibration of the TOFMS instrument was carried out using benzene as the reference. It has been reported that benzene molecule exhibits several sharp (2+1) REMPI transitions in the wavelength region of 365-265 nm. In our experiments, the effusive molecular beam of benzene is multiphoton ionised using the

frequency doubled output of the Nd:YAG pumped (532 nm) dye laser in the 280- 286 nm wavelength region. Upon scanning the dye laser output, we observed that at 284.1 nm a strong ion peak was observed in the time-of-flight spectra, which deteriorates when the wavelength was red/blue shifted by ~ 2 nm. Previously, Grant and co-workers have assigned this strong ion peak at 284.1 nm to (2+1) REMPI signal of $C_6H_6^+$ (at $m/z = 78$).⁸³ Thus, the time of arrival of $C_6H_6^+$ ion at 284.1 nm is used for mass calibration of time-of-flight data.

Figure 2.8 shows the time-of-flight mass spectrum of ethyl bromide monomer at 532 nm laser pulses. Bromine containing peaks are observed in pair in the mass spectra because of two isotopes m/z 79, 81 of similar natural abundance.

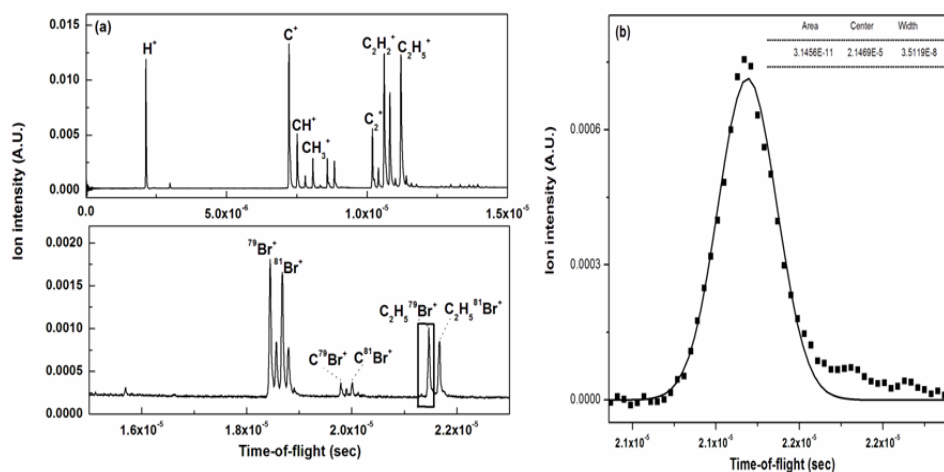


Figure 2.8: (a) Time-of-flight spectra of ethyl bromide monomer recorded at 532 nm. (b) The expanded portion of the spectra corresponding to $C_2H_5^{79}Br^+$ ion (marked portion) is shown along with Gaussian fit for calculating the FWHM of the ion peak.

To calculate the mass resolution of our instrument, the FWHM (Full Width at Half Maxima) for the highest ion peak i.e. $C_2H_5^{79}Br^+$ ($m/z = 108$) ion is calculated using Gaussian fitting of the peak. From the figure 2.10 (b), the arrival time of the ion is 21.47 μs while the FWHM is 35.12 ns. Thus using equation 1.9, the resolution of the instrument is found to be ~ 300 .

$$R = \frac{t}{2\Delta t} = \frac{21.47 \times 10^{-6}}{2 \times 35.12 \times 10^{-9}} \approx 306$$

Chapter 3

Photochemistry of dibromo difluoro methane (CF₂Br₂) monomer and cluster under gigawatt intense laser field

3.1 Introduction

Investigation of halomethanes has received wide attention during recent years, not only due to their important applications in industry and agriculture as refrigerants, flame retardants, aerosols and pesticides, but also due to their impact on atmospheric chemistry. Dibromodifluoromethane [CF₂Br₂ (Halon 1202)] is one such mixed halomethane which has profound implication on atmospheric chemistry because of its high ozone depletion potential [ODP=0.4]. Photolysis of CF₂Br₂ was first reported in 1960 by Mann and Thrush,⁸⁴ using the technique of flash photolysis. They detected CF₂ by optical absorption during the flash photolysis of CF₂Br₂. Based on the observation, it was suggested that the primary dissociation pathway for CF₂Br₂ was molecular elimination of Br₂. While, Walton postulated atomic elimination pathway i.e. dissociation of CF₂Br₂ → CF₂Br + Br to be the major dissociation channel, based on studies carried out upon photo excitation at 265 nm.⁸⁵ In another set of experiments Krajnovich *et al.*⁸⁶ detected CF₂Br⁺ and Br⁺ ions using time-of-flight mass spectrometer as a result of irradiation using 248 nm laser pulses with molecular beam of CF₂Br₂ without detectable molecular elimination channel. This result further supported the dissociation pathway proposed by Walton. In addition, low concentrations of CF⁺ and CF₂⁺ ions were observed in the time-of-flight mass spectrometric studies, which arise due to secondary photo-dissociation of the CF₂Br radical. Time resolved absorption spectra were recorded by Gosnell *et al.*⁸⁷ for photo

dissociated CF_2Br_2 at 248 nm. The major products were found to be CF_2Br and Br indicating the atomic elimination channel. Moreover, based on transient absorption spectra in pulsed CO_2 laser photo-dissociation studies, Vatsa *et al.*⁸⁸ also identified bromine atom elimination channel to be the major dissociation channel for CF_2Br_2 . These authors also reported absorption cross section of CF_2Br radical in the wavelength region of 220-320 nm. van Hoeymissen *et al.*⁸⁹ derived the absorption cross-section of CF_2Br and showed (30±10)% of the primary CF_2Br dissociated spontaneously into $\text{CF}_2 + \text{Br}$ via multi-photon dissociation at 248 nm. Thus, these studies reveal the primary dissociation channel of CF_2Br_2 monomer under the influence of laser pulse. However, the secondary photoproducts are also studied in different experimental conditions. Cameron *et al.*⁹⁰ demonstrate energetics of nascent CF_2 which is produced due to dissociation of CF_2Br_2 in the wavelength range 223-260 nm. Subsequently, Park *et al.*⁹¹ established avoided curve crossing of A_1 and B_1 state in photo dissociation study of CF_2Br_2 at 234 nm and 265 nm using a two-dimensional photo fragment ion imaging technique. Hsu *et al.*⁹² studied Br_2 elimination channel at 248 nm using cavity ring-down absorption spectroscopy.

Though there are large number of reports⁸⁴⁻⁹² dealing with photochemistry of CF_2Br_2 monomer, there is no report on photochemistry of CF_2Br_2 clusters. Thus, present studies were carried out with an aim to understand how degree of aggregation in CF_2Br_2 clusters alters the electronic properties of the system, as well as its photochemical behaviour with respect to its monomer counterpart. Such studies are essential for understanding influence of solvation on reaction dynamics of the molecular species and also for identifying different photo dissociation pathways. In the present study, photo dissociation/ ionisation of CF_2Br_2 monomer and cluster has been studied at 266 nm, 355 nm and 532 nm, using laser pulses of intensity $\sim 10^9$

W/cm^2 . At 266 nm, additional reaction channel is observed in CF_2Br_2 cluster which is otherwise absent in case of monomer studies. Moreover, at 355 and 532 nm, multiply charged atomic ions of carbon, fluorine and bromine have been observed. Generation of energetic multiply charged atomic ions has been ascribed to Coulomb explosion of highly charged cluster. Possible mechanism of generation of multiply charged atomic ions from CF_2Br_2 clusters is explained based on the available literature.

3.2 Experimental details

Details of the experimental setup have been described in Chapter 2. Only information relevant to dibromo difluoro methane (CF_2Br_2) sample is given here. CF_2Br_2 is not a hazardous chemical however it has very high vapour pressure (~ 724 mm of Hg at 25°C ⁹³). Thus, special care has been taken during transfer of CF_2Br_2 to the sample holder.

3.3 Results and Discussion

3.3.1 Multiphoton dissociation/ ionisation of CF_2Br_2 monomer at different wavelengths

Figure 3.1, 3.2 and 3.3 show time-of-flight mass spectra obtained upon interaction of CF_2Br_2 monomer at 266 nm, 355 nm and 532 nm respectively with laser pulses of intensity $\sim 10^9 \text{ W}/\text{cm}^2$. At 266 nm, the major ion signals at $m/z = 12, 31, 50, 79$ and 81 were assigned to $\text{C}^+, \text{CF}^+, \text{CF}_2^+, {}^{79}\text{Br}^+$ and ${}^{81}\text{Br}^+$ respectively. At 355 nm and 532 nm, ion peaks due to $\text{C}^+, \text{F}^+, \text{CF}^+, \text{CF}_2^+, \text{Br}^+$ and CF_2Br^+ were observed however relative ion intensity were different at these two wavelengths. Since no molecular ion signal was observed in the time-of-flight mass spectra at any of these wavelengths, it was inferred that CF_2Br_2 exhibits ladder switching mechanism i.e. undergoes dissociation followed by ionisation. In order to understand the fragmentation mechanism of CF_2Br_2 monomer at different wavelengths, various dissociation channels were investigated. Following three dissociation channels are

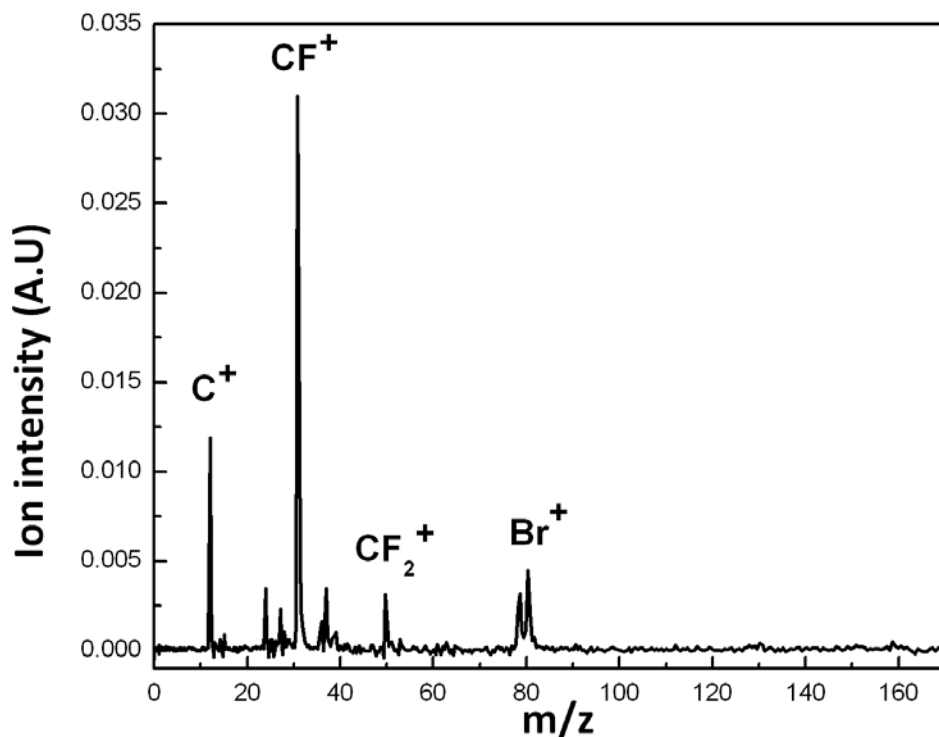


Figure 3.1: Time-of-flight mass spectrum of CF_2Br_2 monomer at 266 nm under laser intensity of $\sim 10^9 \text{ W/cm}^2$.

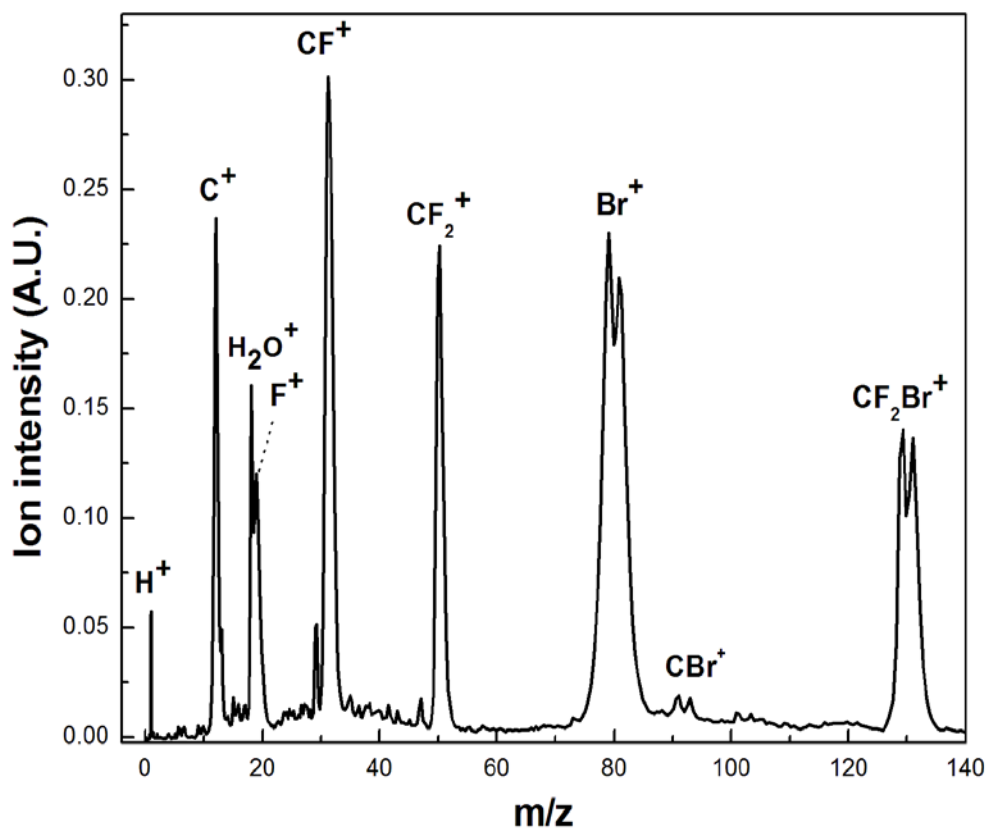
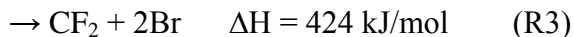
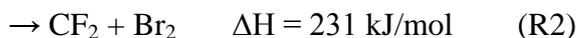


Figure 3.2: Time-of-flight mass spectrum of CF_2Br_2 monomer at 355 nm under laser intensity of $\sim 10^9 \text{ W/cm}^2$.

reported in literature with corresponding enthalpy value ⁹⁰ -



The CF_2Br radical formed through R1 can undergo further photo-dissociation (R4) or unimolecular decay of internally hot radicals (R5).

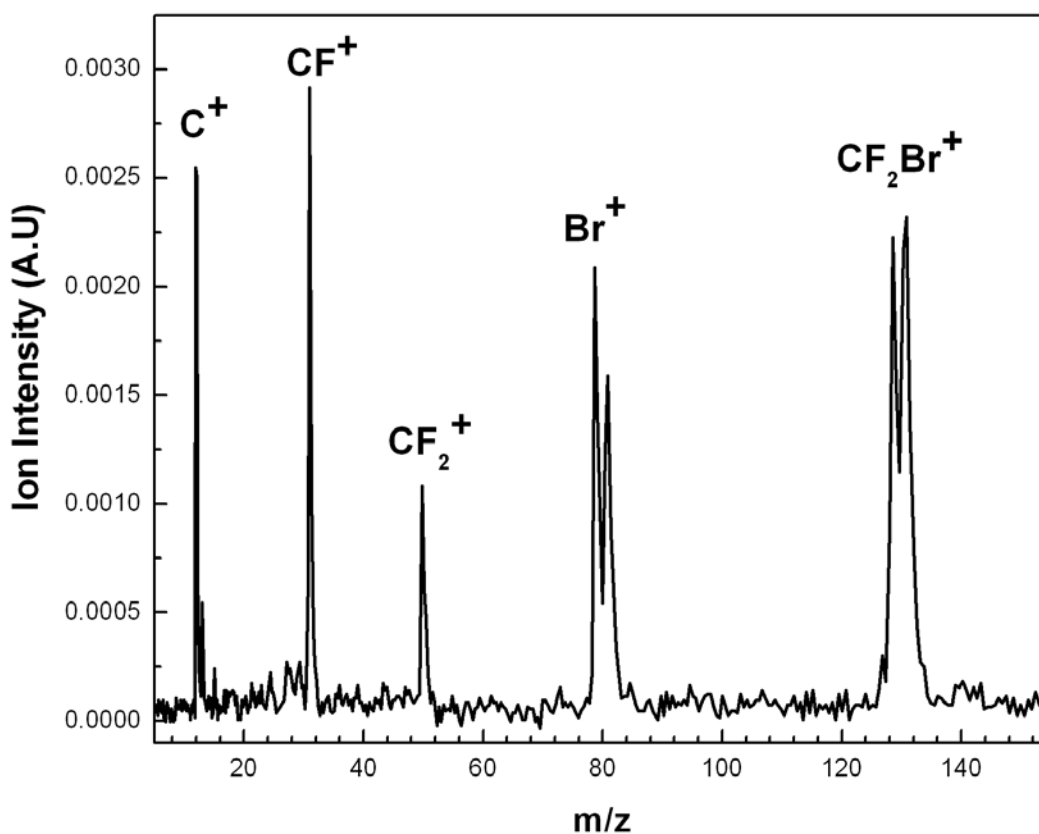


Figure 3.3: Time-of-flight mass spectrum of CF_2Br_2 monomer at 532 nm under laser intensity of $\sim 10^9 \text{ W/cm}^2$.

There is still a controversy in the literature about the primary dissociation channel of CF_2Br_2 . Most of the literature ⁸⁴⁻⁹² deals with of A-band excitation of CF_2Br_2 molecule, which spans from 200 nm to 310 nm with an absorption maximum

at 228 nm. The transition at 266 nm which lies at red edge of the A-band, is expected to originate mainly from $B_1 \leftarrow X$ transition upon excitation of CF_2Br_2 .⁹¹ In the present study, based on time-of-flight mass spectrum at 266 nm, formation of molecular bromine (Br_2) was not observed, thus R2 dissociation channel can be ruled out. Moreover, for R3 dissociation channel, Cameron *et al.*⁹⁰ showed threshold wavelength was at or below 260 nm ($\sim 38450 \text{ cm}^{-1}$) where molecule has sufficient excitation energy to form CF_2 and two atomic Br fragments. Thus, above 260 nm, the primary dissociation channel of CF_2Br_2 is dissociation via R1 channel to form CF_2Br radical and atomic bromine. CF_2Br_2 undergoes dissociation upon absorption ($\sigma_{266 \text{ nm}}^{CF_2Br_2} \sim 7.4 \times 10^{-20} \text{ cm}^2 \text{ molecule}^{-1}$)⁹⁴ of 266 nm photon to form CF_2Br and Br radical. However, no ion signal corresponding to CF_2Br^+ was observed in the mass spectrum which suggests dominance of secondary dissociation process at this wavelength. Thus, CF_2Br radical formed via R1 photo dissociation channel, dissociates ($\sigma_{266 \text{ nm}}^{CF_2Br} \sim 2 \times 10^{-18} \text{ cm}^2 \text{ molecule}^{-1}$)⁸⁸ into CF_2 and Br radical (R4). Ions of CF_2 (IE: 11.44 eV) and Br (IE: 11.81 eV) are produced due to multi-photon ionisation of respective radicals. However, CF_2 radical has good absorption in UV region with maximum at 249 nm ($2.91 \times 10^{-17} \text{ cm}^2 \text{ molecule}^{-1}$)⁹⁵. Thus, at 266 nm, CF_2 further absorbs ($\sigma_{266 \text{ nm}}^{CF_2} \sim 2 \times 10^{-18} \text{ cm}^2 \text{ molecule}^{-1}$) photon to dissociate and form CF radical. CF undergoes multi-photon ionisation to form CF^+ (IE: 9.11 eV) and it is detected as the most abundant ion peak in the mass spectra. Earlier, Park *et al.*⁹¹ showed similar fragmentation pattern in CF_2Br_2 monomer at ~ 265 nm laser pulses where Br (264.9 nm) and Br^* (264.8 nm) were produced due to (2+1) resonance absorption and other fragments were generated due to non-resonant absorption. They have also proposed that the primary dissociation channel at 265 nm was generation of CF_2Br and Br radical (mechanism (R1)) due to absorption of single photon.

At 355 nm and 532 nm, similar fragmentation was observed in the mass spectra with CF^+ as most abundant ion peak. Primary dissociation of CF_2Br_2 molecule leads to generation of CF_2Br radical (R1) which subsequently undergoes ionisation via multi-photon process. Moreover, at 355 nm, CF_2Br^+ shows laser energy dependent secondary dissociation (Figure 3.4). When laser energy was 0.6 mJ/pulse, ion yield of Br^+ was less compared to CF_2Br^+ whereas increasing laser energy to 1.5 mJ/pulse leads to enhancement in the Br^+ ion signal and ion intensity was comparable to CF_2Br^+ ion signal. Further, increase in the laser energy increases Br^+ ion yield above CF_2Br^+ . Thus, CF_2Br^+ undergoes secondary dissociation to Br^+ and CF_2 radical with increase in laser energy and the dissociation channel saturates above laser energy of ~ 1.5 mJ/pulse.

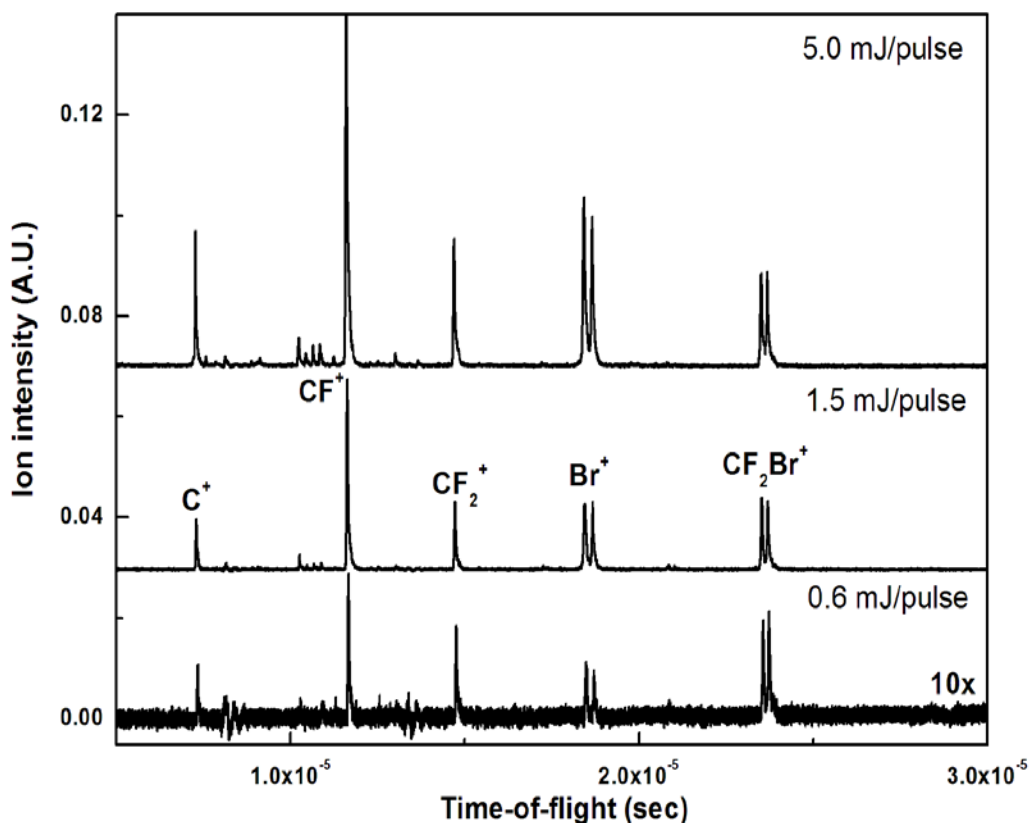
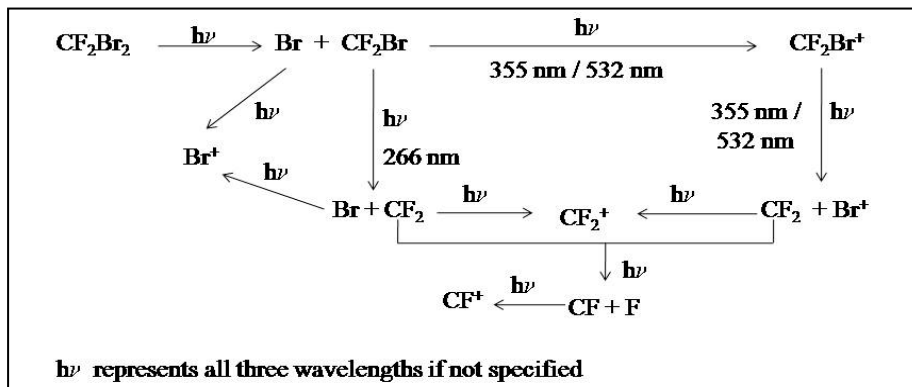


Figure 3.4: Time-of-flight mass spectra of CF_2Br_2 monomer at 355 nm as a function of laser energy.

Thus, based on our experimental observations at different wavelength probable scheme of dissociation/ ionisation of CF_2Br_2 monomer has been shown below-



3.3.2 Ionisation of CF_2Br_2 clusters at different wavelengths

Figure 3.5 represents time-of-flight mass spectrum of CF_2Br_2 clusters at 266 nm under laser intensity $\sim 10^9 \text{ W/cm}^2$. From the spectrum, it is evident that apart from ion signals observed in monomer spectrum, CF_2Br^+ and Br_2^+ ions were observed for CF_2Br_2 clusters at 266 nm. Generation of CF_2Br^+ and Br_2^+ is due to cluster ionization. This was further confirmed by changing the delay between the laser pulse and gas pulse (Figure 3.6). When laser pulse interacted with the cluster region of the gas pulse, CF_2Br^+ and Br_2^+ were formed along with other ions and the ion yield varies with the extent of clustering in the gas pulse. However, no ion signal due to CF_2Br^+ and Br_2^+ was observed when CF_2Br_2 monomer interacts with laser light at 266 nm. For comparison purpose, CF^+ ion signal was plotted in figure 3.6 since it is the most abundant peak in both monomer and cluster spectra at 266 nm. Thus, CF_2Br^+ and Br_2^+ ions were produced from the cluster region and intra-cluster reaction is responsible for generation of these two ions. Generation of CF_2Br^+ ion peak can be attributed due to stabilization of the ion as a result of cluster solvation. Formation of Br_2^+ has also been attributed to stabilization of the ion as a result of cluster solvation. Formation of Br_2^+ has been discussed in detail in the next section.

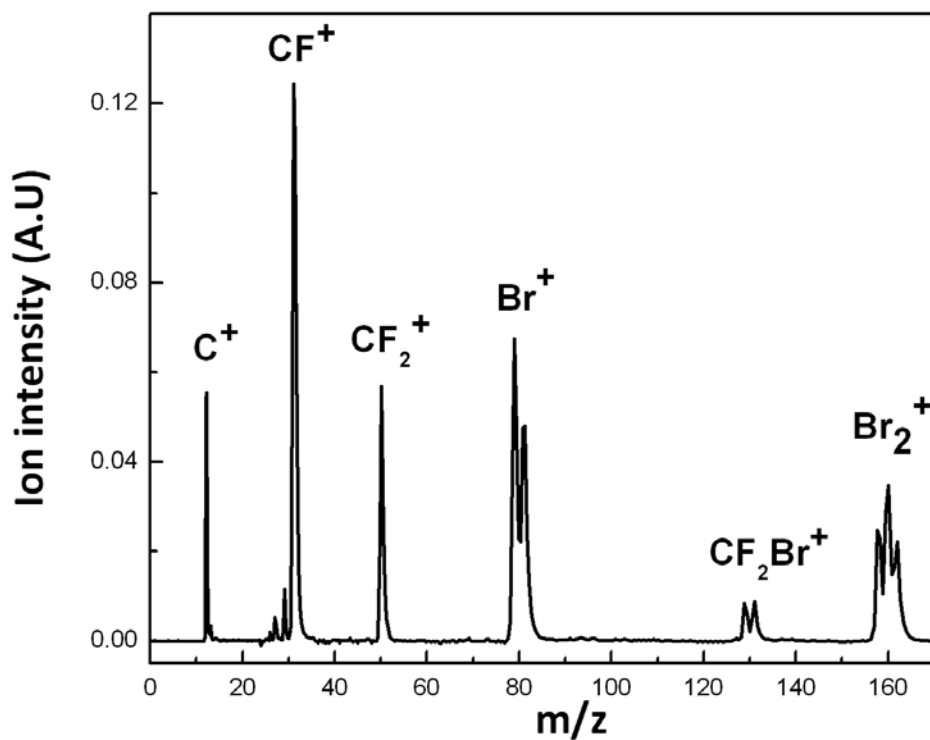


Figure 3.5: Time-of-flight mass spectrum of CF_2Br_2 clusters ionised at 266 nm using laser intensity of $\sim 10^9$ W/cm²

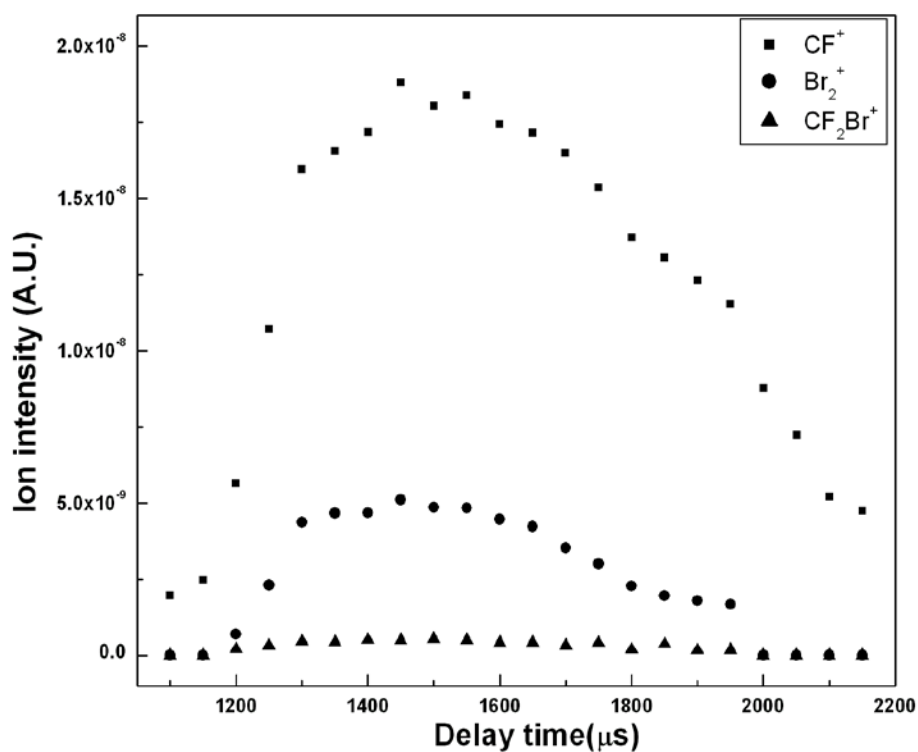


Figure 3.6: Ion intensity of CF^+ , Br_2^+ and CF_2Br^+ as a function of delay between laser and gas pulse at 266 nm

There are ample reports⁹⁶⁻¹⁰¹ on formation of molecular halogen (X_2) in halo-methane clusters under influence of laser pulses with varying pulse duration (ns, ps or fs). X_2^+ can be produced either (a) by the formation of a neutral X_2 molecule via intracluster chemistry, followed by its ionisation or (b) by direct concerted elimination of the X_2^+ ion from ionized clusters.

Sapers *et al.*⁹⁶ first reported the formation of molecular iodide ion from the interaction of methyl iodide clusters $[(CH_3I)_n]$ with ns pulses and supported mechanism (a). Therefore, ionic signal of I_2 was attributed due to the ionisation of the neutral dimer molecule which is produced via sequential dissociation of the two C-I bond of monomers. Using picoseconds laser pulses of 266 nm and 532 nm, Syage *et al.*⁹⁷ also showed formation of I_2^+ from methyl iodide cluster and the origin of I_2^+ formation is attributed due to the multiphoton ionisation of the neutral molecular halogen. Further, Choi *et al.*⁹⁸ ascribed the formation of I_2^+ , from methyl iodide clusters irradiated at 266 and 355 nm with ns laser pulses, to intracluster photochemistry within the neutral manifold and reinforce mechanism (a) for generation of molecular halogen ion. However, Fan *et al.*⁹⁹ investigated alkyl halide clusters using ns laser pulses and laser-induced fluorescence as detection method. They concluded that molecular halogen ion was produced directly from the ionic precursor. Similarly, Vidma *et al.*¹⁰⁰ have argued in favor of mechanism (b) in which photo dissociation of the ionized dimer is the most probable precursor for the formation of I_2^+ . Lockman *et al.*¹⁰¹ also reported formation of I_2^+ from CF_3I clusters and supported (b) mechanism in which photochemical reaction takes place within the cluster environment after multiphoton ionisation. Thus, formation of X_2^+ from molecular cluster is still controversial and there is no definitive explanation which can resolve the issue. Recently, Kosmidis and coworkers¹⁰² performed extensive studies

on different alkyl halide clusters using ps and fs laser pulses which help in understanding the mechanism of formation of molecular halogen. Based on these studies, photochemical reactions are responsible for molecular halogen formation in the ionic manifold. Moreover, dimer of alkyl halide in Head-to-Head (H-H) geometry is preferable over Head-to-Tail (H-T) configuration because of close proximity of the two halogen atoms.¹⁰³ Thus, in H-H configuration of the ionized dimer, two centered three electron (2c, 3e) bond was postulated between the two halogen atoms. This (2c, 3e) bond is responsible for generation of X_2^+ . In case of CF_2Br_2 clusters, no experimental and theoretical work is available in literature. However, in our earlier studies, Br_2^+ was observed in the time-of-flight mass spectra due to interaction of ethyl bromide cluster with ns laser pulses at 266 nm.¹⁰⁴ Based on fluorescence studies by Fan *et al.*,⁹⁹ it was inferred that molecular cluster does not generate neutral Br_2 , however concerted photochemical reaction was responsible in ionic manifold. Thus, Br_2^+ generated from CF_2Br_2 clusters could be due to direct concerted elimination from the ionized cluster ((b) mechanism) and (2c, 3e) bond may be responsible for the photochemical reaction.

At 355 nm, time-of-flight mass spectrum of CF_2Br_2 clusters revealed some unusual peaks due to C^{2+} , F^{2+} and Br^{2+} apart from singly charged dissociated fragments. Generation of multiply charged atomic ions at such low laser intensity is quite interesting. Further, at 532 nm, the charge state of carbon, fluorine and bromine ion increases up to +4, +4 and +5 respectively under similar experimental conditions. Thus, multiply charged atomic ions were observed upon interaction of CF_2Br_2 cluster with nanosecond laser pulses of intensity $\sim 10^9$ W/cm² and the charge state of atomic ions of carbon, fluorine and bromine increases with increasing wavelength. In order to explain the observation at 355 nm and 532 nm, a probable mechanism has been

described based on available literature in the subsequent section.

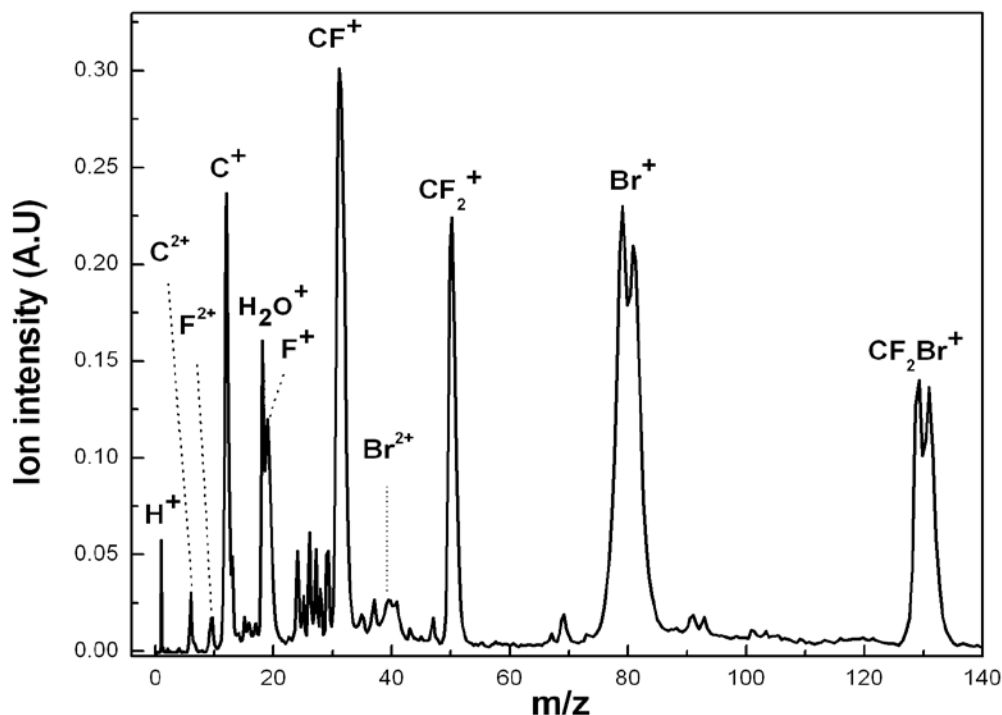


Figure 3.7: Time-of-flight mass spectrum of CF_2Br_2 clusters at 355 nm under laser intensity of $\sim 10^9 W/cm^2$

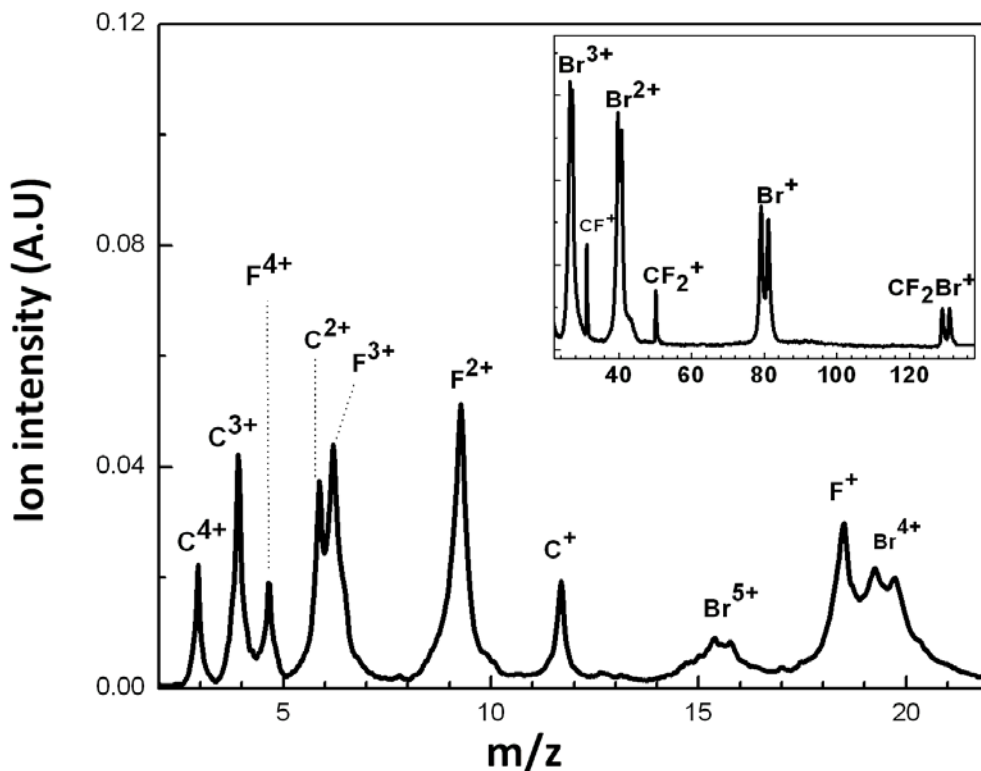


Figure 3.8: Time-of-flight mass spectra of CF_2Br_2 clusters at 532 nm under laser intensity of $\sim 10^9 W/cm^2$

3.3.3 Probable mechanism of multiply charged atomic ion formation in clusters

In order to understand the mechanism of formation of multiply charged ions, primary ionisation process occurring under gigawatt intense laser field is considered. Multiphoton ionisation is expected to be dominant process at a laser intensity $\sim 10^9$ W/cm². To distinguish between these two ionisation processes, Keldysh parameter is calculated for the ionization of CF₂Br₂ molecule. Keldysh parameter is expressed as-

$$\gamma = \sqrt{\frac{I_p}{2U_p}} \quad (3.1)$$

where I_p is ionisation potential of CF₂Br₂ molecule and U_p is ponderomotive energy expressed in eV. Ponderomotive energy (U_p) is expressed as-

$$U_p \text{ (eV)} = 9.33 \times 10^{-14} I \text{ (Wcm}^{-2}\text{)} (\lambda \text{ (}\mu\text{m)})^2 \quad (3.2)$$

where I and λ represents laser intensity and wavelength respectively.

At 532 nm, the ponderomotive energy is found to be $\sim 2.48 \times 10^{-4}$ eV considering I as 5×10^9 W/cm² and λ as 0.532 μ m. Thus, Keldysh parameter (γ) is calculated to be ~ 150 taking I_p of CF₂Br₂ as 11.03 eV. Since $\gamma \gg 1$, the primary ionisation of CF₂Br₂ clusters is via multiphoton process. In order to further verify the ionisation process under our experimental conditions, laser power dependency study has been carried out at 532 nm. Based on our studies, CF₂Br₂ clusters undergo (4+1) non-resonant multiphoton ionisation under gigawatt intense laser field. Laser power dependency was found to be similar for both singly and multiply charged ions of carbon and fluorine (figure 3.9). This result implies that the primary step of multiple charge state formation is via multiphoton ionisation. However, for generation of such multiply charged ions at least 87.14 eV (ionisation energy of F⁴⁺ \leftarrow F³⁺)¹⁰⁵ energy is required from the laser field and some secondary efficient absorption mechanism is necessary for generation of higher charge state of carbon, fluorine and bromine.

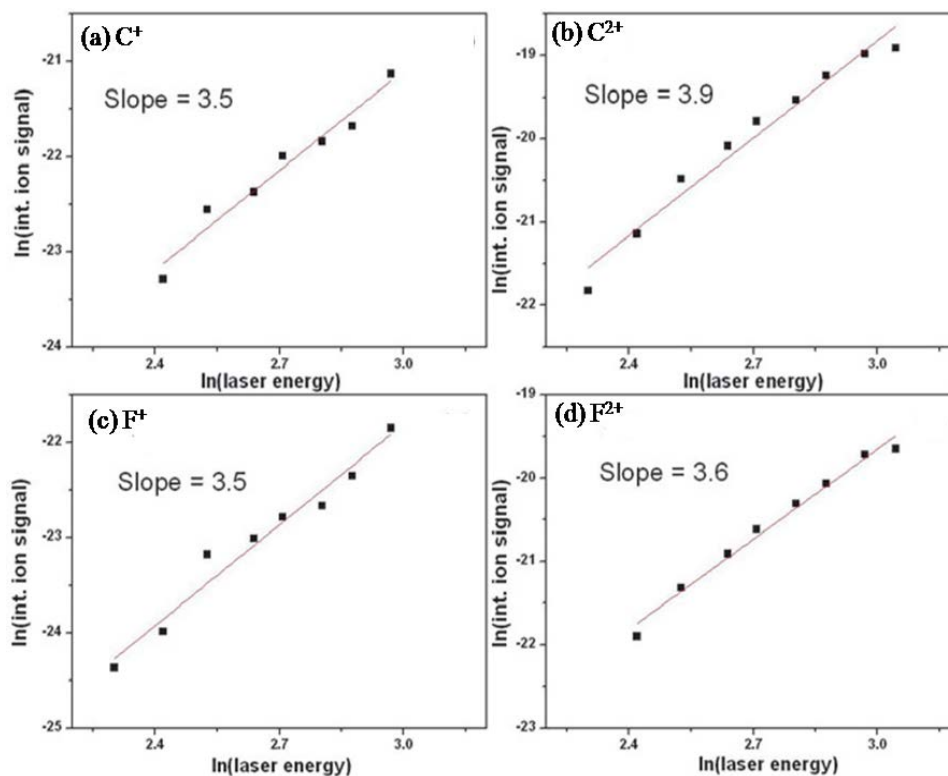


Figure 3.9: Laser power dependency study of (a) C^+ (b) C^{2+} (c) F^+ and (d) F^{2+} ions generated by 532 nm photo ionization of CF_2Br_2 clusters

For understanding the secondary ionisation processes, interaction of electrons with the nanosecond long laser pulses needs to be considered. Electrons are produced within the cluster as result of multiphoton ionisation process at the rising part of the laser pulse. Since multiphoton ionisation rate is expected to be very low it will produce low electron density in the ionized cluster. At such low electron density, the faster electrons which are called outer ionized electrons may escape from the surface of the cluster. Due to removal of outer ionized electron, cluster becomes electrically charged and a macroscopic electric field builds up which prevents the remaining electrons from escaping.¹⁰⁶ The remaining electrons confined in the cluster volume are known as inner ionized electron. The inner ionized electrons which are under the influence of Coulomb field inside the cluster, keep extracting energy from the laser pulse via inverse Bremsstrahlung (IBS) process during electron-ion and electron-neutral collisions. Once the electron energy exceeds the ionisation energy, secondary

ionisation can occur via electron-induced processes, resulting in augmentation of the charge state on the cluster. This sequence of events continues until a stage comes when Coulomb repulsion overcomes the total cohesive energy of the cluster and the multiply charged cluster explodes resulting in formation of multiply charged atomic ions with large kinetic energy.

The rate of energy extraction by the electron via IBS process from the laser pulse is given by equation (3.3) ¹⁰⁷:

$$\frac{dE}{dt} = U_p \times \nu \quad (3.3)$$

Here ν is the collision frequency of the inner ionized electron and is of the order of $\sim 10^{14}$ - 10^{15} Hz ⁶⁴ and U_p is ponderomotive energy of electrons. From equation 3.2, it is clear that as wavelength (λ) increases, ponderomotive energy (U_p) of electrons increases quadratically for a given laser intensity. As a result, net energy extraction by the electron from the optical field is higher at longer wavelength. Thus, higher level of ionisation and charging is expected at longer wavelength which is qualitatively in agreement with the experimental observations.

For better understanding of the mechanism of multiply charged ion formation under gigawatt intense laser field, the above mentioned mechanism is depicted schematically in figure 3.10. Earlier, Li and co workers proposed this model ¹⁰⁸⁻¹¹⁰ for similar laser intensity conditions and our results can also be explained based on the same model. Henceforth, the model will be mentioned as ‘three stage model’ in subsequent chapters of the thesis since cluster explosion process comprise of three step i.e. multiphoton ionisation ignited-inverse bremsstrahlung heating–electron impact ionisation.

It is worth mentioning here that no ion signal corresponding to Ar^+ ($\text{CF}_2\text{Br-Ar}^+$) was observed in the time-of-flight mass spectrum at 355 nm or 532 nm. If Ar

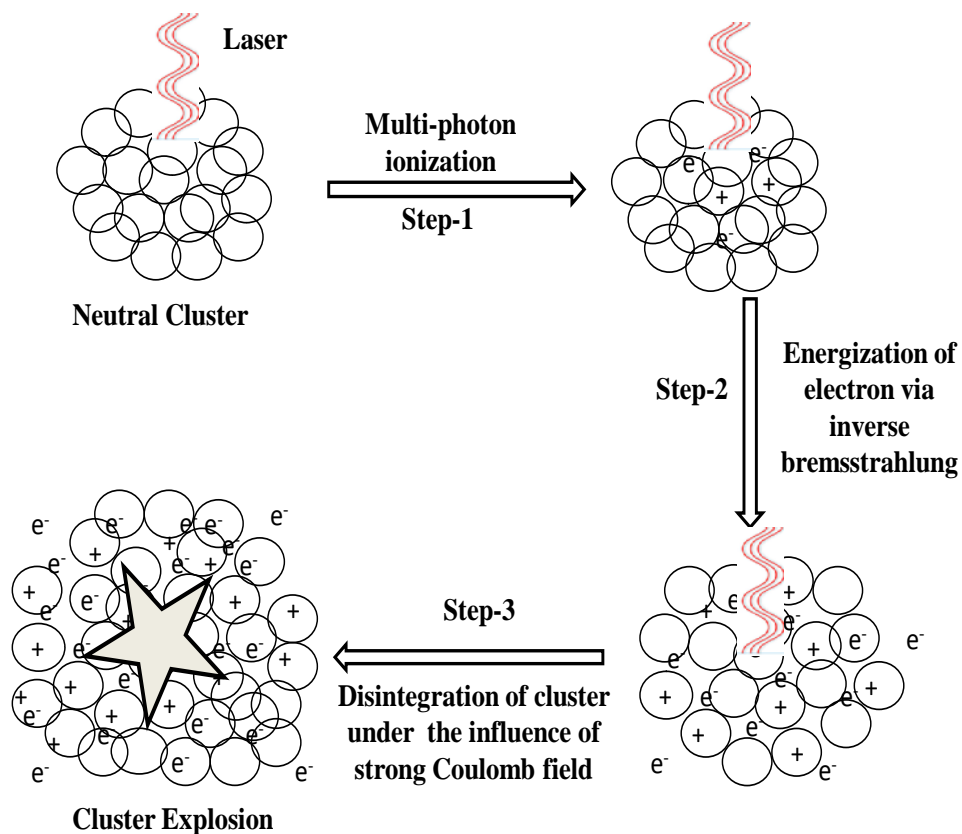


Figure 3.10: Schematic representation of three stage model for the generation of multiply charged ions at an intensity of $\sim 10^9$ W/cm²

atoms had been part of the CF_2Br_2 cluster at the time of ionisation, then Ar^+ signal should have also been observed in the mass spectrum because multiply charged ions are produced at these wavelengths due to random collisions of energized electrons which have higher energy compared to ionisation potential of Ar (15.76 eV). Thus, the experimental results suggest that at the moment of ionisation, Ar atoms are not present in the CF_2Br_2 cluster. From these observations, it is inferred that majority of the Ar atoms evaporate after absorbing the heat generated due to clusterisation.

3.4 Conclusions

Time-of-flight mass spectrometric studies on monomers and clusters of CF_2Br_2 have been studied at 266, 355 and 532 nm using gigawatt intensity laser pulses. On comparison of mass spectra of CF_2Br_2 monomer and cluster photo ionized

at 266 nm, it emerges that clusterization facilitates generation of CF_2Br^+ , Br_2^+ ions which arise as a result of intra-cluster photochemistry. While, when clusters of CF_2Br_2 were subjected to 355 and 532 nm, the clusters were found to generate multiply charged ions eventually leading to violent Coulomb explosion phenomenon. Generation of these multiply charged atomic ions have been ascribed to efficient coupling of laser pulse energy to the cluster based on three stage model comprising of 'multiphoton ionisation ignited-inverse bremsstrahlung heating–electron impact ionisation'.

Chapter 4

Coulomb explosion of C₂H₅Br clusters using nanosecond laser pulses: Determination of kinetic energy of multiply charged ions

4.1 Introduction

Unravelling the mechanism of laser-cluster interaction has been a constant endeavour for last two decades, motivated by the desire to realize benchtop accelerators,^{111,112} highly monochromatic X-ray sources¹¹³ as well as for mimicking nuclear fusion reactions at laboratory scale¹¹⁴. In all such studies, the key driver has been the Coulomb explosion phenomena that occurs upon interaction of clusters with intense (10^{14} - 10^{20} W/cm²) femtosecond laser pulses, which results in generation of multiply charged atomic ions with large kinetic energy.¹¹⁵⁻¹¹⁸ However, a new dimension to these laser-cluster interaction studies has been uncovered by the observation of Coulomb explosion phenomena at comparatively low laser intensity of $\sim 10^9$ W/cm², achieved using nanosecond laser pulses.⁶⁹⁻⁷¹ Generation of such multiply charged atomic ions is in contrast to the threshold laser intensity (I) of $\sim 10^{14}$ - 10^{15} W/cm² (at least five orders of magnitude higher than the intensity used in our experiments) predicted by formula of Augst *et al.*⁴⁸ for generation of multiply charged atomic ions (Equation 4.1).

$$I (\text{W/cm}^2) = 4 \times 10^9 E_i^4 / Z^2 \quad (4.1)$$

Where E_i is ionisation energy of the multiply charged ion (eV) and Z is the charge of the ion. Generation of multiply charged atomic ions upon interaction of cluster with high intensity femtosecond laser pulses has been explained on the basis of optical field ionisation, but it is difficult to account for observation of multiply charged

atomic ions upon interaction with nanosecond laser pulses of very modest (gigawatt) intensity. The electric field associated with a laser pulse having intensity $\sim 10^9$ W/cm² is calculated to be $\sim 10^6$ V/cm based on the formula (equation 4.2)-

$$E \text{ (Vcm}^{-1}\text{)} = 27.45 (I)^{1/2} \quad (4.2)$$

However, for optical field ionisation of an atom or molecule, the required electric field is $\sim 10^9$ V/cm. Thus, the electric field associated with our laser pulse is at least three orders of magnitude lower than the atomic field of atom/molecules. Hence, optical field ionisation process can be safely ruled out under our experimental conditions for generation of multiply charged atomic ions. This has been further affirmed by the value of “Keldysh parameter (γ)”⁵² which is defined as, $\gamma = \sqrt{IE / 2U_p}$ where IE is the ionisation energy and U_p is ponderomotive energy in eV. Under our experimental conditions, typical γ value lie between 100-200, so multi-photon excitation processes are expected to dominate based on the discussion in section 1.4.3 (in chapter 1). However, multi-photon excitation processes alone cannot explain generation of multiply charged atomic ions, which requires coherent absorption of large number of photons from the laser pulse. Above discussion thus throws light on the complexity associated with the interaction of nanosecond laser with clusters and only a highly efficient energy absorption mechanism, which couples the optical field and the cluster can account for generation of multiply charged atomic ions under gigawatt laser intensity conditions.

In chapter 3, results of interaction of CF₂Br₂ clusters with nanosecond laser pulses of intensity $\sim 10^9$ W/cm² have been described which show generation of multiply charged ions of carbon, fluorine and bromine. Generation of multiply charged atomic ions under gigawatt intense laser field has been explained based on three stage cluster ionisation model which comprises of ‘multiphoton ionisation

ignited-inverse bremsstrahlung heating–electron impact ionisation’. However, the model qualitatively explains the observation of Coulomb explosion under our experimental conditions. In order to get a quantitative idea of the phenomenon further studies have been carried out in similar type of cluster system i.e. C_2H_5Br clusters. As discussed in chapter 3, the multiply charged atomic ions are produced with high kinetic energy. However, quantification of the kinetic energy of these ions has not been done. In the present work, an attempt has been made to determine the kinetic energy of multiply charged ions at different wavelength. Moreover, few relevant issues related to cluster ionisation dynamics, like time scale of cluster explosion, effective cluster size, Coulomb stability of multiply charged cluster etc have been described based on the calculation of energization of inner ionised electron under gigawatt intensity laser field.

4.2 Experimental details

Details of the experimental setup have been described in Chapter 2. Only information relevant to ethyl bromide (C_2H_5Br) sample is given here. C_2H_5Br is extremely flammable chemical which is reactive to water and causes eye, skin, respiratory tract irritation. Thus, transfer of the sample has been carried out in glove box taking adequate safety precautions.

4.3 Results & Discussion

4.3.1 Interaction of C_2H_5Br clusters with 266, 355 and 532 nm laser pulses: Observation of multiphoton dissociation/ionisation and Coulomb explosion

Figure 4.1 represents the time-of-flight mass spectrum for ethyl bromide clusters irradiated by 266 nm laser pulse of intensity $\sim 5 \times 10^9$ W/cm². Ion signals corresponding to H^+ , CH_n^+ ($n=0-3$), $C_2H_5^+$, Br^+ , $C_2H_5Br^+$, Br_2^+ , $C_2H_5(C_2H_5Br)_n^+$ ($n=1-4$) were observed in the mass spectrum. All these observed masses could be assigned

to singly charged species, which arise as a result of multiphoton dissociation/ionisation of ethyl bromide cluster. Here it is worth mentioning about ion signal at m/z 158, 160 and 162 with a relative intensity ratio of approximately 1:2:1, observed only at this wavelength. These ion signals have been assigned to the formation of molecular bromine ion – Br_2^+ , which can be produced by a) formation of neutral Br_2 molecule via intra-cluster chemistry, followed by its ionisation or b) direct concerted elimination of the Br_2^+ from ionized clusters of ethyl bromide. Fan and co-workers⁹⁹ have studied photo dissociation of dimers and other small clusters of $\text{C}_2\text{H}_5\text{Br}$ at 248 and 193 nm using laser induced fluorescence spectroscopy for characterization of products. Based on their study, it was inferred that clusters of ethyl bromide do not generate molecular halogen (Br_2) as product upon excitation at either wavelength. Thus, the only other possibility for the generation of Br_2^+ is concerted photo dissociation of the ionized ethyl bromide clusters $(\text{C}_2\text{H}_5\text{Br})_n^+$ ($n>2$) which is suggested to be the most probable source of the molecular bromine ion, Br_2^+ .

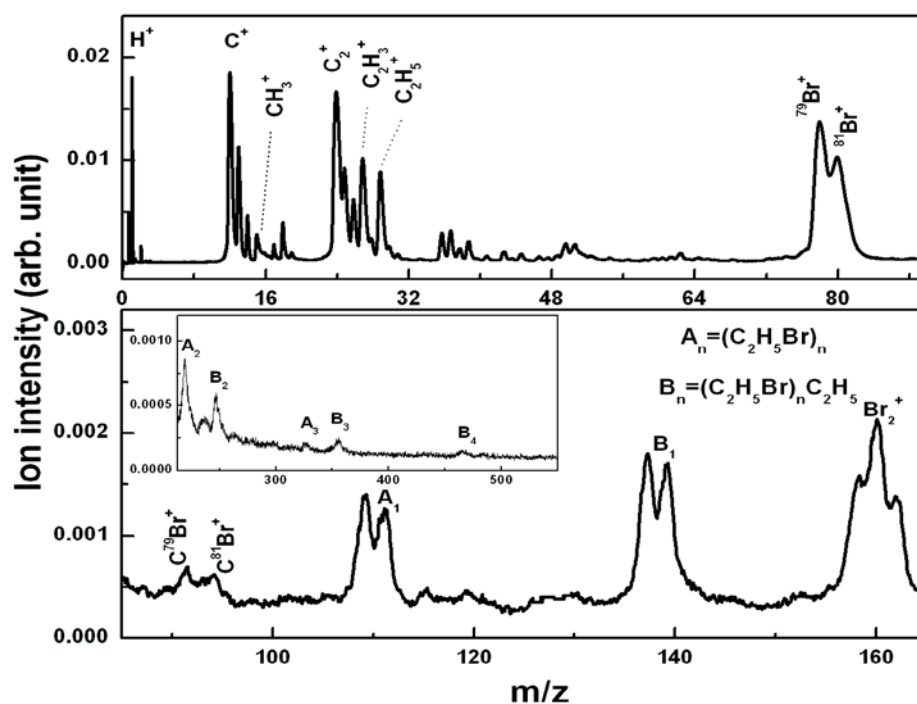


Figure 4.1: Time-of-flight mass spectra of ethyl bromide clusters ionised at 266 nm using laser pulses of intensity $\sim 10^9 \text{ W/cm}^2$

Under similar experimental conditions, the time-of-flight mass spectra obtained when C_2H_5Br clusters were interacted with 355 and 532 nm laser pulses and are depicted in figure 4.2 and 4.3 respectively. At 355 nm, the mass spectrum shows weak ion signals corresponding to C^{2+} and Br^{2+} ions along with other singly charged fragment ions observed at 266 nm. While at 532 nm, multiply charged atomic ions of carbon (up to C^{4+}) and bromine (up to Br^{5+}) were observed along with other singly charged ions. These multiply charged atomic ions observed at 355 and 532 nm arise as a result of efficient laser-cluster interaction resulting in Coulomb explosion of $(C_2H_5Br)_n$ clusters and exhibit broad and split profiles, indicating that these ions are associated with significant amounts of kinetic energy.

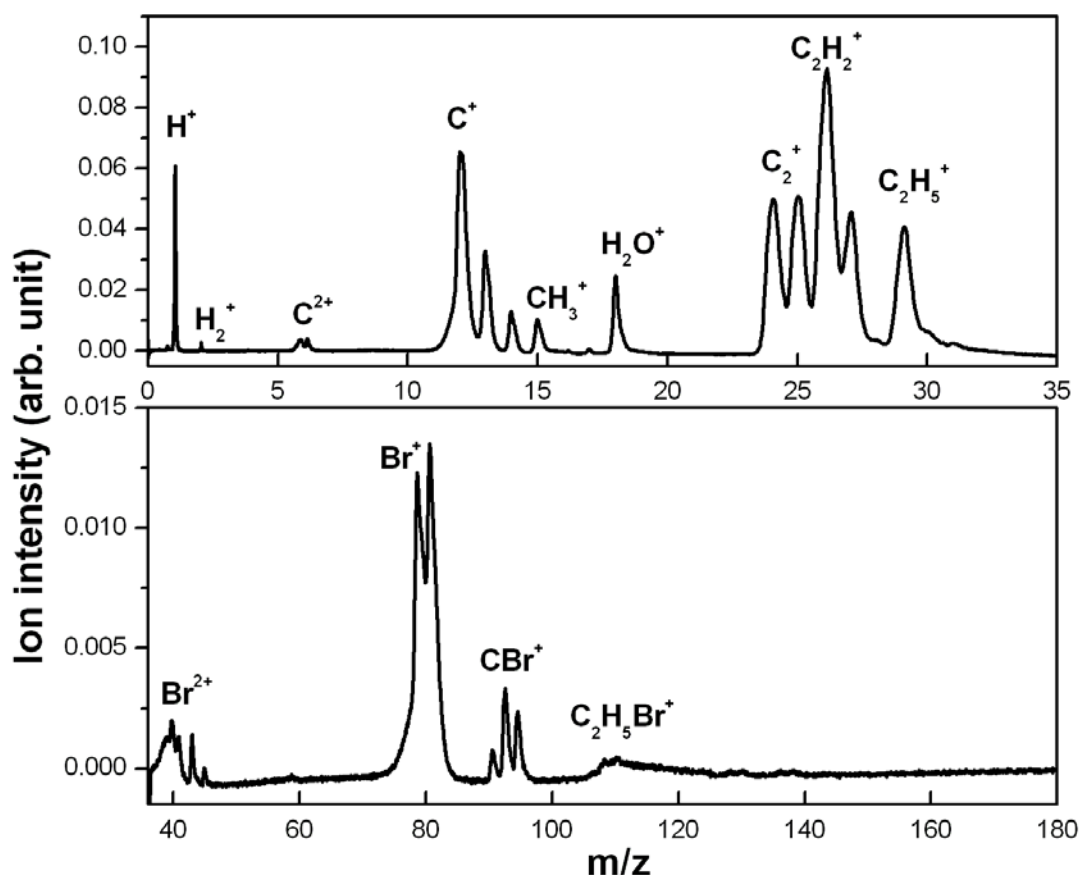


Figure 4.2: Time-of-flight mass spectra of ethyl bromide clusters ionised at 355 nm using laser pulses of intensity $\sim 10^9$ W/cm²

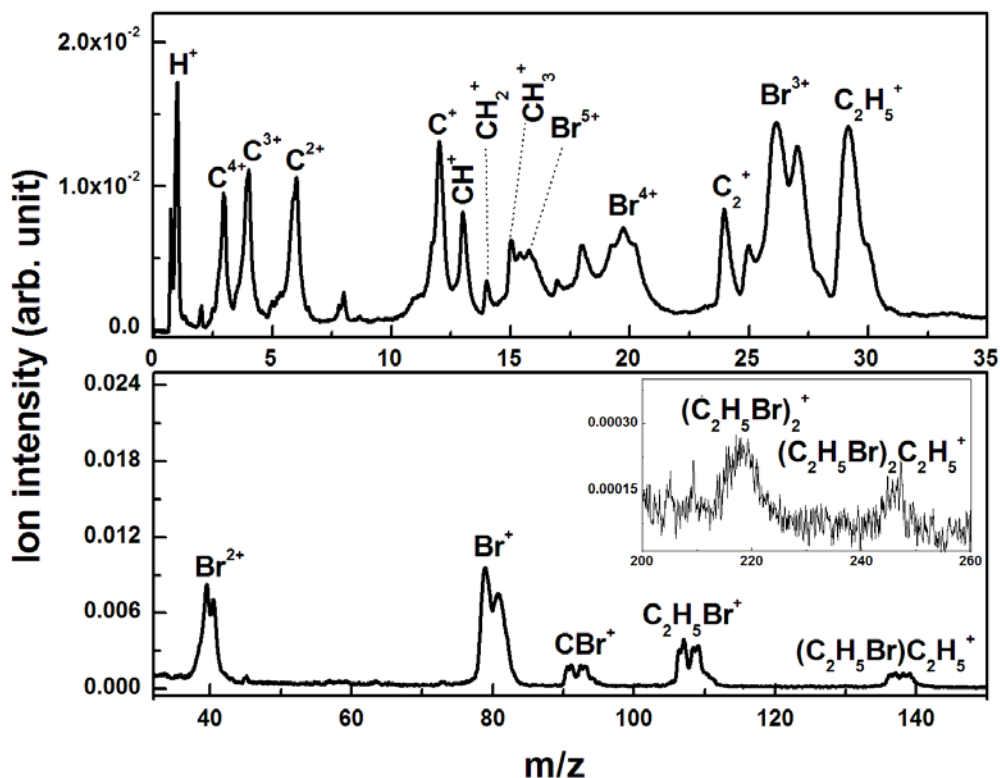


Figure 4.3: Time-of-flight mass spectra of ethyl bromide clusters at 532 nm. Inset shows ion signal for cluster fragments of ethyl bromide.

4.3.2 Determination of kinetic energy of multiply charged carbon and bromine ions due to interaction of ethyl bromide clusters at 355 and 532 nm

(a) Peak splitting method

During cluster disintegration, multiply charged ions fly apart in all direction from the interaction zone i.e. towards the detector and opposite to the detector direction. For each ion peak, the fraction of ions moving towards the detector are referred as forward component and fraction of ions travelling away from the detector are called backward component. The forward ion component reaches the detector early in time because of its initial kinetic energy along the detector direction. On the other hand, backward ion component moves opposite to the applied electric field, as a result, this bunch of ions slows down, stops and turns around towards the detector and reaches at a later time. Thus, for an energetic ion peak, forward and backward ion component constitute a broad asymmetric peak in the time-of-flight mass spectra

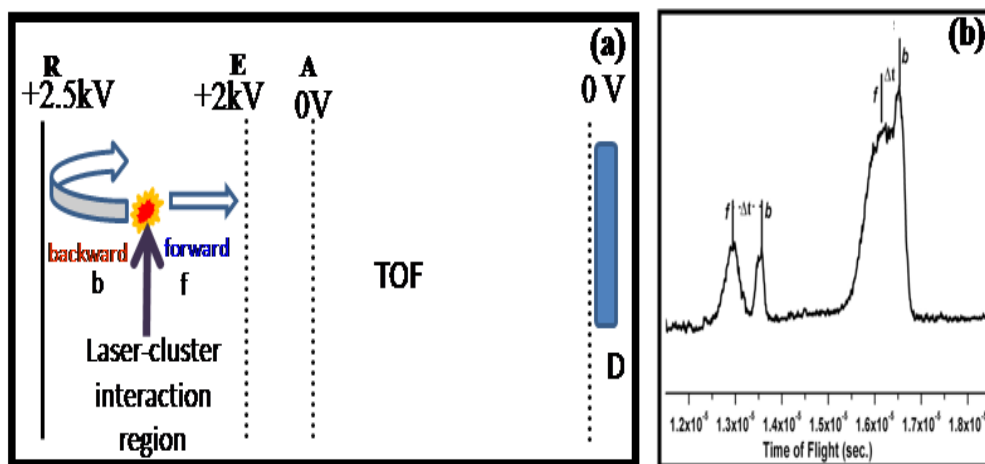


Figure 4.4 (a) Direction of motion of energetic multiply charged ions in the ion optics of time-of-flight mass spectrometer showing turn around motion of backward ions and direct motion of forward ions (b) asymmetric peak shape of multiply charged ions in time-of-flight mass spectra

(figure 4.4). Using the difference in arrival time of forward and backward ion, kinetic energy can be determined. The electric field applied in the dual stage time-of-flight mass spectrometer is shown in figure 1.2 (in chapter 1). The time spent by forward and backward ion peak in the extraction region is as follows³⁷:

$$T_{forward} = \frac{\sqrt{2m}}{ZE} [U_0 + ZES_a - \sqrt{U_0}] \quad (4.3)$$

$$T_{backward} = \frac{\sqrt{2m}}{ZE} [U_0 + ZES_a + \sqrt{U_0}] \quad (4.4)$$

Where U_0 is initial kinetic energy of the ion, E is the electric field (V/cm), z represents the charge of the ion and S_a is the initial position of ion formation (in cm).

$$\Delta t = T_{backward} - T_{forward} = \frac{\sqrt{2m}}{ZE} [2\sqrt{U_0}] \quad (4.5)$$

Squaring both sides and rearranging, we get

$$U_0 = \frac{\Delta t^2 Z^2 E^2}{8m} \quad (4.6)$$

Substituting the conversion factor of the units in equation 4.6, the kinetic energy of multiply charged ions can be expressed as

$$E_{kin} (eV) = 9.65 \times 10^{-7} \frac{\Delta t^2 n^2 F^2}{8m} \quad (4.7)$$

Here Δt is the time difference (in ns) between the forward and backward component of the ion signal for a particular mass, F is a static electric field ($V\text{ cm}^{-1}$) applied for ion extraction, n is charge of the ion, m is mass of the ions in atomic units (Dalton (Da)). Since the kinetic energy of multiply charged ions are determined based of the split nature of the ion peak, this method is commonly known as ‘Peak splitting method’.

Peak splitting method has been used to calculate the kinetic energy of the multiply charged ions of carbon which are listed in Table 4.1. It is to be noted that the kinetic energy of multiply charged ions of carbon increases with increase in charge state for a particular wavelength. Moreover, kinetic energy of C^+ and C^{2+} ions observed in 532 nm experiments is much higher as compared to that of 355 nm experiments.

(b) Retarding potential method

For calculating the kinetic energy of multiply charged bromine ions, the above mentioned method based on the difference in arrival time could not be applied due to merger of the forward and backward components arising from two bromine isomers i.e. ^{79}Br and ^{81}Br (since the individual components could not be resolved due to their large kinetic energy). Hence, the method based on retardation field⁷¹ was employed for measuring the kinetic energy of multiply charged bromine ions.

The modified ion optics is shown in figure 4.5, where repeller and extractor are kept under same potential and the ions are moving towards the detector because of the kinetic energy acquired due to Coulomb explosion of cluster. With increase in extractor voltage (marked as E), only those ions would reach the detector which have kinetic energy above the retardation field. Mass spectra have been recorded with

increase in retardation field in steps of 50 V/cm. The area under the peak indicates the ion yield of the particular charge state having kinetic energy equivalent to the retardation field. Thus, kinetic energy of each charge state of bromine has been calculated based on retarding potential method.

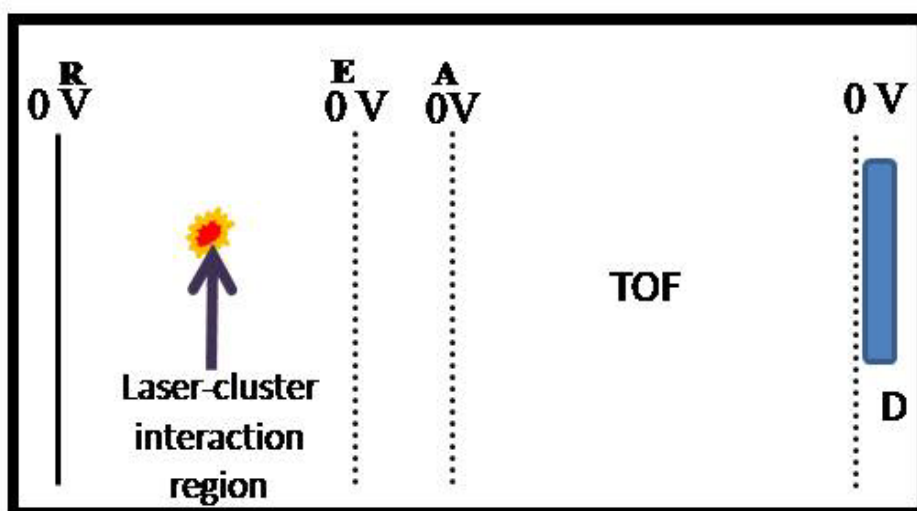


Figure 4.5: Ion optics arrangement for determination of kinetic energy of multiply charged bromine ions using retarding potential method

In figure 4.6, the representative mass spectra have been plotted as a function of increasing retardation potential at an interval of 100 V/cm and representative spectra are shown here. However, actual experiments have been done by increasing retardation potential at an interval of 50 V/cm. Based on the retardation potential value, kinetic energy of multiply charged bromine ion has been derived and is listed in table 4.1. During these experiments, since the mass spectrometer had to be operated in single-focusing condition, the mass resolution was poor, as evident from the mass spectra presented in figure 4.6.

It must be noted here that the peak splitting method provides most probable ion kinetic energy while the retardation field method offers the maximum kinetic energy of the ions. Hence, the tabulated kinetic energy of multiply charged bromine

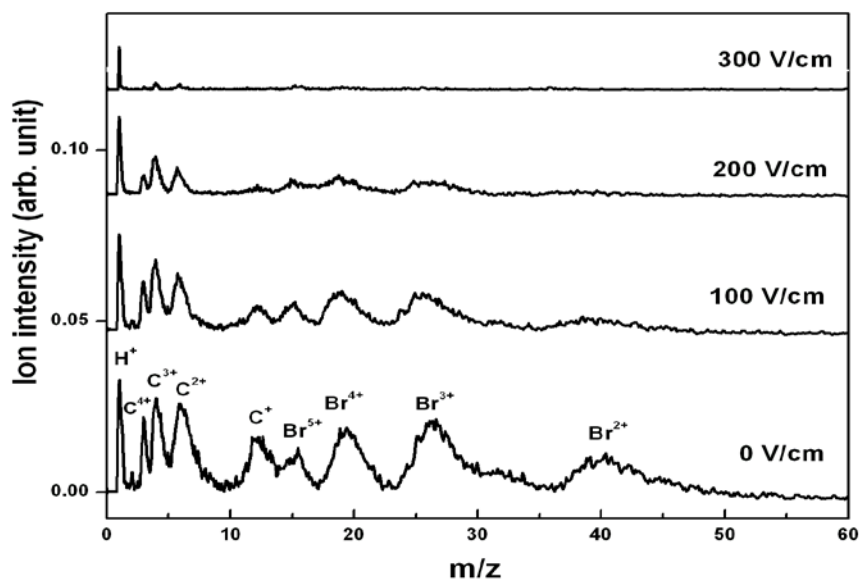


Figure 4.6: Representative time-of-flight mass spectra of ethyl bromide clusters at different retardation potential

ions measured by retarding potential method is much higher than those of multiply charged carbon ions measured by peak splitting method. Based on these measurements, we find a simultaneous increase in the charge state and kinetic energy of the multiply charged atomic ions (Table 4.1). This is in contrast to the case of molecules, where the singly and doubly/triply charged ions generated upon Coulomb explosion of multiply charged molecular ion, essentially have the same kinetic energy,^{119, 120} since higher charge states were generated by subsequent ionisation of singly charged ions released from the dissociation of the doubly (and/or triply)

Table 4. 1: Kinetic energy of multiply charged atomic ions of carbon and bromine measured for ionisation of ethyl bromide clusters at 532 and 355 nm.

Method of determination	Peak splitting method				Retarding potential method				
	C ⁺	C ²⁺	C ³⁺	C ⁴⁺	Br ⁺	Br ²⁺	Br ³⁺	Br ⁴⁺	Br ⁵⁺
Charge state	C ⁺	C ²⁺	C ³⁺	C ⁴⁺	Br ⁺	Br ²⁺	Br ³⁺	Br ⁴⁺	Br ⁵⁺
Kinetic energy (eV) at 532 nm	~14	~180	~343	~495	-	~400	~750	~1000	~1250
Kinetic energy (eV) at 355 nm	~4	~50	Not Observed		Could not be calculated because of low ion yield			Not Observed	

charged parent ion as a result of Coulomb explosion. These results thus indicate that under our experimental conditions the multiply charged ions are direct products of disintegration of ethyl bromide cluster, which has been highly charged prior to undergoing Coulomb explosion.

4.3.3 Laser power dependency study of ethyl bromide clusters at 266, 355 and 532 nm

For understanding the photochemistry of ethyl bromide clusters at different wavelengths, it is imperative to focus on excited electronic states of ethyl bromide molecule. Like other alkyl halides, the lowest energy electronic transition for C_2H_5Br corresponds to dissociative \tilde{A} band, centered at ~ 6.1 eV. In addition, there are large number of Rydberg excited states in the 6.7-10.1 eV region.¹²¹ Thus, under our experimental conditions at all the laser wavelengths studied, the ethyl bromide clusters have been ionised via multiphoton excitation to Rydberg states and the role of dissociative \tilde{A} band is insignificant. This is supplemented by power dependence of integrated charge density measurements carried out at different laser wavelengths. Details of the charge density measurement have been described in chapter 8. In brief, charge density is the total amount of charge produced per unit volume in the interaction zone. In this experiment, charge density of the interaction zone has been measured for a particular wavelength at varying laser energy. Figure 4.7(a) and 4.7(b) show ln-ln plot of integrated charge density vs laser energy, where a slope of 1.7 and 1.6 obtained at 266 and 355 nm respectively suggests that the cluster undergoes (2+1) photon ionisation mediated via Rydberg state at ~ 9.32 and 7eV, respectively.

Similarly at 532 nm, as a slope of 3.5 was obtained in ln-ln plot of integrated charge density vs laser energy, the cluster ionisation is mediated via the Rydberg state at ~ 9.32 eV (Figure 4.7(c)). Thus, at all the three wavelengths the primary process is multiphoton ionisation of the cluster assisted by the Rydberg states, at the leading

edge of the laser pulse. Though the primary step at all the three wavelengths is similar, our time-of-flight mass spectra depict altogether different behavior. At 266 nm, the main process is multiphoton dissociation/ionisation. On the other hand at 355 nm, multiphoton dissociation/ionisation coupled with weak Coulomb explosion was observed, while at 532 nm, a strong Coulomb explosion has been observed, as explained above.

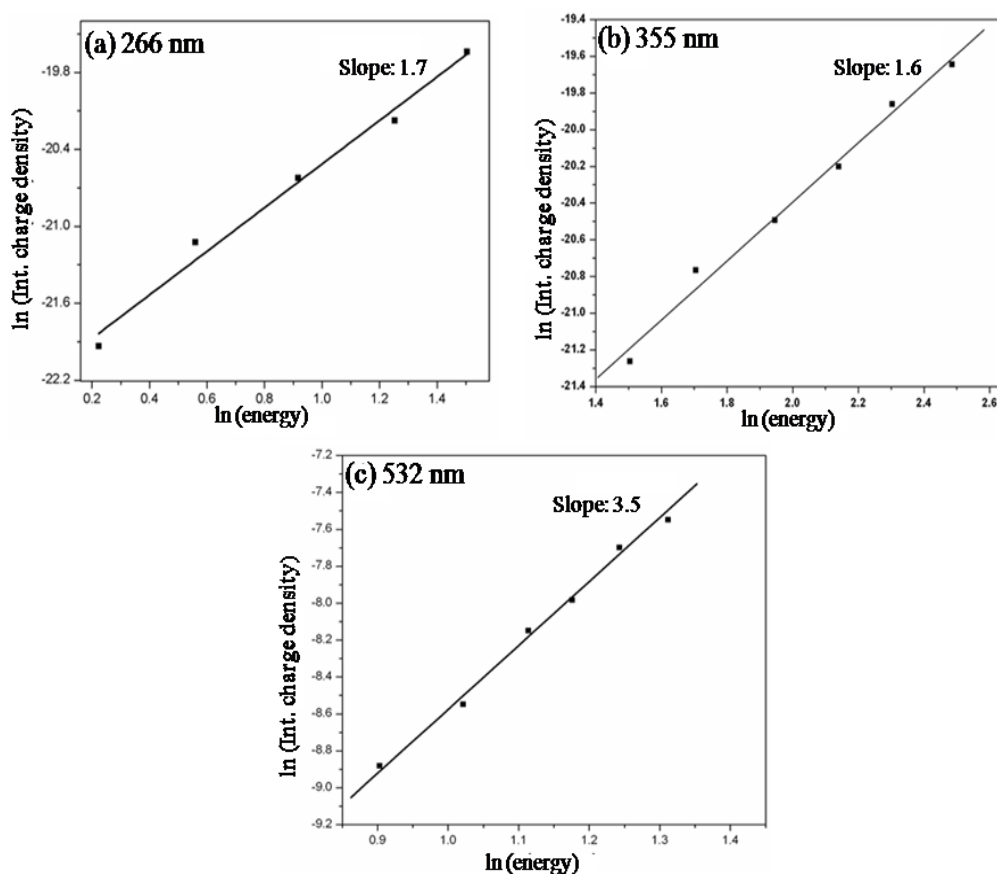


Figure 4.7: *ln-ln plot of charge density as a function of laser energy for ionisation at (a) 266 nm (b) 355 nm and (c) 532 nm laser wavelength*

4.3.4 Different aspects of cluster explosion mechanism

Upon interaction of nanosecond laser pulses of intensity $\sim 10^9$ W/cm² with C₂H₅Br clusters, multiply charged ions of carbon and bromine have been observed. The charge state of atomic ions of carbon and bromine increases with laser wavelength. In chapter 3, results of interaction of CF₂Br₂ clusters with gigawatt laser pulses were presented and as can be seen, observations are similar in both cluster

system. The results in the present study can also be explained qualitatively based on three-stage cluster ionisation mechanism as described in Chapter 3 (section 3.3.3). However, the three-stage cluster ionisation mechanism cannot conclusively explain the absence of multiply charged ions at 266 nm, as the ponderomotive energy at 266 and 532 nm differ by a factor of 4, which could be compensated partially by higher collision frequency of inner ionized electron at 266 nm (see Table 4.2). To resolve this issue, we have calculated average kinetic energy gained by electron under our experimental conditions at the three different wavelengths using equation (4.8), assuming that upon ionisation of the cluster at the leading edge of the laser pulse the cluster survives for ~ 1 ns before disintegrating (for a hypothetical case).

$$\frac{dE}{dt} = U_p \times v \quad (4.8)$$

Our calculations suggest that the average energy gained by the inner ionized electron in 1 ns would be ~ 73 eV, 50 eV and 37 eV at 532, 355 and 266 nm respectively (Table 4.2). At 532 nm, the highest observed ionic charge states of carbon and bromine have ionisation energy [IE(C⁴⁺)= 64.49; IE(Br⁵⁺) =59.9 eV see Table 4.3]¹⁰⁵ less than that of electron energy (~ 73 eV). Thus, observation of such charge state can be explained based on the electron heating mechanism. However, in case of 355 and 266 nm, if inner ionised electrons interact with optical field of laser for 1 ns, than the expected energy gain is ~ 50 eV and ~ 37 eV respectively which is much higher than the observed charge state. Ionisation energy of highest observed charge state at 266 nm and 355 nm are ~ 11.85 eV (Br⁺), ~ 24.38 eV (C²⁺) respectively. Thus, from the calculation it is very clear that inner ionised electron interacts with laser field for shorter duration at 266 nm and 355 nm as compared to 532 nm. Hence, the ionised cluster interacts with the laser field for different duration of time at

Table 4.2: Laser wavelength and the corresponding ponderomotive energy for intensity of $\sim 5 \times 10^9 \text{ W/cm}^2$. Electron-ion collision frequency is assumed to be of the order of laser frequency.⁶⁴ The total energy gained by electron is derived by taking product of ponderomotive energy and the average number of collisions experienced by the caged electron in $\sim 1 \text{ ns}$.

Wavelength (nm)	Ponderomotive energy (Up) in eV	Collision frequency (s^{-1})	Average number of collisions in $\sim 1 \text{ ns}$ (v)	Energy gained by e^- (eV)
532	1.33×10^{-4}	5.62×10^{14}	$\sim 5.5 \times 10^5$	~ 73
355	5.88×10^{-5}	8.45×10^{14}	$\sim 8.5 \times 10^5$	~ 50
266	3.30×10^{-5}	1.12×10^{15}	$\sim 1.1 \times 10^6$	~ 37

Table 4.3: Ionisation energy of different charge states of carbon and bromine ions¹⁰⁵

Charge state	Ionisation energy (eV) of carbon (C^{n+})	Ionisation energy (IE) of bromine (Br^{n+}) (eV)
+1	11.26	11.85
+2	24.38	21.87
+3	47.88	36.08
+4	64.49	47.42
+5	392.07	59.9
+6	489.98	88.92
+7	-	103.37
+8	-	193.44

different wavelength. At higher wavelength, partially ionised cluster interact via quasifree electrons with laser pulses for longer duration and as a result of that the electron energy increases and at some stage crosses the ionisation energy for the next level of ionisation which are then observed as higher charged states in time-of-flight mass spectrometer.

Here it is pertinent to mention about some recent experiments carried out on Coulomb explosion of inert gas clusters using few-cycle (~ 10 - 12 fs) laser pulses.^{122,123} In case of few-cycle pulses, there is insufficient time for the cluster to undergo

expansion (Coulombic and hydrodynamic). In these experiments the maximum ion energies were measured to be much lower than those obtained when longer pulses (~ 100 fs) of the same laser intensity ($\sim 10^{14}$ W/cm²) were used. This suggests that the efficiency of the laser-cluster interaction and resultant ion energies depend critically on the overall duration of interaction. On the contrary, in our experiments due to comparatively long duration of the laser pulse, the cluster expansion cannot be neglected completely and would become significant once large number of charge centers have been generated within the cluster upon interaction with laser, finally resulting in disintegration of the cluster. Thus for our experiments, the energy accumulated in the cluster would be governed by the period for which the ionized cluster interacts with nanosecond laser pulse before undergoing disintegration.

Based on the calculations reported in table 4.2 and above discussion, it can be concluded that under our experimental conditions the ionized cluster survives only for sub nanosecond duration within the interaction zone of the laser although the laser pulse duration is much longer (~ 9 ns). As a result, the inner ionized electrons are unable to extract energy from the laser pulse to the extent expected on the basis of calculations assuming no expansion as reported in table 4.2. Hence, our observation cannot be explained merely on the basis of three-stage cluster ionisation mechanism.

In addition, it is essential to take into account the meta-stability of multiply charged cluster, generated by electron ionisation mechanism (assisted via IBS), which is under the influence of laser pulse. For instance, there are several reports where Coulomb instability of multiply charged clusters has been studied and it has been demonstrated that the lifetime of a multiply charged cluster, having certain charge N , increases with increase in cluster size due to the ability of the larger cluster to delocalize the given charge over larger cluster surface. Also it has been reported that

the multiply charged cluster must exceed a critical cluster size, in order to be stable (or at least metastable).¹²⁴ For example, critical size deduced for triply charged argon cluster ions is $[\text{Ar}_{226}]^{3+}$.¹²⁵ Similarly for $(\text{CO}_2)_n$ clusters, the critical cluster size for doubly, triply and quadruply charged cluster corresponds to $n=44$, 108 and 216 respectively.¹²⁶ Thus, the Coulomb instability of multiply charged cluster and rate of energy extraction from the optical field at different laser wavelengths can shed more light in understanding the results obtained in the present study. In our experiments, the adiabatic expansion conditions used for generation of ethyl bromide clusters were kept identical at 266, 355 and 532 nm. Hence it can be safely assumed that the average size of ethyl bromide cluster irradiated at these laser wavelengths is same. Upon interaction with the initial part of the laser pulse, these clusters undergo inner and outer ionisation as a result of multiphoton excitation process, coupled with other parallel processes like dissociation, evaporation, fragmentation, fission and intra cluster ion-molecule reactions, etc. Since these ionized clusters are still in the sea of photons, the electron induced ionisation of the cluster by inner ionized electrons via IBS process will become significant in addition to further multiphoton excitation/ionisation of the cluster. But as a result of above mentioned parallel processes, which are expected to be more significant at 266 and 355 nm due to their higher photon energy, the average cluster size at these two wavelengths would diminish rapidly as compared to the clusters exposed to 532 nm laser pulse. Thus, the average lifetime of the ionized cluster before it undergoes disintegration is much shorter (due to their inability to sustain higher charge states owing to their smaller resultant cluster size) at 266 and 355 nm, as a result the laser-cluster interaction is less efficient. While at 532 nm, in addition to higher ponderomotive energy, due to larger effective size (even after undergoing other parallel processes) the cluster is able

to sustain higher charge before disintegration. An added advantage offered by larger cluster size, is its ability to retain the inner ionized electrons for relatively longer time before the inner ionized electrons escape from the cluster volume, as a result the average time an inner ionized electron spends in extracting energy from the laser pulse would be more at 532 nm. Based on the above discussion, it can be concluded that in case of gigawatt laser induced Coulomb explosion, average size of cluster plays a dominant role in efficient interaction of laser with cluster which has not been given much significance so far.

4.4 Conclusions

Ethyl bromide clusters irradiated with laser pulses of intensity $\sim 10^9$ W/cm² exhibit diverse wavelength dependent photochemistry. At 266 nm, the ethyl bromide clusters were found to undergo multiphoton dissociation/ionisation. While at 355 and 532 nm, the clusters exhibited Coulomb explosion phenomenon leading to generation of multiply charged atomic ions with large kinetic energy. Our studies suggest that the mechanism which leads to cluster ionisation and Coulomb explosion is driven by complex multistep process which are strongly coupled i.e. Rydberg state mediated multiphoton ionisation of cluster-followed by energization of electrons (via IBS process) resulting in multiple ionisation of cluster, which subsequently undergoes Coulomb explosion. The phenomenon shows strong wavelength dependence and observed charge state as well as kinetic energy of ions is enhanced with increasing wavelength. The wavelength dependency observed in the present study has been explained on the basis of Coulomb stability of ethyl bromide clusters, which is a function of cluster size.

Chapter 5

Coulomb explosion phenomenon in methyl iodide clusters irradiated by gigawatt intense laser field: Effect of cluster size, laser polarisation and doping in clusters

5.1 Introduction

Interaction of nanosecond laser pulses of intensity $\sim 10^9$ W/cm² with molecular clusters leads to generation of multiply charged atomic ions with high kinetic energy. In chapter 3 and 4, results of interaction of CF₂Br₂ and C₂H₅Br clusters have been presented at different wavelengths and kinetic energy of multiply charged ions were determined. Observation of such high level of ionisation under gigawatt laser field can be understood based on the three stage cluster ionisation model which comprises of multiphoton ionisation ignited-inverse bremsstrahlung heating-electron impact ionisation. However, apart from three stage model, other parameters such as cluster size, Coulomb stability of cluster, electron retention time also play important role as discussed in chapter 4. In order to get deeper understanding of these aspects, further studies have been carried out in similar type of cluster system i.e. methyl iodide cluster which has an ionisation energy of ~ 9.54 eV and sufficient vapour pressure (400 mm of Hg at NTP) to produce clusters easily.

Methyl iodide clusters are one of the most studied system in laser-cluster interaction studies where laser pulse duration has been varied from femtosecond to nanosecond regime. Castleman and co-workers extensively studied methyl iodide clusters using femtosecond laser pulses of intensity $\sim 10^{15}$ W/cm² at two different wavelengths. At 795 nm, study of interaction of methyl iodide clusters was carried out using different carrier gas and charge state of iodine and carbon were observed in

reflectron time-of-flight mass spectrometer. The heavier carrier gas (Ar) facilitates production of larger clusters allowing higher charge states (I^{15+} and C^{4+}) to be formed. However, the lighter carrier gas (He) leads to smaller iodine charge state distribution (I^{7+} and C^{4+}) and smaller kinetic energy of these multiply charged ions.⁶⁵ At 397 nm, charge state of iodine has been reduced to +7 when Ar is used as carrier gas and the charge state remains similar even when He was used as carrier gas. Based on the observation, they have concluded that for longer wavelength (795 nm) fluence plays an important role in formation of higher charge state species whereas atomic ion fragments formed using a blue wavelength (397 nm) have a much smaller charge state distribution and exhibit moderate fluence dependence.⁶⁶ These experimental observations were supported by molecular dynamic simulation which predicts the temporal evolution of a cluster system after the ionisation event.¹²⁷ Using picoseconds laser pulses of intensity $\sim 10^{12}$ - 10^{13} W/cm², Kosmidis and coworkers studied methyl iodide clusters at 266 nm, 532 nm and 1064 nm. Multiply charged ions of iodine and carbon were observed at 532 nm and 1064 nm and charge state of these atomic ions was found to increase with wavelength. The explosion of the multiply charged cluster ions is found to be isotropic, while an asymmetric charge distribution prior to their fragmentation is observed. According to the authors, clusters are initially singly ionized by multiphoton absorption and an internal electric field is created within the cluster. This results in a higher distortion of the internal barriers and an increased ionisation of the cluster which finally explodes leading to energetic multiply charged ion production.¹²⁰ In nanosecond regime, Li and coworkers have studied interaction of methyl iodide clusters with different harmonics of Nd:YAG laser having intensity $\sim 10^{10}$ - 10^{11} W/cm². At 266 nm and 355 nm, charge state of fragment ions were limited to +1 whereas at 532 nm and 1064 nm generation of energetic multiply charged

atomic ions of carbon and iodine were observed ultimately leading to Coulomb explosion. Charge states of iodine and carbon were found to increase with laser wavelength.¹²⁸ However, for a particular wavelength the charge state of multiply charged ions remains the same and increase in laser intensity does not enhance the charge state. The increase in laser intensity linearly enhances the kinetic energy of multiply charged ions.¹²⁹ For the observation of multiply charged atomic ions at such low laser intensity, they have proposed a three stage model which comprises of multiphoton ionisation ignited-inverse bremsstrahlung heating–electron impact ionisation (mentioned in section 3.3.3 in chapter 3).¹⁰⁸ In order to support the electron impact ionisation for generation of multiply charged ions, electron energy has been measured using retarding potential method as a function of laser intensity and wavelength. However, the maximum electron energy is found to be lower than the ionisation energy required for the highest observed charge state in the time-of-flight mass spectra. In order to explain the disparity, screening effect of electrons is considered on ionisation energy of multiply charged ions.¹¹⁰ Further, Sharma *et. al*⁶⁹ have showed Coulomb explosion of methyl iodide clusters using nanosecond laser pulses at even lower laser intensity ($\sim 10^9$ W/cm²). Based on the experimental results, the charge states of iodine and carbon ions are found to increase with laser wavelength. Moreover, kinetic energy of ions and electrons are measured using peak splitting and retarding potential method. These observations can be qualitatively explained by the above mentioned three stage cluster ionisation model.

In the present work, methyl iodide clusters have been ionised using nanosecond laser pulses of intensity $\sim 10^9$ W/cm² and experiments have been carried out to understand the mechanism of multiple ionisation of atoms. In the first set of experiments, average size of methyl iodide clusters has been varied by changing the

pulsed valve nozzle and time-of-flight mass spectra are monitored at different wavelengths. Since size plays an important role in determining the property of a given cluster, these experiments were carried out with an aim to investigate the effect of clusterisation on ionisation dynamics under gigawatt intense laser field. Secondly, kinetic energies of multiply charged ions of carbon and iodine produced due to interaction of methyl iodide clusters with nanosecond laser pulses were measured using the peak splitting method. During peak splitting method, certain extraction voltage is applied to the multiply charged ions and kinetic energy of the particular ion is determined based on the split time of the peak. Thus, experiments have been carried out to investigate whether there is any effect of extraction field on kinetic energy of multiply charged ions. Thirdly, effect of laser polarisation has been studied on ion yield and kinetic energy of multiply charged ions produced as a result of interaction of methyl iodide clusters with nanosecond laser pulses. Laser polarisation has been varied parallel and perpendicular to the time-of-flight axis and mass spectra are compared at different polarisation condition. Finally, studies have been carried out using doped methyl iodide clusters instead of pure clusters. In chapter 3 and 4, interaction of nanosecond laser pulses has been focussed on different pure molecular clusters such as CF_2Br_2 and $\text{C}_2\text{H}_5\text{Br}$. However, in mixed clusters, doping plays an important role in altering ionisation dynamics compared to its pure form. Thus, doped methyl iodide clusters were ionised with nanosecond laser pulses and results have been compared with pure clusters.

5.2 Experimental details

Details of the experimental set up have been described in Chapter 2 and only a brief description relevant to this work is being given here. Methyl iodide sample

(Purity ~ 99.5 %) was procured from Sigma-aldrich and used for cluster formation without further purification. Helium gas (3 atm pressure) was used as carrier gas for supersonic expansion of methyl iodide sample. Two different nozzles (0.6, 0.8 mm) were used for generation of methyl iodide clusters of different sizes.

Ionisation was carried out using fundamental (1064 nm) as well as different harmonics (532 nm, 355 nm and 266 nm) of a pulsed Nd : YAG nanosecond laser. For some experiments, a dye laser ($\lambda_{em} = 563$ nm) was also used for ionisation. For generation of 563 nm, a Quantel dye laser [TDL 70] with Rhodamine 6G solution in ethanol was pumped by the second harmonic of the Nd : YAG laser. The pulse energy of the dye laser could be varied by changing the pump laser energy. An iris was introduced just prior to entering in the ionisation chamber to make sure that central homogeneous portion of the laser beam is used for these experiments.

In order to understand the effect of laser polarisation on multiply charged ions of carbon and iodine, the polarization of 532 nm laser was rotated by placing a half wave plate ($\lambda/2$ plate) in the path of laser beam. A combination of polariser and analyser has been used in order to define 0° . Analyser is nothing but another polariser. Thus, the second polariser is termed as analyser. If placed perpendicularly, minimum light will come out from polariser –analyser arrangement and this amount was measured by using laser power meter. Similarly highest energy at the laser power meter corresponds 0° angle between polariser and analyser. Again, 0° is defined as the direction of the laser polarization parallel to the TOF axis. In the present experiment, time-of-flight mass spectra were recorded from 0° – 360° , with step size 45° degrees. Subsequently, ion yield and kinetic energy of different multiply charged atomic ions were plotted as a function of laser polarisation angle.

5.3 Results and Discussion

5.3.1 Effect of cluster size on the charge state of atomic ions at different wavelengths

Large number of experimental and theoretical studies have been performed to understand the evolution of different properties of cluster as a function of their size. Jortner and co-workers theoretically studied the energetic, quantum, electronic, spectroscopic and electro-dynamic size effect in clusters by using cluster size equation.²⁵ Using density functional theory, He *et al.*¹³⁰ optimised the structure geometry and stability of different cluster size of lead sulfide and predicted the optical properties as function of cluster size. Experimentally Miyazaki *et al.*¹³¹ demonstrated the effect of cluster size on electronic spectroscopy of benzene – water clusters. Thus, cluster size plays a crucial role in determining the property of the cluster and this prompted us to study the ionisation phenomenon of methyl iodide cluster as a function of its size.

Methyl iodide clusters of different average size were produced by changing the nozzle diameter of pulsed valve. First set of experiments were carried out with nozzle diameter of 0.6 mm and laser wavelength has been varied at selected wavelengths of UV and visible region (i.e at 266 nm, 355 nm, 532 nm and 563 nm) at laser intensity of $\sim 10^9$ W/cm². At 266 nm, singly charged ions of C⁺, CH₃⁺, I⁺ and CH₃I⁺ were observed with I⁺ as the most intense peak alongwith cluster fragments like (CH₃)₂I⁺, I₂⁺, CH₃I₂⁺ and (CH₃I)₂⁺. However, there is no signature of multiply charged ions of carbon and iodine (figure 5.1(a)). When laser wavelength was changed to 355 nm, similar mass spectra were observed and once again multiply charged ions are absent (figure 5.1(b)). However when laser wavelength was shifted to 532 nm, multiply charged ions of carbon and iodine started appearing. Charge state of carbon and bromine are observed up to +3 at 532 nm (figure 5.1(c)). When laser wavelength

is further increased to 563 nm, charge state of carbon and iodine increased to +4 and +5 respectively (figure 5.1(d)). An attempt has been made to ionize methyl iodide clusters at 1064 nm. However, no ion signal was observed in the time-of-flight mass spectra. This could be because of higher number of photon requirement for multiphoton ionisation of methyl iodide clusters at 1064 nm. Thus, the results of methyl iodide clusters show similar trend as observed for other molecular clusters i.e. charge state of multiply charged ions increases with wavelength and the observation can be explained based on the three stage cluster ionisation mechanism (section 3.3.3).

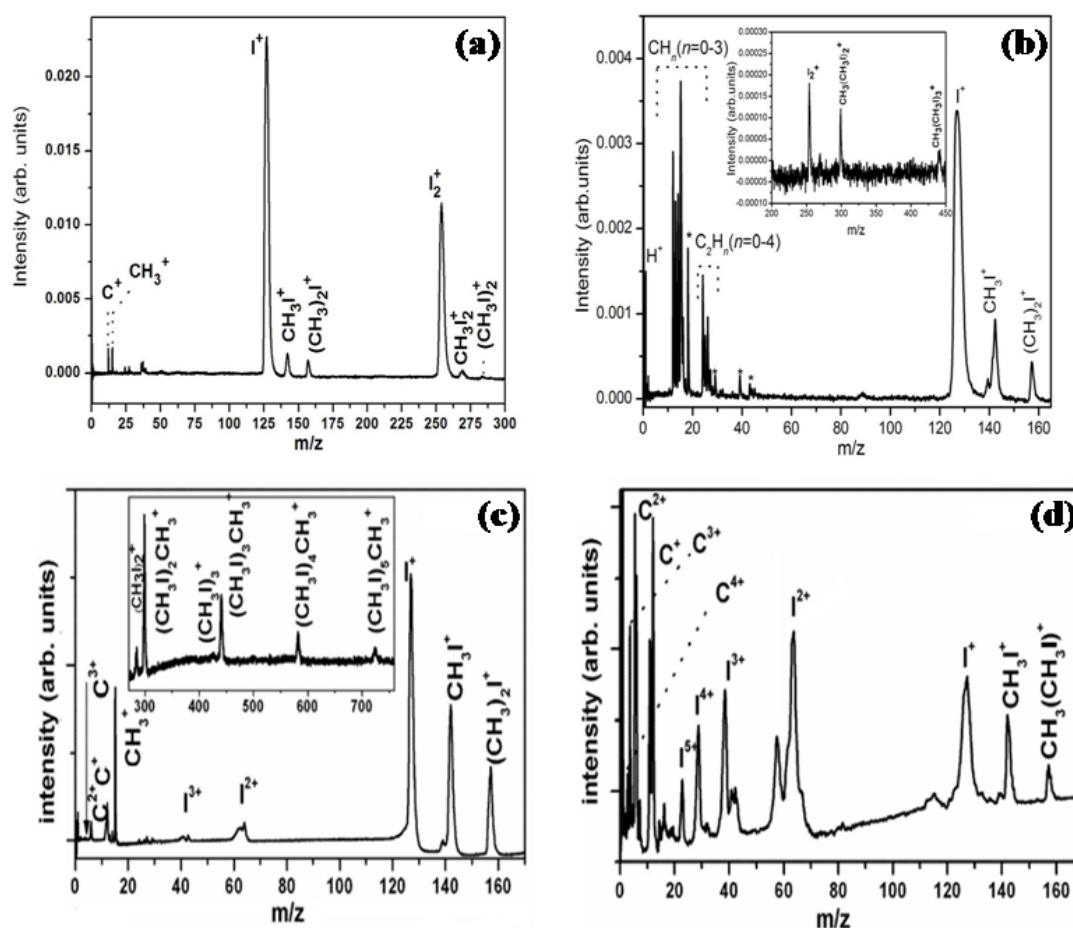


Figure 5.1: Time-of-flight mass spectra of methyl iodide clusters using 0.6 mm nozzle diameter at (a) 266 nm* (b) 355 nm (c) 532 nm and (d) 563 nm. * Time-of-flight mass spectra of 266 nm have been taken from reference 69.

In second set of experiments, nozzle diameter was increased to 0.8 mm and clusters so produced were ionised with different harmonics of nanosecond Nd:YAG laser pulses. As reported for 0.6 mm nozzle, at 266 nm, only singly charged ions of CH_3^+ , I^+ , CH_3I^+ , $(\text{CH}_3)_2\text{I}^+$ and I_2^+ are observed (figure 5.2(a)). However, at 355 nm, multiply charged ions of carbon and iodine started appearing in the mass spectrum. The charge state of carbon and iodine ion was limited to +2 (figure 5.2(b)). When laser wavelength was increased to 532 nm, charge state of carbon and iodine ions was found to increase up to +4 (figure 5.2(c)). Further, methyl iodide clusters on ionisation with 1064 nm laser pulses, showed dramatic increase in iodine ion charge state. Charge state of iodine ion increased to +11. However, charge state of

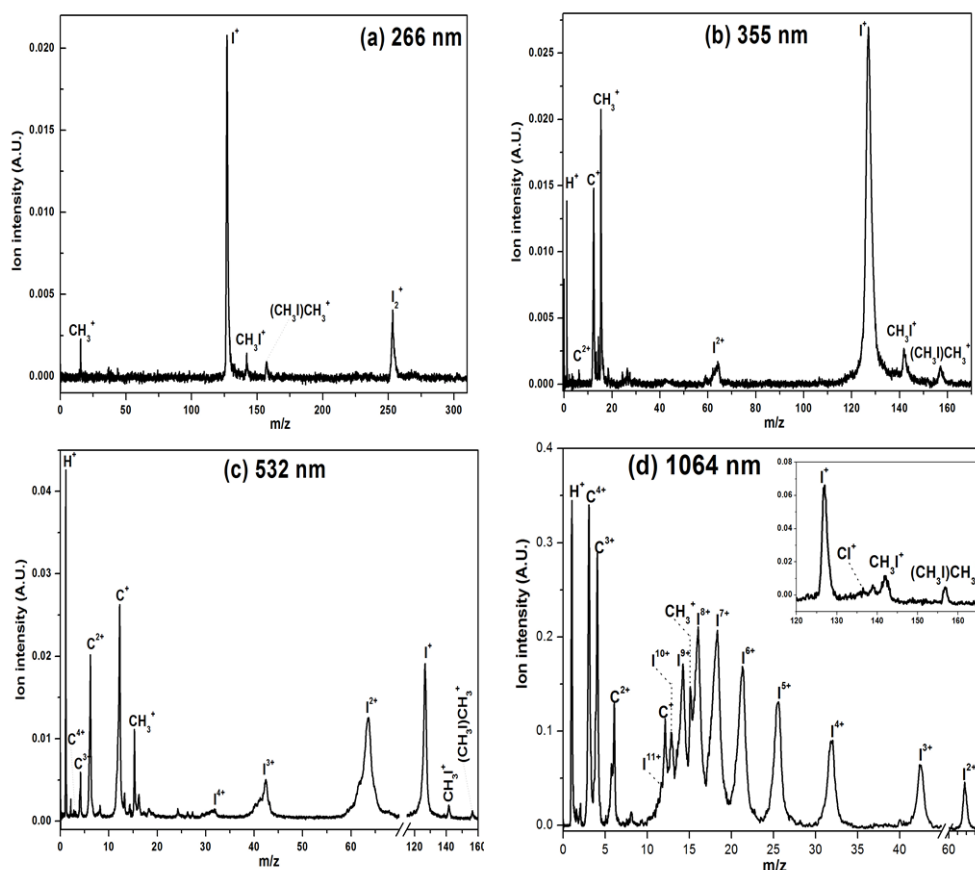


Figure 5.2: Time-of-flight mass spectra of methyl iodide clusters using 0.8 mm nozzle diameter at (a) 266 nm (b) 355 nm (c) 532 nm and (d) 1064 nm

carbon ions is limited to +4 because of very high ionisation energy of C^{4+} (~ 392 eV). Thus, similar trend has been observed in results of methyl iodide clusters produced using bigger diameter nozzle i.e. charge state of multiply charged ions increases with wavelength. Here it is worth mentioning that methyl iodide clusters produced by 0.8 mm nozzle diameter could be ionised by 1064 nm laser pulses however no ion signal was observed at this wavelength with clusters produced by 0.6 mm nozzle diameter. Higher intensity was used in case of 1064 nm which might be sufficient to induce multiphoton ionisation. Typically, the threshold laser intensity for observation of Coulomb explosion at 532 nm is found to $\sim 2 \times 10^9$ W/cm² however for 1064 nm the value is about 2.5 times more ($\sim 5 \times 10^9$ W/cm²).

If we compare the results of methyl iodide cluster produced by different nozzles at a given wavelength, then the effect of cluster size can be rationalised. At 355 nm, clusters produced by 0.6 mm nozzle diameter, gives rise to only singly charged ionic species. However, clusters produced by 0.8 mm nozzle diameter, were able to generate doubly charged carbon and iodine ions. Thus, for generation of multiply charged atomic ions under gigawatt intense laser conditions, a threshold cluster size is required. However, the size of methyl iodide clusters required for formation of multiple charge state can't be quantified because of inapplicability of the empirical formula (Hagena's parameter) for cluster size determination under our experimental conditions. Further, at 532 nm, with increase in cluster size, charge state of carbon and iodine has increased. Thus, bigger cluster size helps in inducing more charge state in the ionised clusters. This observation can also be explained based on the three stage cluster ionisation model (Chapter 3: section 3.3.3). According to the model, the inner ionised electrons are energised via inverse bremsstrahlung mechanism process and the higher charge states are produced in the cluster due to

electron ionisation. The larger cluster size helps in retaining the inner ionised electrons for longer duration and the electrons interact for more time with the laser pulse. As a result, the energy gained by the electron in larger cluster would be more and subsequently leading to higher charge state formation under laser intensity conditions. Thus, cluster size plays an important role in formation of multiply charged species under gigawatt intensity conditions.

5.3.2 Effect of extraction field on kinetic energy of multiply charged ions of carbon and iodine

Methyl iodide clusters produced using 0.6 mm nozzle diameter were ionised with 532 nm laser pulses and kinetic energy of multiply charged ions of carbon and iodine was measured based on peak splitting method. As described in earlier chapter (section 4.3.2), peak splitting method is based on the difference of arrival time of forward and backward ion peak for determination of kinetic energy of multiply charged ions. Thus, kinetic energy of different charge state of carbon and iodine were determined using the above mentioned method and listed in Table 5.1. It is evident from the table that kinetic energy of multiply charged ions of carbon and iodine increases with charge state.

In order to verify whether there is any effect of extraction field on kinetic energy of Coulomb exploding multiply charged ions, extraction field of the ions in the time-of-flight mass spectrometer has been varied in the range of 250 V/cm to 600 V/cm and kinetic energy of different charge states has been measured. Since the peak splitting method relies on the time difference of the forward and backward peak of the ion peak, the extraction field has been changed in the limited range during the experiment so that resolution of forward and backward peak is sufficient to determine kinetic energy. Figure 5.3 shows kinetic energy of different charge states of carbon and iodine ions at different extraction voltage in time-of-flight mass spectrometer.

Table 5.1: Kinetic energy of multiply charged atomic ions on 532 nm photo ionisation, based on arrival time difference ‘ Δt (in nanoseconds)’ between forward and backward ion peak of mass m (in amu), calculated using formula ‘ $E_{\text{kin}} = 9.65 \times 10^{-7} \Delta t^2 n^2 F^2 / 8m$ ’, where F is the static electric field for ion extraction in V cm^{-1} and n is the charge of the ion.

Charge state	Kinetic energy (eV)
C^+	29 ± 6
C^{2+}	115 ± 30
C^{3+}	325 ± 26
I^+	18 ± 2
I^{2+}	114 ± 12
I^{3+}	376 ± 25

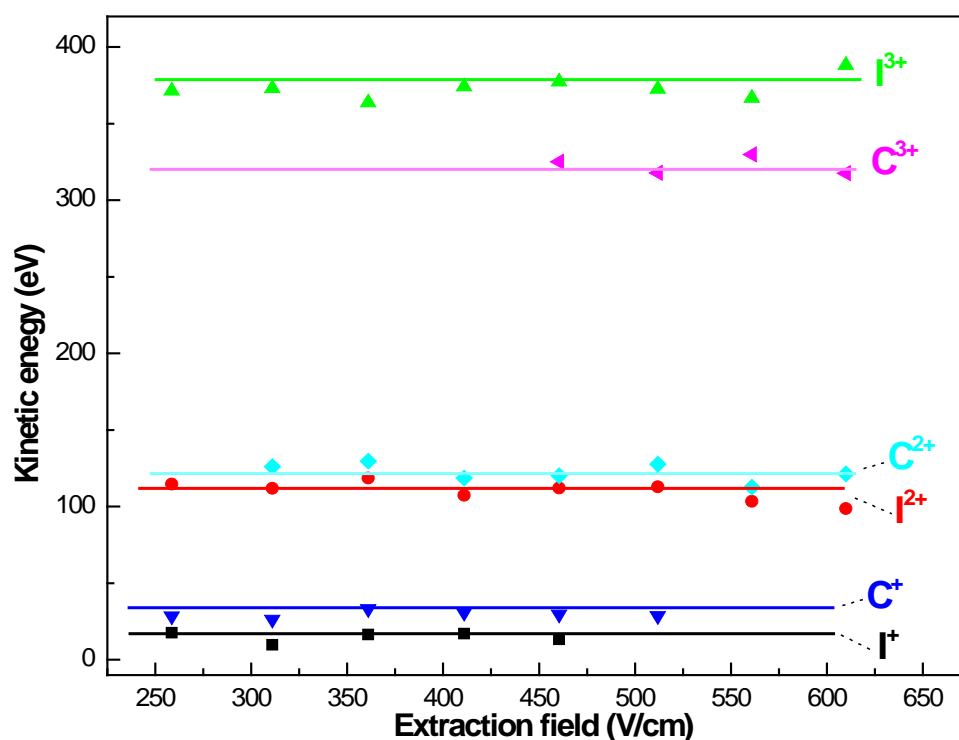


Figure 5.3: Kinetic energy of multiply charged ions of carbon and iodine as a function of extraction field in time-of-flight mass spectrometer for 532 nm photo ionisation

From the figure, it is clear that the kinetic energy of multiply charged ions is more or less same (within statistical fluctuation) even though the extraction field has been changed by a factor of 2.4. Thus, the kinetic energy measured by this method is a manifestation of the strong Coulomb repulsive forces in the ionized cluster and remains unaffected by the externally applied electric field for ion extraction.

5.3.3 Effect of laser polarisation on ion yield and kinetic energy of multiply charged ions

Laser polarisation plays an important role in determining the spatial distribution of the fragment ions formed due to laser-cluster interaction. In literature, symmetric as well as asymmetric ion distribution has been reported under different experimental conditions.^{132,133} Kumarappan *et al.*¹¹⁶ experimentally showed asymmetric explosion in argon cluster (~ 40,000 atoms/cluster) where laser polarisation direction of the intense femto second laser plays a decisive role for the observation. Kosmidis and co-workers^{134,135} studied the ejection anisotropy of fragments produced from different alkyl halide clusters using picosecond and femto second laser pulses. Their study reveals that majority of the ions are ejected in a direction parallel to the laser polarization vector. Theoretical studies show that a multiply charged cluster can decay either by binary/ tertiary fission or by Coulomb explosion. The former is spatially anisotropic via one axis elongation of the charged cluster forming two large fragments. On the other hand, Coulomb explosion process is isotropic with small ionic fragments expanding radially.¹³⁶ However, these theoretical studies have been performed for high laser intensity cases (10^{14} – 10^{20} W/cm²) and no information is available regarding the spatial distribution of fragment ions in case of nanosecond laser induced Coulomb explosion. Therefore, in order to understand the effect of laser polarization on the phenomenon of Coulomb explosion of clusters

under our experimental conditions, laser polarization dependent mass spectroscopic experiments were carried out.

Figure 5.4 (a) and (b) illustrate time-of-flight mass spectra of CH_3I clusters (produced using 0.6 mm nozzle diameter) recorded under parallel (0°) and (b) perpendicular (90°) laser polarization with respect to the time-of-flight axis at 532 nm.

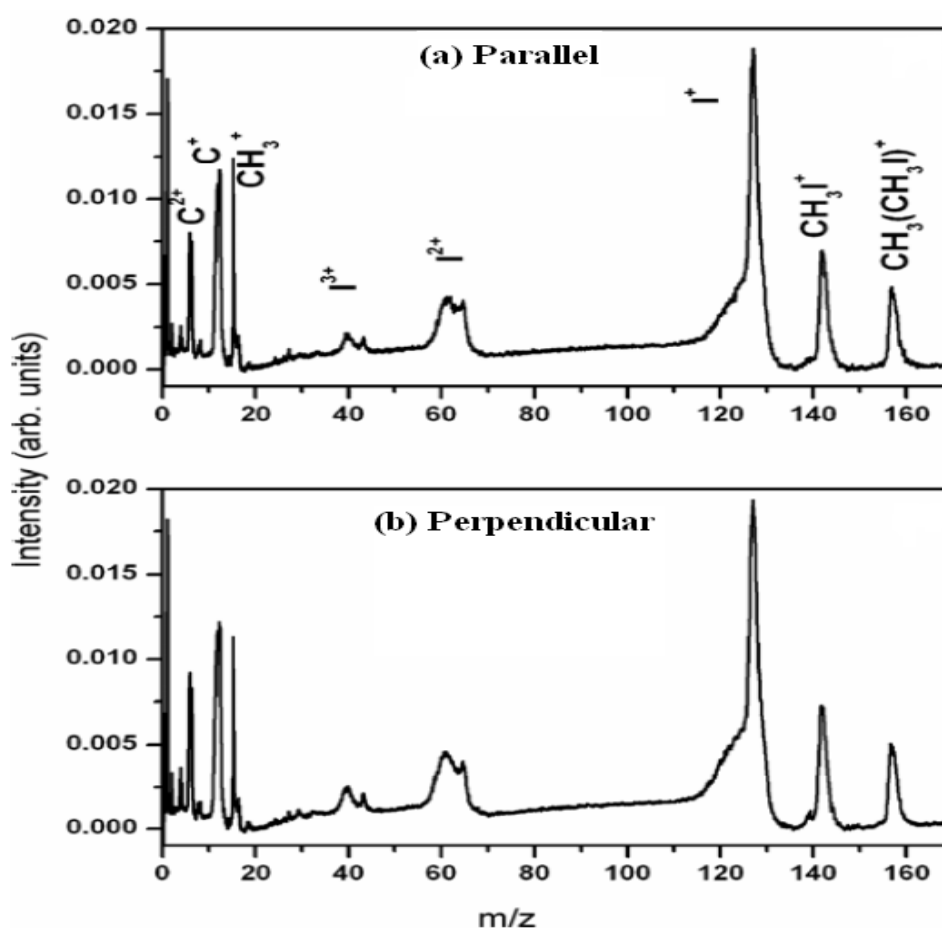


Figure 5.4: Time-of-flight mass spectra of ions produced by photo ionisation of CH_3I clusters at 532 nm (a) parallel (0°) and (b) perpendicular (90°) polarization with respect to time-of-flight axis

From the figure, it can be realized that, the fragmentation pattern as well as the ion intensity distribution are found to be similar, suggesting isotropic disintegration of multiply charged CH_3I cluster. Moreover, the transient electric field due to

nanosecond laser pulses having intensity $\sim 10^9$ W/cm² is not sufficient to align the Coulomb exploded multiply charged ions in a particular direction and thus the mass spectra at parallel and perpendicular polarization remains same in terms of speciation as well as ion intensity.

Figure 5.5 shows kinetic energy of multiply charged ions C^{2+} , C^{3+} , I^{2+} and I^{3+} as a function of polarization angle of laser beam with respect to time-of-flight axis. Similarly, figure 5.6 shows variation in ion yield of multiply charged ions as a function of laser polarization angle with respect to the time-of-flight axis. From these figures, it is clear that the ion yields as well as their kinetic energies are found to be independent of laser polarization angle, thus indicating that the Coulomb explosion process induced by nanosecond laser in clusters is isotropic.

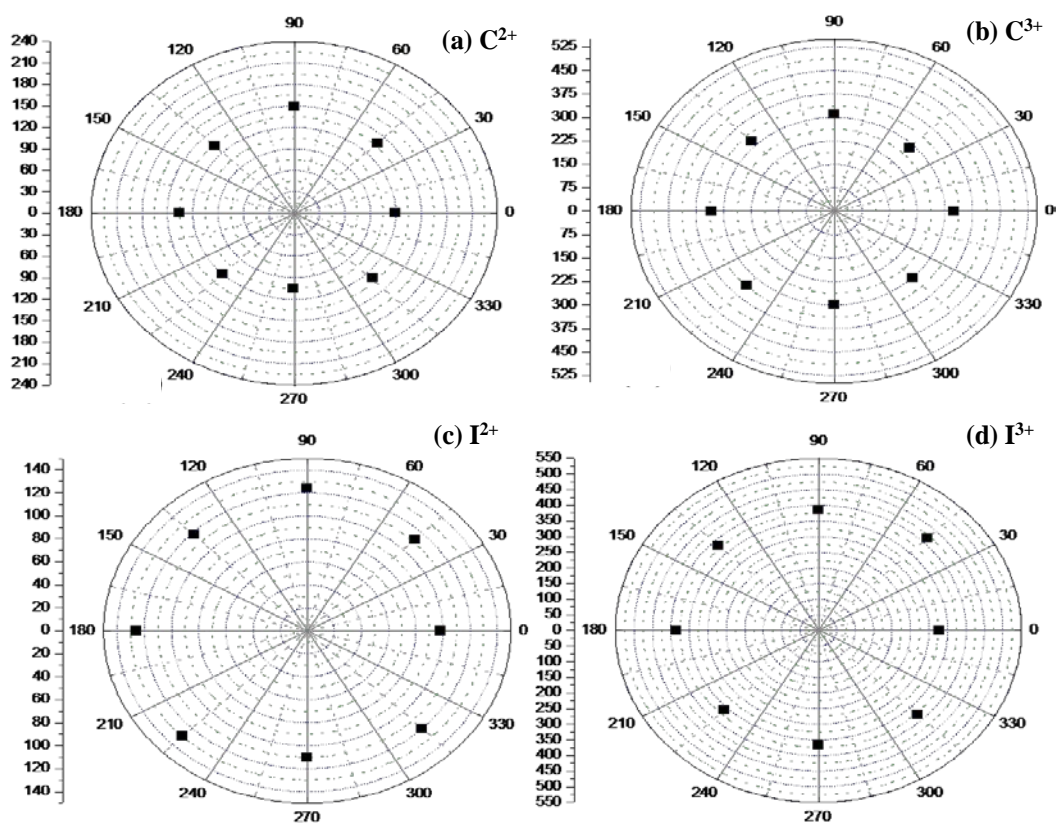


Figure 5.5: Variation in kinetic energy of multiply charged ions (a) C^{2+} (b) C^{3+} (c) I^{2+} and (d) I^{3+} as a function of plane of polarisation

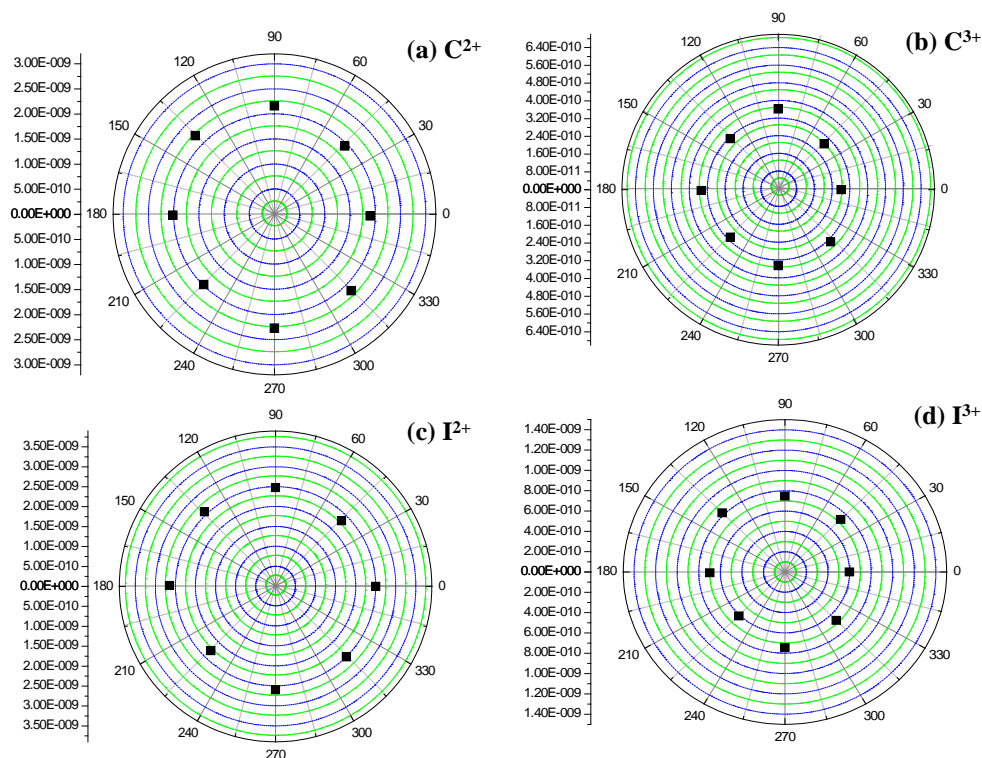


Figure 5.6: Variation in ion yield of multiply charged ions (a) C^{2+} (b) C^{3+} (c) I^{2+} and (d) I^{3+} as a function of plane of polarisation

5.3.4 Effect of dopant in cluster ionisation dynamics

When clusters are made up of similar constituent they are called homogeneous cluster whereas presence of more than one cluster constituents produces heterogeneous clusters or mixed clusters. If a particular constituent is found to be much less compared to other constituent in the mixed clusters than the cluster system can be termed as doped cluster where the constituent with lower concentration acts as the dopant. Dopant plays an important role in altering the property of the mixed cluster and that is subsequently reflected in their photophysical/chemical behaviour. For example, Jha *et al.*¹³⁷ observed enhancement in X-ray yield and generation of hotter electrons, when Ar clusters were doped with H_2O . Intra-cluster ion molecule reaction has been observed in benzene doped water clusters.¹³⁸ Thus, an attempt has been made to generate mixed clusters i.e. neutral methyl iodide cluster along with some dopant molecule. Photo ionisation of the doped molecular system was then

studied using time-of-flight mass spectrometry to see what is the fate of dopant molecule which does not absorb laser radiation.

In the present set of experiments, methyl iodide was doped with water. Following are the reasons why we have chosen water as dopant under our experimental conditions-

(i) Water has higher ionisation energy (12.62 eV) as compared to that of methyl iodide (9.54 eV). This higher ionisation potential of water reduces the multiphoton ionisation probability of the water significantly as compared to that of methyl iodide molecules/clusters under identical laser excitation conditions. Thus, methyl iodide is only ionisable species via multiphoton ionisation process under our experimental conditions which would help in understanding the ionisation process in mixed clusters.

(ii) Further, water has much lower vapour pressure (25 mm of Hg at 25⁰ C) as compared to that of methyl iodide (437 mm of Hg at 25⁰ C). Hence on co-expansion, the methyl iodide clusters have minor contribution from dopant water molecules.

(iii) Another requirement from experimental point of view is the fact that, the multiply charged ions of dopant should be different from carbon and iodine and should be unambiguously assignable. Water meets all these criteria as well as it is easily available in the pure form. So water was chosen as dopant.

No ion signal arising due to interaction of water clusters with laser pulse could be observed under our experimental conditions when pure H₂O clusters generated by supersonic expansion of H₂O vapors at room temperature seeded in 1–5 atm pressure of the helium are subjected to 563 nm laser pulses of gigawatt intensity. As mentioned above, the probable explanation for this observation could be lower multiphoton ionisation cross-section of water clusters at 563 nm. However, when

water doped methyl iodide clusters (generated by supersonic expansion of CH_3I and water sample mixed in 9:1 ratio (by volume) are subjected to 563 nm laser radiation, these doped clusters are found to undergo Coulomb explosion resulting in generation of energetic multiply charged atomic ions of oxygen (up to O^{4+}) in the time-of-flight mass spectra along with other multiply charged atomic ions of carbon and iodine. Therefore, this study demonstrates that doping of methyl iodide clusters with water leads to induction of Coulomb explosion in dopant water which now forms an integral part of methyl iodide cluster. These results show that Coulomb explosion is a collective property of the cluster as a whole and individual molecular properties do not play significant role.

Apart from that, this method provides an alternate pathway to ionize molecules or molecular clusters which have high ionisation energy and could not be ionized in pure form under low laser intensity conditions. The low ionisation energy molecule (in this case methyl iodide) is ionized via multiphoton ionisation under gigawatt intense laser field. Thus providing the quasifree inner ionized electron in the cluster and the electron gains energy from the laser field via inverse bremsstrahlung process. When electron energy crosses the ionisation energy of the dopant molecule, single ionisation is induced in the dopant molecule (in this case H_2O). Further increase in the electron energy leads to generation of doubly charged ions of dopant molecule and the process keeps on repeating itself. Thus, the energized electron ionizes the cluster constituents indiscriminately and causes multiple ionisation of both $(\text{CH}_3\text{I})_n$ and the dopant $(\text{H}_2\text{O})_n$. These doped cluster experiments also reveal an additional proof of electron heating mechanism for generation of multiply charged ions under gigawatt intense laser field.

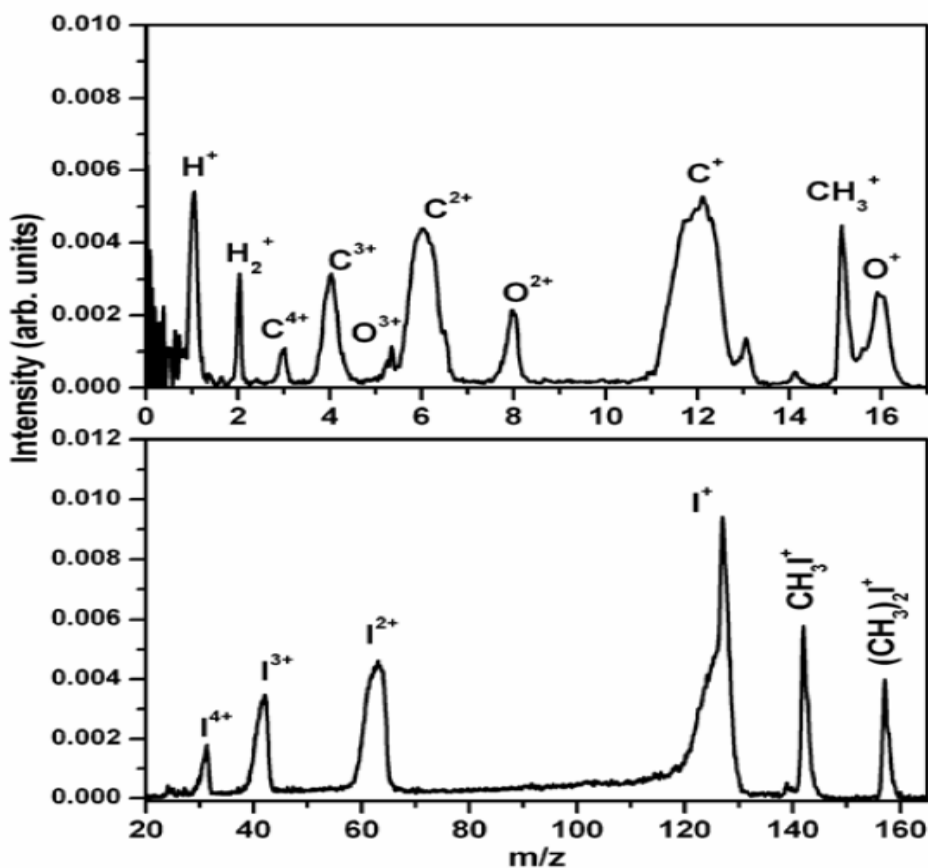


Figure 5.7: Time-of-flight mass spectra of $\text{CH}_3\text{I}-\text{H}_2\text{O}$ mixed clusters when subjected to 563 nm laser pulses at an intensity of $\sim 10^9 \text{ W/cm}^2$.

5.4 Conclusions

In conclusion, we have carried out nanosecond laser induced Coulomb explosion studies in methyl iodide clusters by varying several experimental parameters and effect of these parameters has been investigated on generation of multiply charged ions. First of all, cluster size of methyl iodide has been varied by changing the nozzle diameter and irradiated with different wavelengths. From the time-of-flight mass spectra, it can be concluded that there is a threshold cluster size required for generation of multiply charged ions under gigawatt intense laser field and charge state of the ions increases with cluster size. However, the threshold cluster size for methyl iodide cluster can't be estimated because of inapplicability of the Hagena's empirical parameter under our expansion conditions. Secondly, effect of extraction

field on kinetic energy of multiply charged ions has been studied. It has been demonstrated that the large kinetic energy of multiply charged ions is a result of violent explosion of the ionized cluster and extraction field has no effect on kinetic energy of these ions. Moreover, polarization angle of laser has been varied using half wave plate and time-of-flight mass spectra have been recorded. Ion intensity and kinetic energy of different multiply charged ions were found to be independent of the laser polarization angle and cluster explodes isotropically in the interaction region. The studies have also been extended to mixed cluster where water is used as dopant in methyl iodide clusters. In mixed cluster experiments, Coulomb explosion has been induced in dopant molecule which gives rise to multiply charged ions of oxygen (from H₂O) along with other ions of carbon and iodide (from CH₃I). This result also suggests that electron heating mechanism is responsible for multiply charged atomic ion formation under gigawatt intense laser field.

Chapter 6

Interaction of xenon clusters with nanosecond laser pulses: Determination of minimum cluster size and threshold laser intensity for observation of multiply charged ions

6.1 Introduction

In the previous chapters (3, 4 and 5), interaction of nanosecond laser pulses of intensity $\sim 10^9$ W/cm² with different molecular clusters such as CF₂Br₂, C₂H₅Br and CH₃I has been described. Multiply charged atomic ions were observed with high kinetic energy in time-of-flight mass spectra. In order to understand the mechanism of formation of multiply charged atomic ions under such low laser intensity conditions, several laser and cluster parameters were varied and results obtained were explained based on the available literature. However, molecular clusters have inherent complications such as presence of several dissociation channels, energy dependent electron attachment processes leading to formation of metastable negative ions etc. which complicate understanding of multiply charged ion formation. These complications can be eliminated if studies are carried out using inert gas atomic clusters. Therefore, xenon clusters were chosen and interacted with nanosecond laser pulses of intensity $\sim 10^9$ W/cm².

Most of the earlier reported studies deal with interaction of xenon cluster with highly intense laser pulses of ultra short duration and explosion dynamics has been studied as a function of laser wavelengths and cluster size. In different experiments, wavelength of ionisation has been varied from IR to soft x-ray region. Ditmire *et al.*⁶¹ have studied interaction of xenon clusters (consisting of 2500 atoms) with 800 nm femtosecond laser pulses of intensity 2×10^{16} W/cm². Multiply charged xenon ions

were observed up to +40 state with kinetic energy as high as 1 MeV. Springate *et al.*¹³⁹ have performed experiments under similar laser conditions and showed that clusters consisting of $\sim 10,000$ atoms is optimum in order to generate maximum kinetic energy ions. Observation of such highly energetic and multiply charged xenon ions was explained based on efficient heating of the nanoplasma electrons by the intense laser pulse.¹⁴⁰ According to the nanoplasma model, the clusters are assumed to be initially neutral spheres with uniform temperature and density. There will be no gradients in density and temperature in the cluster during further evolution of the nanoplasma. The plasma is heated due to the interaction with the laser radiation which is described by collisional absorption (inverse bremsstrahlung).¹⁰⁷ Castleman and coworkers¹⁴¹ studied interaction of xenon clusters at 624 nm having laser intensity $\sim 10^{15}$ W/cm². They reported multiply charged xenon ions with charge states up to +20. Observation of such high charge state at 624 nm is accounted using ionisation ignition model. According to this model, after the initial ionisation events, the parent ion cores are inertially confined to the cluster because the much lighter electrons depart quickly, leaving the ion field unscreened. This results in a very large and inhomogeneous electric field. This large field lowers the ionisation barrier and enables subsequent ionisation events to occur, which in turn further increases the field and lowers the ionisation barrier. Hence, the fields created by the initial ionisation events “ignite” the cluster to undergo subsequent ionisation. Further, interaction of Xe_N (N= 1-30,000) has been studied using 98 nm free electron laser pulses of intensity $\sim 10^{13}$ W/cm² by Wabnitz *et al.*⁷ Multiply charged xenon ions up to +8 were observed as a result of interaction of xenon clusters with free electron laser. Under such short laser wavelength, inverse bremsstrahlung heating mechanism is found to be ineffective because of low ponderomotive energy of electrons. Role of resonant intermediate

states has been emphasized for generation of such multiple charge state of xenon.¹⁴² These experimental results have been complemented by theoretical model which predicts that recombination contributes significantly to the ionisation dynamics and large fraction of neutrals exist within the core resulting from the recombination.¹⁴³ Moreover, even at a wavelength of 13.9 nm (intensity $\sim 2 \times 10^{10}$ W/cm²) generation of multiply charged xenon ions up to Xe⁴⁺ has been reported, which arise due to inner shell (4d) ionisation of xenon cluster ($\sim 20,000$ atoms/cluster).¹⁴⁴

Laser interaction studies have also been carried out on xenon clusters as a function of cluster size. It has been demonstrated that in the small cluster regime the dynamics of the cluster expansion is controlled by the Coulombic forces^{145, 146} while for comparatively larger clusters, the hydrodynamic force dominates the cluster expansion dynamics^{147, 148}. When xenon clusters were subjected to few cycle laser pulses, the order of charge state as well as the kinetic energy of xenon ions generated are found to be significantly lower, as a result of inefficient laser-cluster coupling due to ultrashort interaction time-scale.¹²² Additionally the ion yield in few cycle pulse studies was found to be independent of the cluster size, which is in sharp contrast to results obtained at comparatively longer laser pulse duration of 150 fs. Thus above studies clearly demonstrate that cluster size, laser wavelength and laser-cluster interaction time-scale play decisive roles in determining the charge state, yield and kinetic energy of multiply charged atomic ions.

In the present work, photoionisation of xenon cluster has been studied using nanosecond long laser pulses as a function of wavelength and cluster size. Laser wavelength has been varied from UV (266 and 355 nm) to visible (532 nm) region at a laser intensity of $\sim 10^9$ W/cm². Multiply charged ions of xenon could be observed in time-of-flight mass spectrum at all three wavelengths and the charge state of xenon

increases with increasing wavelength. Earlier, Luo *et al.*¹⁴⁹ have reported generation of Xe¹¹⁺ upon irradiation of xenon clusters (0.4 MPa, 0.5 mm nozzle) with 532 nm pulses of slightly higher laser intensity ($I \sim 10^{11}$ W/cm²). Moreover, cluster size of xenon (Xe_N) has been varied (N varies from 10-10,000) to determine the threshold cluster size required for generation of multiply charged xenon ions. With increase in the cluster size, the ion kinetic energy was found to increase whereas threshold laser intensity for generation of multiply charged ion decreases. Apart from that, experiments have been carried out in water doped xenon cluster to understand the effect of dopant in ionisation dynamics of atomic clusters.

6.2 Experimental details

Details of the experiments have been described in Chapter 2 and only a brief description relevant to this work is being given here. Clusters were produced by supersonic expansion of pure xenon gas (purity = 99.999 %) using a pulsed nozzle source. Size of the xenon cluster has been varied by modifying expansion conditions i.e. using different diameter nozzle (0.3 and 0.8 mm) and by changing the stagnation pressure (0.5 - 4 atm) of xenon gas. Average size of xenon cluster $\langle \text{Xe}_N \rangle$ is estimated using the empirical formula of Hagena. The dimensionless Hagena's parameter (Γ^*) is expressed as⁷⁷ -

$$\Gamma^* = k \frac{(d / \tan \alpha)^{0.85}}{T_0^{2.29}} P_0 \quad (6.1)$$

Where d is the nozzle diameter (μm), α the expansion half angle ($\alpha=45^\circ$ for sonic nozzles, $\alpha<45^\circ$ for supersonic nozzles), P_0 the stagnation pressure (mbar), T_0 the pre-expansion temperature (Kelvin) and k a constant related to the bond formation. The average size of the cluster in terms of the number of atoms per cluster can be written as¹⁵⁰ -

$$N \cong 33 \left[\frac{\Gamma^*}{1000} \right]^{2.35} \quad (\Gamma^* \leq 10^4) \quad (6.2)$$

$$N \cong 100 \left[\frac{\Gamma^*}{1000} \right]^{1.8} \quad (\Gamma^* > 10^4) \quad (6.3)$$

Using equation 6.2 and 6.3, average cluster size of xenon was estimated under a given set of expansion conditions.

6.3 Results and Discussion

6.3.1 Effect of laser wavelength on photo ionisation of xenon clusters

Figure 6.1 represents time-of-flight mass spectrum of $\langle \text{Xe}_{11400} \rangle$ clusters photo ionised with 266 nm laser pulses (intensity $\sim 10^9 \text{ W/cm}^2$). The spectrum depicts generation of multiply charged atomic ions of xenon up to +3 state (IE (Xe^{3+}): 32.1 eV) at 266 nm. Under similar experimental conditions, on changing the photoionisation wavelength to 355 nm, the highest observed charge state of xenon ions increased to +6 (IE (Xe^{6+}): 71.8 eV). (figure 6.2), while for the case of photoionisation at 532 nm, generation of multiply charged xenon ions up to +10 (IE (Xe^{9+}): 202 eV) (figure 6.3) was observed. Therefore, it is very clear from the spectra that charge state of multiply charged xenon ions increases with increasing laser wavelength. Apart from that, cluster fragments at different wavelength have been shown in respective graphs. At 266 nm, Xe_2^+ to Xe_{14}^+ were observed whereas only dimer (Xe_2^+) signal could be detected at 355 nm. However, no ion signal due to cluster fragment was observed at 532 nm. This could be because of differential charging of the ionized cluster at different wavelengths. Formation of higher charge states at longer wavelengths can be qualitatively understood in terms of three stage cluster ionisation model [as described in Chapter 3 (3.3.3)]. However, since the charge state of xenon at all three wavelengths is higher compared to the molecular clusters thus energization of inner ionized electron is expected to be higher

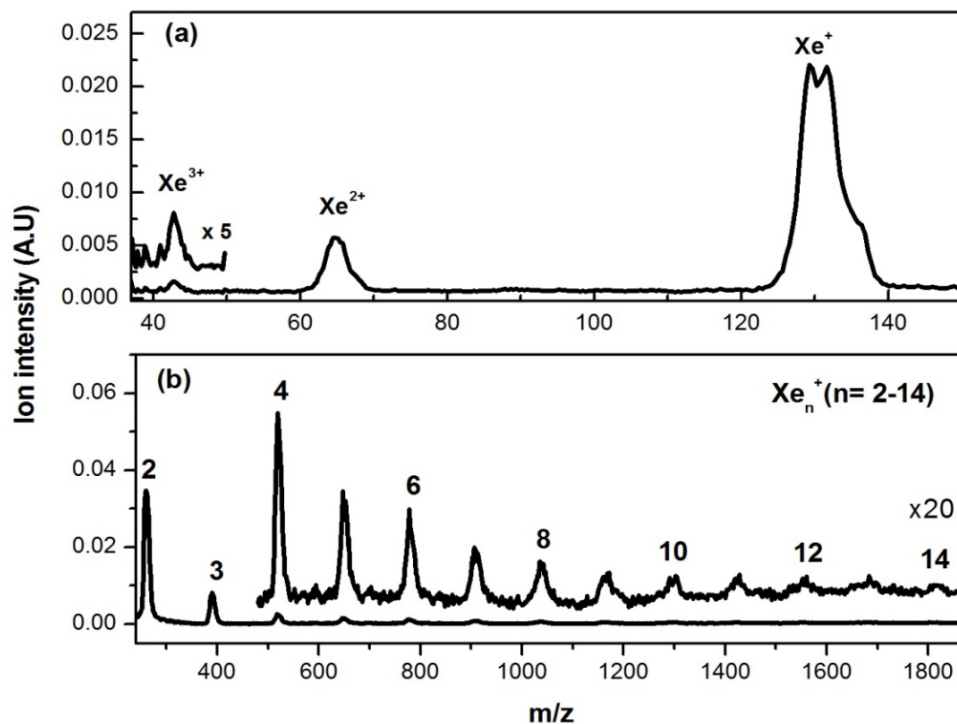


Figure 6.1: Time-of-flight mass spectrum of xenon clusters subjected to photo ionisation by 266 nm laser pulse of intensity $\sim 10^9 \text{ W/cm}^2$. (a) depicts multiply charged ions up to +3 while (b) represents the cluster ion fragments up to Xe_{14}^+ .

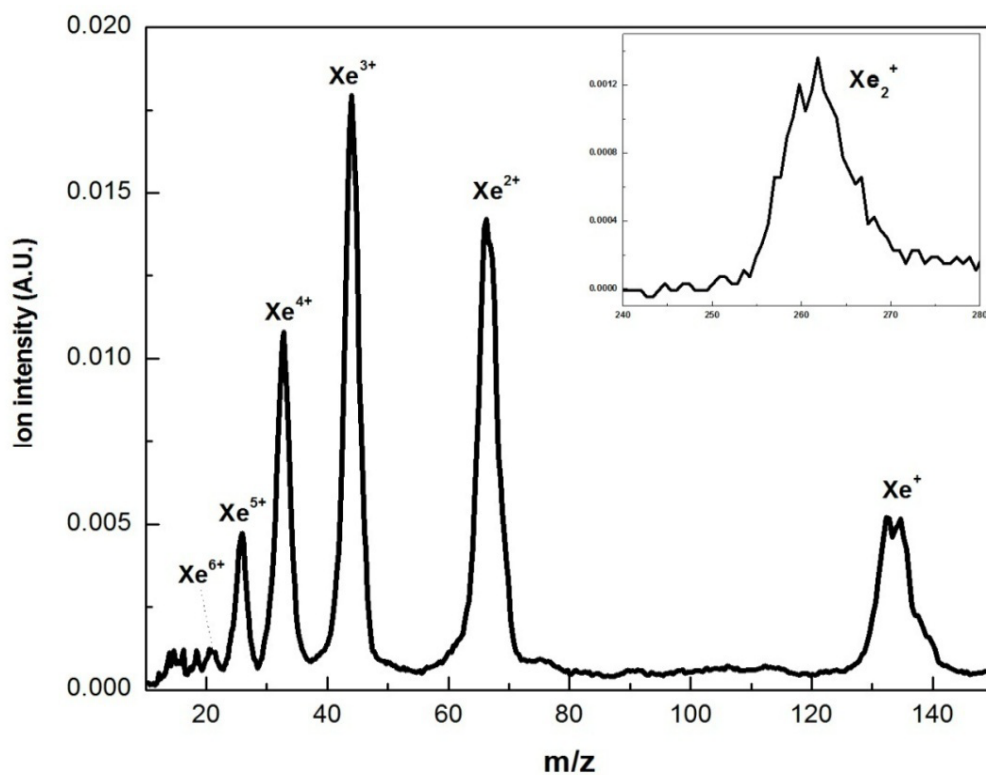


Figure 6.2: Time-of-flight mass spectrum of xenon clusters subjected to 355 nm photo ionisation by laser intensity $\sim 10^9 \text{ W/cm}^2$. Inset depicts xenon dimer ions observed in the mass spectrum.

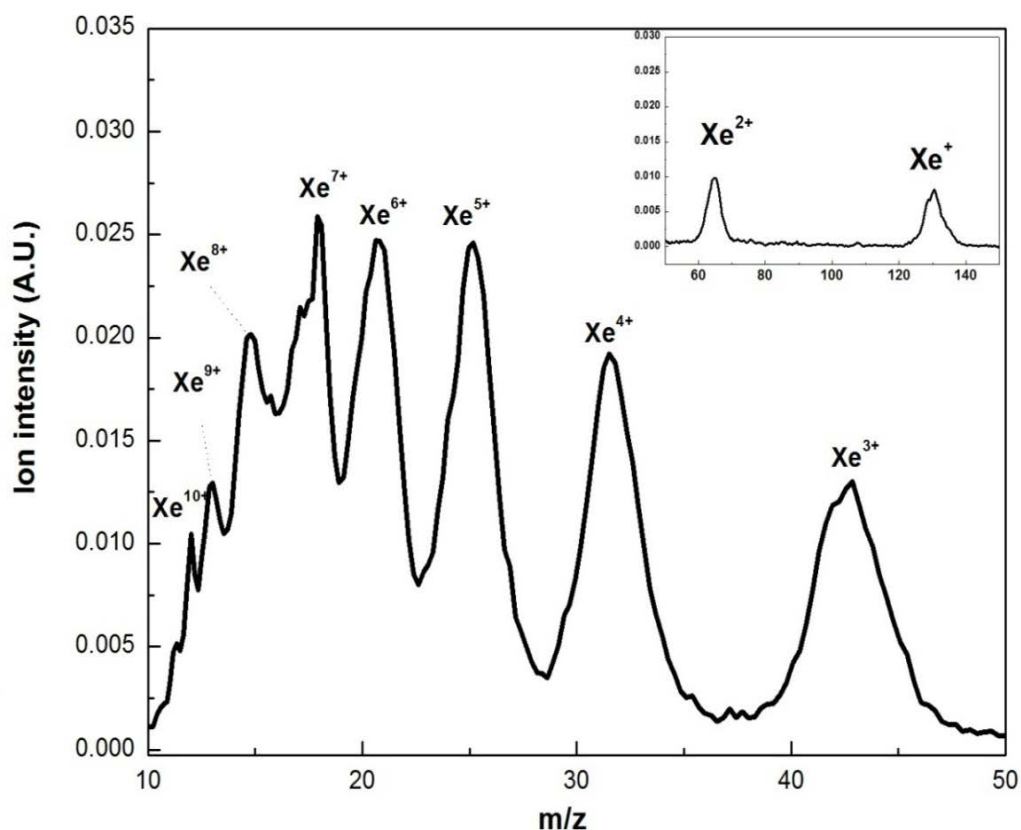


Figure 6.3: Time-of-flight mass spectrum of xenon clusters subjected to photo ionisation by 532 nm laser pulse of $\sim 10^9$ W/cm². Singly and doubly charged xenon ions are shown in the inset.

in atomic cluster as compared to their molecular counterpart under similar experimental conditions.

In Chapter 5, it was observed that size of cluster affects the charge states of atomic ions for ionization at a given wavelength. However, in case of methyl iodide cluster, the average size for generation of multiply charged ions can't be estimated because $(\text{CH}_3\text{I})_n$ clusters are produced by using a carrier gas (Helium gas) and the Hagen's empirical formula is not applicable to such experimental conditions. In xenon clusters, average size of the cluster interacting with the laser pulse can be calculated based on the empirical formula and an attempt has been made to estimate the minimum cluster size which undergoes multiple ionisation.

6.3.2 Determination of threshold cluster size for observation of multiply charged ions

Out of the three wavelengths that have been used under our experimental conditions, 532 nm is found to produce highest charge state of the xenon ions (Xe^{10+}), hence this wavelength was employed for threshold cluster size determination. In order to determine, the threshold cluster size for observation of multiply charged ions, average cluster size has been varied from tens of atoms to thousand of atoms of xenon. For generation of small xenon clusters, 0.3 mm nozzle diameter is employed and cluster size is varied by changing the back up pressure. Figure 6.4(a) shows mass spectrum on irradiation of $\langle \text{Xe}_{17} \rangle$ with 532 nm laser light. Singly charged cluster ions (up to Xe_4^+) were observed and multiply charged ions are completely absent. However, irradiation of $\langle \text{Xe}_{50} \rangle$ resulted in a completely different mass spectrum (figure 6.4(b)). Multiply charged xenon ions are clearly seen in the mass spectrum. Therefore, the minimum cluster size for observation of multiply charged xenon ions under gigawatt laser intensity irradiated with 532 nm laser light lies between $17 < N < 50$ where N is the number of atoms in the xenon cluster. This result can be rationalized on the basis of the three stage cluster ionisation mechanism dealing with extraction of laser energy by cluster confined quasi-free electrons resulting in generation of multiply charged ions. $\langle \text{Xe}_{17} \rangle$ clusters undergo multiphoton ionisation leading to generation of cluster fragments in the mass spectra. $\langle \text{Xe}_{17} \rangle$ cluster can be assumed to be similar to $\langle \text{Xe}_{13} \rangle$ icosahedra structure where one xenon atom is surrounded by 12 xenon atoms (first shell). In contrast, $\langle \text{Xe}_{50} \rangle$ can be compared to $\langle \text{Xe}_{55} \rangle$ with an extra shell of xenon atoms ($R \sim 10 \text{ \AA}$). Thus, the results of the present study show that clusters having only one shell are not able to extract enough energy from the laser field to cause multiple ionisation. On the other hand, slightly bigger clusters having one extra shell of xenon atoms does cause multiple ionisation. We

thus conclude that photoionised electrons in $\langle Xe_{17} \rangle$ are not retained inside the cluster as quasi free electrons for a period long enough to extract energy and cause multiple ionisation unlike those in $\langle Xe_{50} \rangle$.

In the second set of experiments, 0.8 mm diameter nozzle was used and by varying the stagnation pressure of xenon gas, clusters of average size ranging from $\langle 600 \rangle$ to $\langle 11400 \rangle$ atoms could be investigated. However, as can be seen from figure 6.5, increasing the cluster size from 600 to 11400 did not change the experimentally observed highest charge state of xenon ions beyond +10 which is present even for the case of $\sim \langle 50 \rangle$ atom xenon cluster, though the individual ion signal increases with cluster size. With increase in cluster size, one would expect efficient caging of the inner ionised electrons in a larger cluster, which would subsequently cause an enhancement in the charge state, as well as the kinetic energy of the multiply charged atomic ions. Such a behavior was previously observed in our studies on methyl iodide

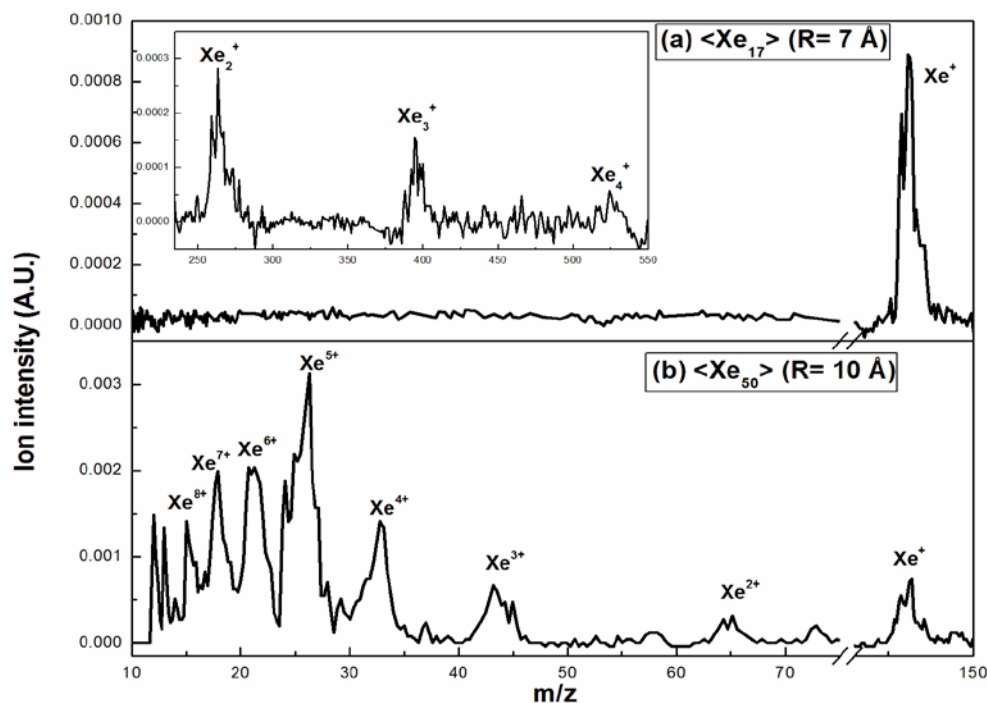


Figure 6.4: Time-of-flight mass spectra of xenon clusters photo ionised by 532 nm laser pulses of intensity $\sim 10^9 \text{ W/cm}^2$; nozzle diameter: 0.3 mm at (a) 0.5 atm (Xe_{17}) and (b) 0.8 atm (Xe_{50}) pressure of xenon

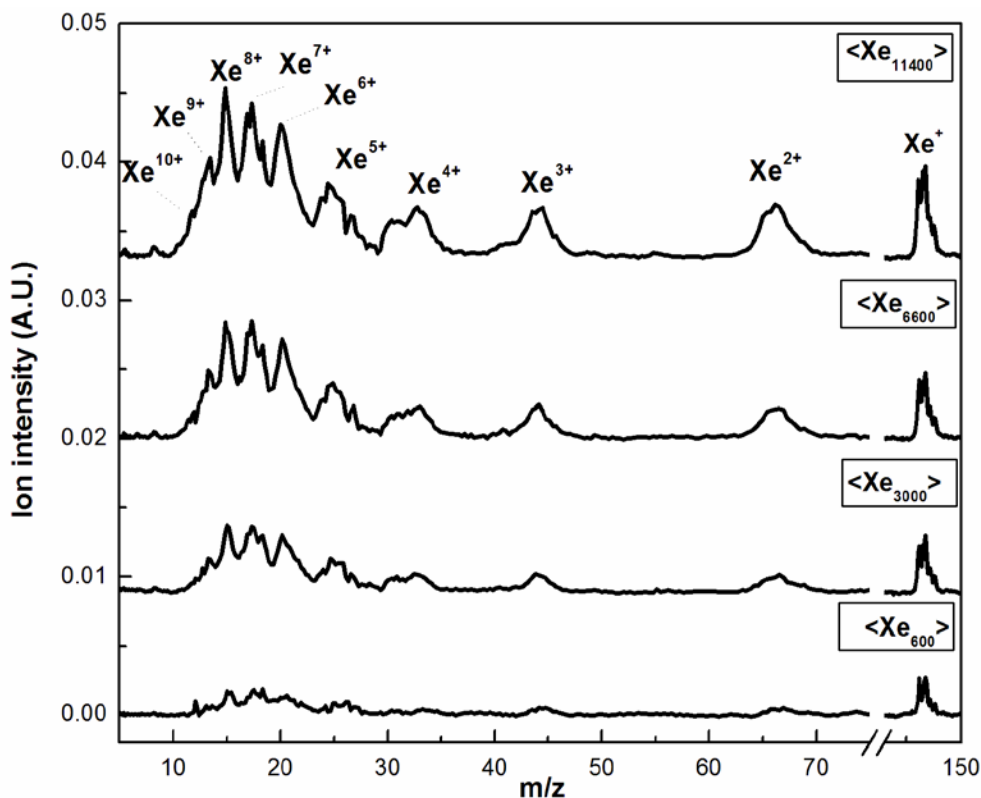


Figure 6.5: Time-of-flight mass spectra of xenon clusters as function of cluster size (Ionisation wavelength: 532 nm, Intensity: $\sim 10^9$ W/cm², Nozzle diameter: 0.8mm)

clusters (Chapter 5), tetramethyl silane doped Ar clusters,¹⁵¹ under similar experimental conditions. However, no enhancement in the charge state of the xenon ions could be observed. Therefore, the kinetic energy of multiply charged xenon ions was measured as a function of cluster size and results are reported in the next section.

6.3.3 Kinetic energy of multiply charged xenon ions as a function of cluster size

Kinetic energy of multiply charged xenon ions was measured based on retarding potential method as described in detail in chapter 4 (section 4.3.2). In this method, the energy analysis of the multiply charged ions is carried out prior to the extraction of the ions in the time-of-flight mass spectrometer. To estimate the kinetic energy of ions, mass spectra were recorded in which the retarding field was progressively increased in steps of 50 V/cm. Kinetic energy of multiply charged xenon ions as a function of cluster size at 532 nm is shown in figure 6.6 (also see table 6.1). From

the table, it is clear that xenon ions with multi-keV kinetic energy are produced as a result of interaction of 532 nm laser pulses with xenon cluster. Further, with increase in cluster size, the kinetic energy of multiply charged atomic ions also increases. Thus, the results show that clusters of larger size help in heating quasi free electrons more efficiently, which in turn produces higher number of charge centers within the cluster prior to explosion. As a result, the total potential energy accumulated within a larger cluster would be comparatively higher. Coulomb potential (E_{coul}) of an ion at a distance r ($r \leq R$, R : cluster radius) inside the cluster having N number of atoms is given by¹⁵²-

$$E_{\text{coul}}(r, q, N) = \frac{Nq^2 r^2}{R^3} \quad (6.4)$$

Here it is assumed that the cluster is homogeneously charged by the laser pulse with charge q per ion.

Table 6.1: Kinetic energy of multiply charged xenon ions as a function of cluster size for ionization at 532 nm, measured using retarding potential analyzer

Charge state	Kinetic Energy (in keV)			
	Cluster size			
	<Xe ₁₀₀ > (R=12.7 Å)	<Xe ₅₀₀ > (R=21.7 Å)	<Xe ₂₀₀₀ > (R=34.4 Å)	<Xe ₅₀₀₀ > (R=46.7 Å)
Xe ²⁺		-	-	0.4
Xe ³⁺	-	-	0.3	1.2
Xe ⁴⁺	-	0.4	1.6	3.2
Xe ⁵⁺	0.5	1.3	3.5	6.0
Xe ⁶⁺	0.9	3.3	6.0	9.6
Xe ⁷⁺	1.8	4.6	7.70	11.2
Xe ⁸⁺	2.0	6.0	9.6	12.8
Xe ⁹⁺	2.3	6.8	10.8	14.4

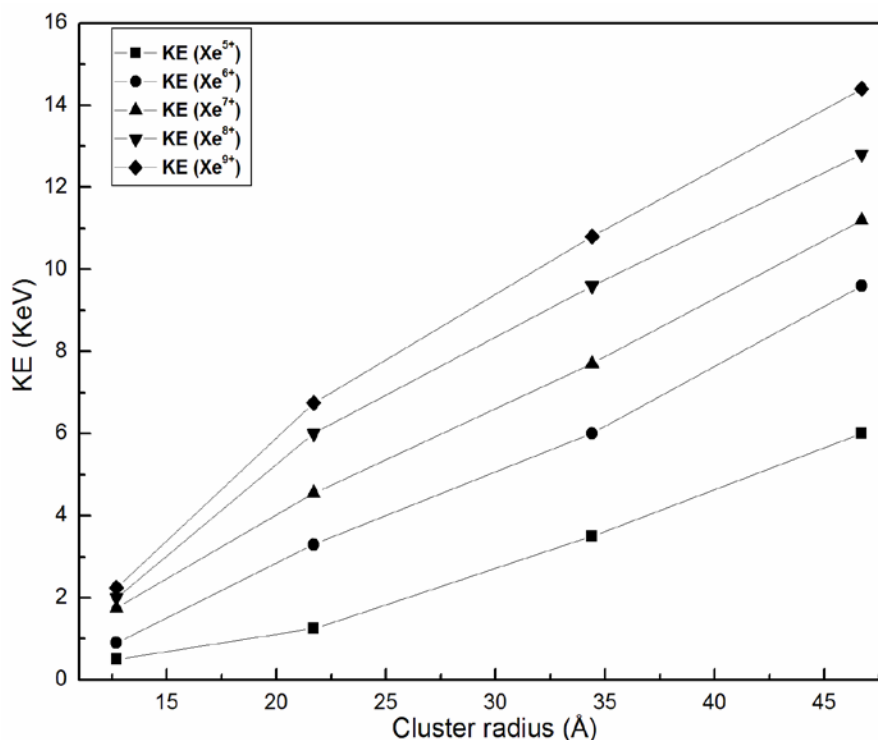


Figure 6.6: Kinetic energy of multiply charged ions of xenon as a function of cluster size ionised at 532 nm

Thus, the highest potential energy of an ion would be at cluster radius $r = R$ and the modified equation is given by -

$$E_{Coul}(R, q, N) = \frac{Nq^2}{R} \quad (6.5)$$

Based on the area under the peak of different multiply charged ions of xenon, average charge state at 532 nm is estimated, assuming similar detection efficiency for multiply charged ions. The average charge (q) per ion has been calculated to be ~ 5 under our experimental conditions. Therefore, E_{Coul} depends on N and R . As N increases with size, potential energy of larger clusters will also increase. However, increasing cluster radius leads to decrease in potential energy. As a result, effective increase in potential energy will be governed by the ratio i.e. N/R . During cluster explosion, the potential energy of the cluster gets transformed into the kinetic energy of the ions. In figure 6.7, normalized value of N/R and kinetic energy of Xe^{5+} (for instance) is plotted as

function of cluster size which shows similar behavior in accordance with the arguments given above. Hence, we conclude that though the charge state does not increase, overall ionisation is significantly higher in larger clusters as compared to smaller clusters. The enhanced ionisation is ultimately reflected in the kinetic energy of multiply charged ions after cluster explosion.

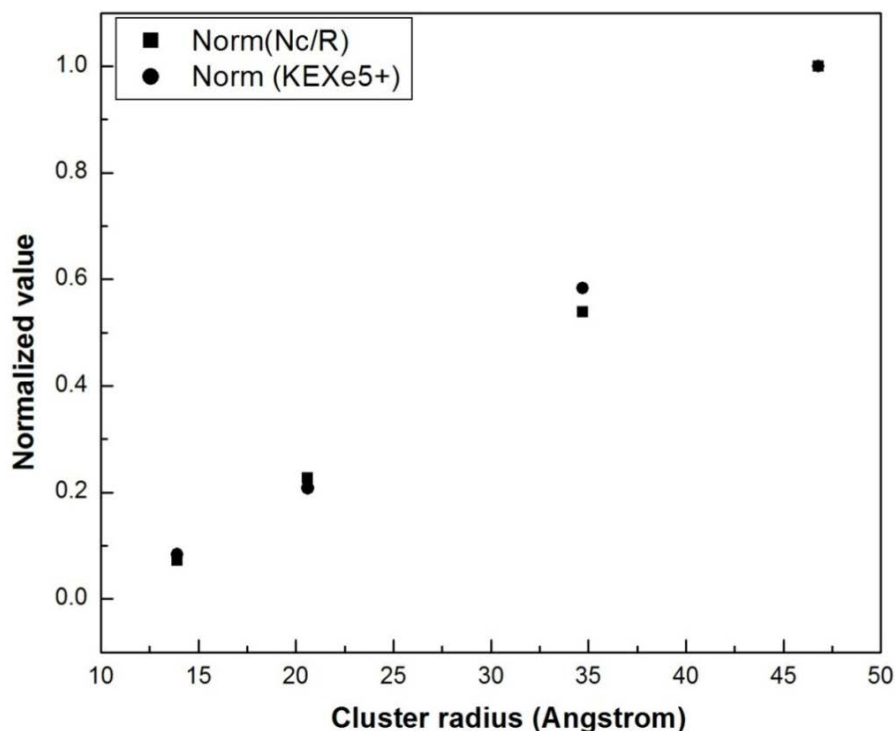


Figure 6.7: Normalized value of N/R and kinetic energy of Xe^{5+} ions plotted as a function of cluster size

6.3.4 Threshold laser intensity for observation of Coulomb explosion as a function of cluster size

In this section, an attempt has been made to determine threshold laser intensity for generation of multiply charged atomic ions as a function of cluster size. Figure 6.8 represents threshold laser intensity required for observation of multiply charged xenon ions as a function of cluster size. It can be seen from the figure that the threshold laser intensity decreases with cluster size. Over the average cluster size of $\sim \langle Xe_{50} \rangle$ to $\sim \langle Xe_{11,400} \rangle$, the threshold laser intensity varies from $9.6 \times 10^9 \text{ W/cm}^2$ to 3×10^9

W/cm^2 . Combining this observation with the results from the previous section, it can be concluded that efficiency of ionisation increases with increasing cluster size, so that same charge states can be produced using lower laser intensity.

The total ionisation in a cluster comprises of contribution from the primary multiphoton ionisation and secondary electron ionisation processes. Multiphoton ionisation which is the first step, leads to generation of singly charged cluster ions and electrons. Subsequently the energisation of the electron by the remaining portion of

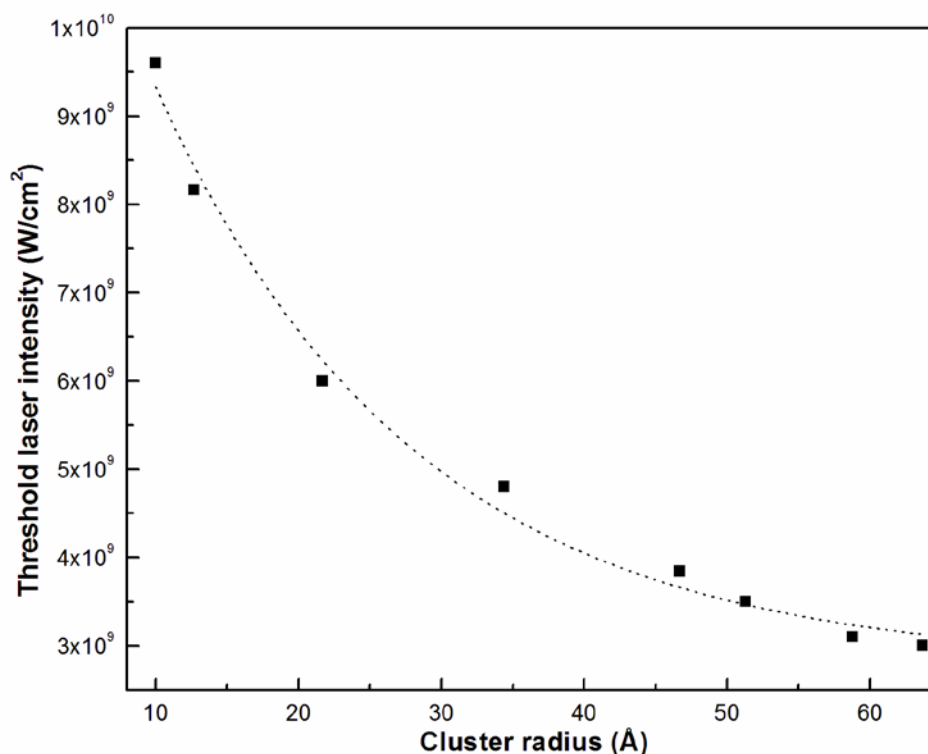


Figure 6.8: *Threshold laser intensity for observation of multiply charged ions of xenon as a function of cluster size*

the laser pulse leads to generation of multiply charged xenon ions by the electron ionisation mechanism. For multiphoton ionisation of clusters of different sizes, ionisation energy plays an important role. In general, with increase in cluster size, ionisation energy decreases. Gantefoer *et al.*¹⁵³ have reported lowering in ionisation potential of xenon clusters, based on studies carried out using synchrotron radiation

source (Table 6.2). Their study showed that ionisation energy drops from 12.13 eV

(for atomic case) to 10.20 eV for clusters as small as Xe_{20} and approach bulk ionisation energy of 9.7 eV for larger clusters. Since present set of experiments were done for $\langle \text{Xe}_{50} \rangle$ to $\langle \text{Xe}_{11,400} \rangle$, it is expected that cluster ionisation energy attains nearly constant value (between 9.76 to 10.06 eV as calculated using scaling laws). Thus, irrespective of the cluster size, same number of photons are required for the multiphoton ionisation of the cluster to produce singly charged xenon ion. However, the multiphoton ionisation cross-section of a cluster is expected to increase with the number of atoms. As a result, similar ionisation probability can be achieved in larger cluster with comparatively lower laser intensity. Moreover, secondary ionisation process i.e. electron ionisation depends on the electron flux present within the cluster and the electron temperature. Since, maximum charge state is found to be same for all cluster size, maximum electron

Table 6.2: Ionisation energy of xenon cluster as a function of size¹⁵³

Xenon species (n)	Ionisation energy (eV)
1	12.13
2	11.09
3	10.88
4	10.81
5	10.75
6	10.72
7	10.68
8	10.63
9	10.57
10	10.54
11	10.54
12	10.40
13	10.38
14	10.34
15	10.33
16	10.28
17	10.26
18	10.26
19	10.24
20	10.20
∞	9.70

temperature is expected to be similar. However, electron flux can be different in clusters of different size because of differential electron escape probability. Therefore, increased cluster size helps in facilitating both multiphoton ionisation and electron ionisation within the cluster which is subsequently reflected in the lowering of threshold laser intensity for generation of multiply charged ions.

6.3.5 Ionisation of water doped xenon clusters at 532 nm laser pulses

In chapter 5, results of doped molecular cluster have been presented where water is used as dopant in methyl iodide cluster. Here, doped atomic clusters has been irradiated with 532 nm laser pulses of intensity $\sim 10^9$ W/cm² and the resulting ions were observed in time-of-flight mass spectrometer. In chapter 5, it has also been explained why water was chosen as dopant. Similar explanation is valid for present experiment also. During the experiment, water has been taken in the sample cell and pure xenon gas was passed above pure water. The mixture was supersonically expanded through the pulsed valve nozzle and water doped xenon clusters were produced. Figure 6.8 represents the time-of-flight mass spectra of water doped xenon clusters ionised at 532 nm. From the spectra, it is evident that multiply charged ions of oxygen (from H₂O) were observed along with Xeⁿ⁺. Thus, the doped atomic cluster results shows similar trend as that of doped molecular clusters. In both cases, dopant molecule (H₂O) is not ionisable in its pure form under our laser intensity conditions. However, when low ionisation energy atom or molecular clusters are mixed with dopant, Coulomb explosion has been induced in dopant molecule leading to generation of multiply charged atomic ions of oxygen. Thus, the experimental results further confirm that Coulomb explosion process is collective property of the cluster and individual atomic/ molecular property does not play any role. Moreover, multiply charged atomic ions were produced due to indiscriminate heating of the energized

electron in the ionized clusters and leads to the formation of multiply charge ionic state of oxygen along with xenon.

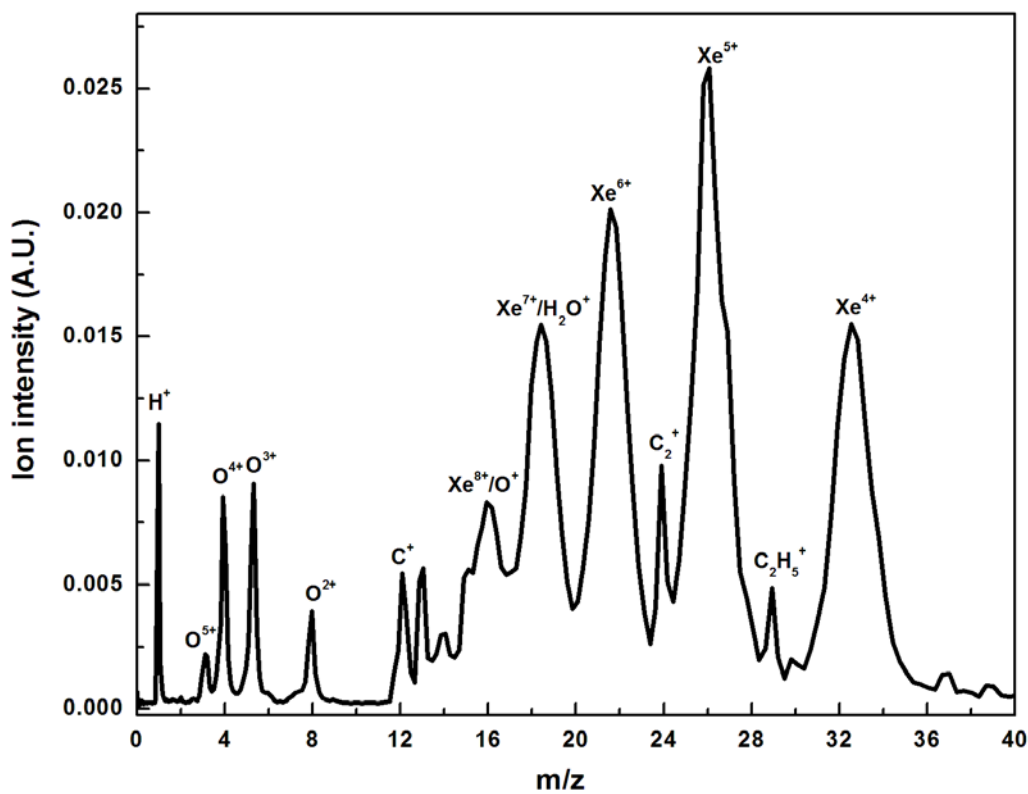


Figure 6.8: Time-of-flight mass spectrum of water doped xenon clusters irradiated by 532 nm laser pulses of intensity $\sim 10^9$ W/cm². Multiply charged ions of oxygen were observed along with multiply charged xenon ions. C⁺, C₂⁺ and C₂H₅⁺ appear in the mass spectra because of background diffusion pump oil.

6.4 Conclusions

In summary, photoionisation of xenon clusters has been investigated at an intensity of $\sim 10^9$ W/cm² under different experimental parameters, using time-of-flight mass spectrometer. The efficiency of laser-cluster interaction was found to increase with laser wavelength, resulting in generation of multiply charged xenon ions (up to Xe¹⁰⁺) with large kinetic energy at 532 nm. Generation of multiply charged atomic ions has been explained on the basis of efficient heating of cluster by electrons liberated initially upon multiphoton ionisation of xenon atoms inside the cluster. For observation of multiply charged ions under gigawatt intensity conditions, based on

size dependent cluster studies, threshold cluster size for xenon has been estimated to be $17 < N < 50$. Increase in cluster size of xenon beyond the threshold size, enhances the kinetic energy of the multiply charged atomic species without increasing the charge state. The enhancement in kinetic energy of the multiply charged ions in larger cluster has been attributed to the ability of larger cluster to accumulate comparatively higher charge prior to Coulombic disintegration. Presence of multiply charged oxygen ions in water doped xenon cluster further confirm that the Coulomb explosion phenomenon is a collective property of the cluster and atomic and molecular properties do not play any role.

In the end it is relevant to qualitatively compare present results on atomic clusters with those obtained for molecular clusters. Though the laser-cluster interaction mechanism leading to generation of multiply charged atomic ions is same for both atomic and molecular clusters, however molecular clusters exhibit complex cluster photo-dynamics due to contribution by undesired additional intra-cluster photochemical processes like – energy dependent electron attachment, photodissociation, vibrational excitation, ion-molecule reactions etc. Present studies suggest that the coupling of laser energy with clusters is more efficient for the atomic clusters, as evident from kinetic energy and highest multiply charged atomic ion observed in the time-of-flight mass spectrum, under similar experimental conditions. Besides estimation/quantification of cluster size for atomic clusters is rather straightforward due to accessibility of well established scaling laws, which helps in less ambiguous interpretation of the experimental results.

Chapter 7

Laser-cluster interaction under gigawatt intense laser field: Detection of negative ions

7.1 Introduction

A negative ion is an atom or a molecule to which an extra electron has been attached, giving the whole system a net negative charge. Electron is not attracted by a neutral atom/ molecule, however the electron will polarize the atom/molecule when it is brought near to the electron cloud surrounding the atom/molecule and this will induce an electric dipole moment. This induced electric dipole moment can in turn attract the electron which then becomes trapped in an induced electric dipole potential. The energy release when an electron is added to a neutral atom/molecule to form a negative ion is defined as electron affinity. In general, attachment of electron to atom/ molecule is an exothermic process and exothermicity of the electron attachment process determines the stability of negative ion.

In laser-cluster interaction, detection of negative ions is not so easy and only limited reports are available in literature. Moustazis *et al.*¹⁵⁴ have demonstrated generation of negative ions as a result of interaction of 30 TW Ti-sapphire laser pulses with CH₄ and CD₄ clusters using Thomson parabola mass spectrometer. Negative and positive ions of H, D and C were observed with a maximum energy up to 70 keV for laser intensity of 10¹⁸ W/cm². Based on experimental findings, they have concluded that negative ions are produced as a result of double electron attachment to the positive ions. Ter-Avetisyan *et al.*¹⁵⁵ have produced highly energetic negative ions as a result of interaction of femtosecond laser pulses (35 fs) having intensity ~10¹⁹ W/cm² with water and heavy water micro droplets. The maximum energies for the D⁻

and O^- are 0.3 MeV and 1.3 MeV respectively, which is only a few times lower compared to those for positively charged ions. Further Nakamura and co-workers¹⁵⁶ studied generation of negative ion formation and their acceleration in laser plasmas due to interaction of 35 fs laser pulses (130 mJ) with CO_2 clusters. When a cluster target is irradiated by an intense laser pulse and the Coulomb explosion of positively charged ions occurs, the negative ions are accelerated inward. This observation is termed as 'Coulomb implosion' of negatively charged ions in the laser plasma. Under such experimental conditions, the highest energy of negative ions is found to be several times lower than that of positive ions. The maximum energy of positive C^{4+} ions is 4.8 MeV and that of negative ions (C^-) is 0.6 MeV. This observation is in sharp contrast to the earlier observed results where kinetic energy of negative ions is found to be similar to that of positive ions. Moreover, the Coulomb implosion model is theoretically supported using 2-dimensional particle-in-cell simulations.^{74, 157} Recently, Krishnamurthy and coworkers¹⁵⁸ also observed negative ion formation as a result of interaction CO_2 clusters with femtosecond laser pulses of intensity 2×10^{16} W/cm². However, they have opposed Coulomb implosion model under their experimental conditions. The absence of any negative ion signal from single, isolated cluster suggests that intra-cluster mechanisms, such as Coulomb implosion, are not dominant in small clusters (of a few nm). Besides, their analysis reveals that the obvious mechanisms of charge reduction i.e. electron-ion recombination and normal charge transfer fail to explain the large fraction of negative ions observed in measurements. They show that it is the electronic excitation of the hot dense plasma is responsible for the large yield of negative ions.

In the present work, laser-cluster interaction studies have been carried out in different molecular clusters such as CF_2Br_2 and CH_3I clusters and possibility of

negative ion formation has been explored. In chapter 3 and 5, generation of singly and multiply charged positive ions has been presented in these molecular clusters and the observation of such energetic ions is explained based on the three stage cluster ionisation model. According to this model, prior to the cluster explosion, neutral atoms, ions and electrons are in close proximity within the cluster volume. Electron attachment to neutral atoms may lead to generation of negative ions. Thus, an attempt has been made to detect negative ions in the interaction zone by changing the polarity of channel electron multiplier detector. Moreover, effect of negative ion formation on Coulomb explosion phenomena under gigawatt intense laser field has been discussed.

7.2 Experimental details

Details of the experimental method are given in Chapter 2 along with the description of the detector i.e. channel electron multiplier (CEM) (section 2.6.2). In previous experiments, CEM detector has been configured for detection of positive ions. The electrical connections of the detector for detection of positive ions are shown in figure 7.1 (a). Negative high voltage is applied at point “A” while point “B” of the CEM detector has been grounded which creates a positive electric gradient throughout channel of the detector. The secondary electrons produced due to impingement of positive ions on the lead silicate coating move through the positive electric gradient of the channel of CEM detector. The ion signal is collected from the collector part of the detector. However, for detection of negative ions, the above explained electrical circuit of the CEM is not suitable. In order to create the positive electric gradient in the channel of detector, point “A” has been grounded and positive high voltage is applied to point “B”. Moreover, a circuit containing 1 M Ω resistance and 33 pF capacitor is also used between the collector and the oscilloscope (as shown in figure 7.1 (b)).

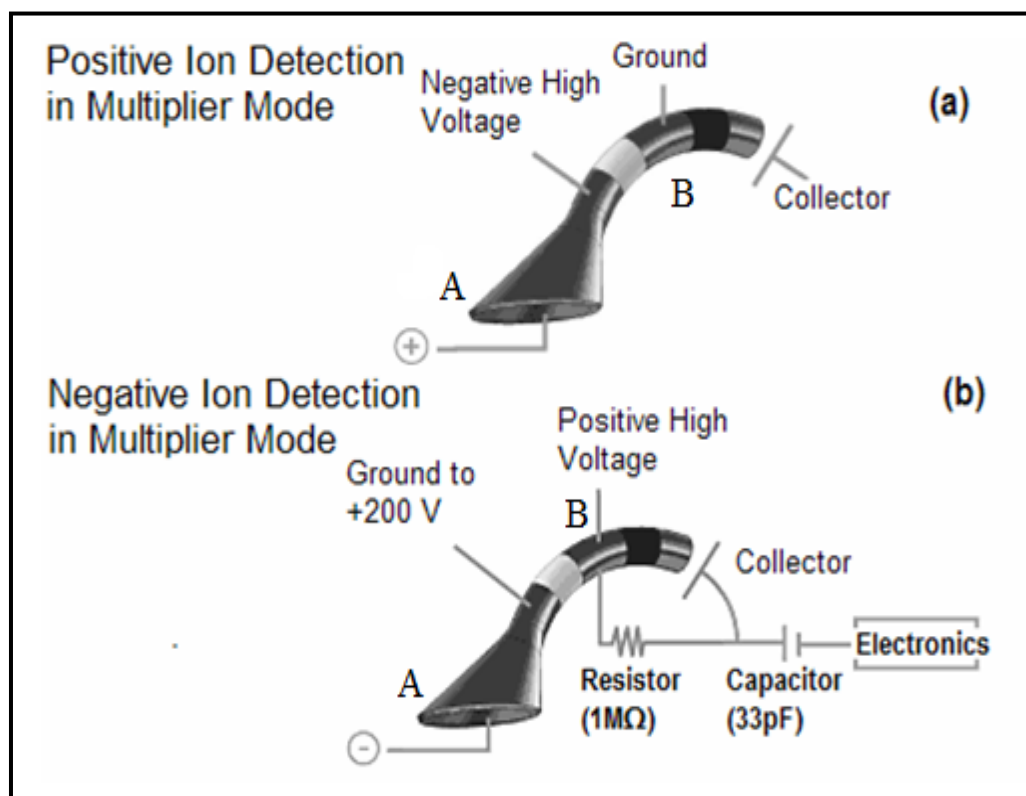


Figure 7.1: Electrical connections of channel electron multiplier for detection of (a) positive ions and (b) negative ions

7.3 Results & Discussion

7.3.1 Detection of negative ions in photo ionisation CF_2Br_2 clusters under gigawatt intense laser field

CF_2Br_2 clusters were produced using 0.8 mm nozzle diameter and made to interact with different harmonics of Nd:YAG laser. Figure 7.2 represents time-of-flight mass spectrum of negative ions generated due to interaction of CF_2Br_2 clusters with 532 nm laser pulses having intensity $\sim 10^9 \text{ W/cm}^2$. Weak signals of negative ions are observed in the mass spectra. In negative ion spectra, the most abundant species is Br^- which has a high electron affinity (-3.354 eV).¹⁵⁹ Moreover, other negative ions such as F^- , Br_2^- and $(\text{CF}_2\text{Br}_2)\text{Br}^-$ are also observed in the time-of-flight mass spectra. No ion peak due to CF_2Br_2^- was observed in the mass spectra because of exceptionally low lifetime ($\sim 4.5 \text{ ps}$).¹⁵⁹

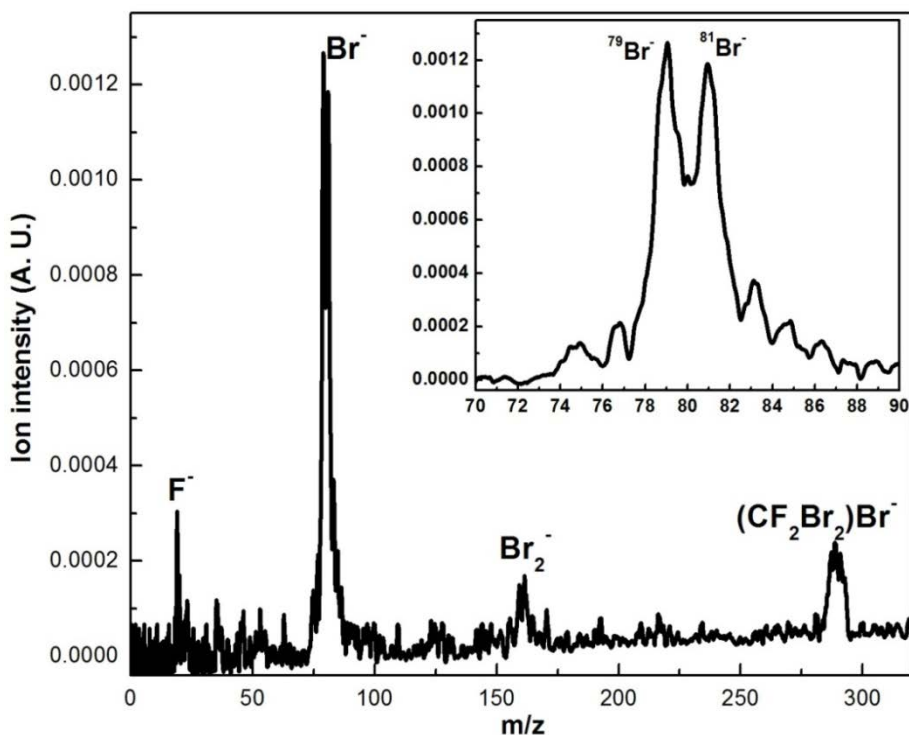
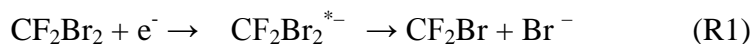


Figure 7.2: Negative ion time-of-flight mass spectra of CF_2Br_2 clusters photoionised at 532 nm for a laser intensity of $\sim 10^9 \text{ W/cm}^2$. Two isotopes of bromine (^{79}Br and ^{81}Br) are shown in inset.

Negative ion formation in CF_2Br_2 molecule has been reported in collision reactions carried out with velocity selected $K(np)$ Rydberg atoms. Br^- was the most abundant peak with small signal due to Br_2^- without any ion signal due to molecular anion.¹⁵⁹⁻¹⁶¹ Generation of negative ions from CF_2Br_2 molecule can be attributed to dissociative electron attachment process, where low energy electron attaches to the neutral molecule and leads to formation of excited state anion which finally undergoes dissociation to form Br^- and Br_2^- .¹⁶⁰



R1 reaction is an exothermic reaction since electron affinity of bromine ($\sim 3.358 \text{ eV}$) is greater than dissociation energy ($\sim 3 \text{ eV}$) of C-Br bond. With the increase in exothermicity of the reaction, potential energy of negative ion state becomes lower which in turn increases the probability of low energy electron

attachment. Moreover, the electron attachment cross section depends on electron energy $[E (e^-)]$. CF_2Br_2 molecule has a very high electron attachment cross-section of $\sim 1.2 \times 10^{-13} \text{ cm}^2$ at an electron energy of 0.001 eV. However, with increasing electron energy, electron attachment cross-section decreases drastically ($\sigma(CF_2Br_2) < 10^{-17} \text{ cm}^2$ when $E (e^-) > 1 \text{ eV}$).¹⁶² Though there are few reports¹⁵⁹⁻¹⁶² in the literature regarding negative ion formation of CF_2Br_2 monomer, there is hardly any report on negative ion formation of CF_2Br_2 clusters. Langer *et al.*¹⁶³ have reported negative ion formation in analogous cluster system i.e. CF_2Cl_2 cluster using low energy (0-15 eV) electron impact. Based on their studies, molecular anion ($CF_2Cl_2^-$) is observed in quadrupole mass spectrometer when electron energy was $\sim 0 \text{ eV}$. Moreover, solvated cluster fragments such as $(CF_2Cl_2)_nCl^-$ and $(CF_2Cl_2)_nF^-$ ($n \geq 7$) were observed in studies carried out using low energy electron. In negative ion spectrum of CF_2Br_2 cluster, the yield of solvated cluster ions are much less under our experimental conditions because of excessive cluster disintegration under gigawatt intense laser field at 532 nm. Further, no F^- containing solvated cluster ion was observed in our mass spectra. This observation suggests less facile C-F bond breaking (bond energy $\sim 5.05 \text{ eV}$ ¹⁶⁴) in CF_2Br_2 compared to C-Br bond (bond energy $\sim 2.98 \text{ eV}$ ¹⁶⁴). Negative ion intensity of F^- , Br^- in the mass spectra is also in accordance with the dissociation energy of these two bonds.

Generation of negative ions in CF_2Br_2 clusters can also be explained based on dissociative electron attachment. For dissociative electron attachment, electron energy has to be low so that the electron attachment cross-section is high. However, we have not measured electron energy in CF_2Br_2 clusters at 532 nm because of instrumental limitation. To get the idea of electron energy, one should consider the ionisation process under our experimental conditions. Based on three stage model (described in

section 3.3.3), first step is multiphoton process where (4+1) non resonant process leads to primary ionisation. Thus, the energy of the photoelectrons is ~ 0.6 eV after multi-photon ionisation (considering 532 nm photon energy and ionisation potential of CF_2Br_2). Subsequently, the photoelectrons gain energy via IBS process which in turn lowers the electron attachment probability. Thus, the negative ions are produced in our study as a result of the attachment of the photoelectrons produced after multiphoton ionisation and detected in the time-of-flight mass spectrometer.

7.3.2 Detection of negative ions in photo ionisation CH_3I clusters under gigawatt intense laser field

Methyl iodide clusters were generated with pulsed valve having 0.8 mm nozzle diameter and ionised with different harmonics of Nd: YAG laser. Time-of-flight mass spectra of positive ions have been presented in chapter 5 (Figure 5.2). Negative ions signal observed as a result of interaction of methyl iodide clusters with laser pulses of 532 nm is shown in figure 7.3. In the mass spectra, I^- could be observed along with higher mass signals like $(\text{CH}_3\text{I})\text{I}^-$ and $(\text{CH}_3\text{I})_2\text{I}^-$.

Negative ion formation has been extensively studied in methyl iodide using different experimental techniques and rate constant of electron attachment to CH_3I molecule has been determined. Low energy electron attachment to CH_3I , especially in the thermal energy region, has been studied by various workers using a variety of experimental methods such as electron swarm (ES)¹⁶⁵, flowing afterglow/Langmuir probe (FALP)¹⁶⁶, high-Rydberg beam (HRB),^{167,168} threshold photoionisation (TPI),¹⁷⁰ electron cyclotron resonance¹⁷¹ and even pulse radiolysis technique¹⁷². In high energy range of 0-50 eV, Nagesha *et al.*¹⁷³ studied negative ion formation in methyl iodide. They have observed H^- , CH^- along with I^- at specific resonant energies due to dissociative electron attachment of CH_3I .

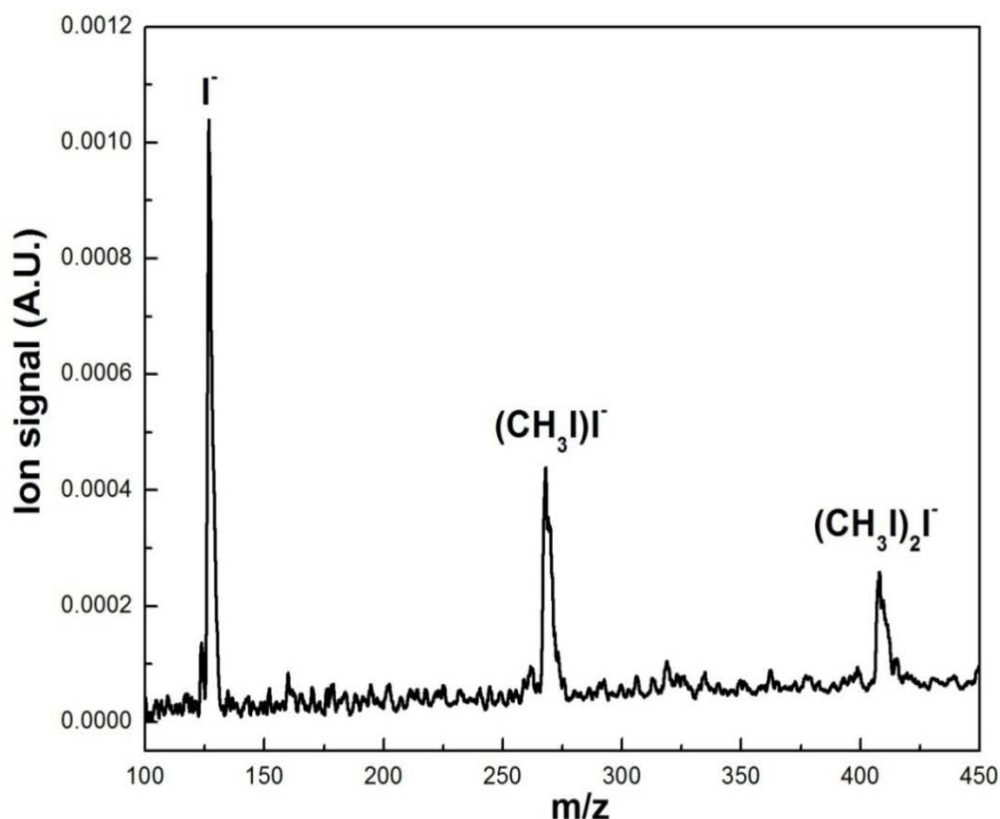


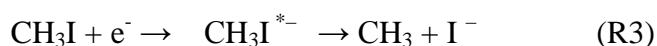
Figure 7.3: Negative ion time-of-flight mass spectrum of CH_3I clusters photoionised at 532 nm

Further, absolute electron attachment cross-sections have been derived using relative flow technique. The large electron attachment cross-section ($5.8 \times 10^{-15} \text{ cm}^2$) at non zero energies is attributed due to s-wave scattering process due to electron/ molecule interaction. These experimental observations are supported by ab-initio molecular orbital calculations which derive information based on ground state potential energy surfaces of CH_3I and CH_3I^- and their various dissociation products.¹⁷⁴

The above results are for electron attachment process taking place in single, isolated CH_3I , however few studies have been carried out in CH_3I clusters. Using laser photoelectron attachment technique coupled with mass spectrometric ion detection, Weber *et al.*¹⁷⁵ measured the relative rate coefficient for formation of $(\text{CH}_3\text{I})_n\text{I}^-$ ($n=0-2$) ions over the electron energy range 0-100 meV. Based on the experimental observation and R-matrix calculation, these authors concluded that

clusterisation plays an important role in dissociative electron attachment process. Kosmidis and co-workers¹²⁰ studied negative ion formation in methyl iodide clusters photoionised with picoseconds laser pulses of intensity $\sim 10^{12}$ - 10^{13} W/cm². From the analysis of the mass spectra, these authors attributed main peaks to H⁻ and I⁻ negative ions. Smaller peaks corresponding to C_xH_y⁻ (x = 1, 2 and y = 1, 2) have also been recorded. According to these authors, the negative ion formation in the laser-cluster interaction is very helpful for the understanding of the cluster ion stability.

Under our experimental conditions, negative ions like (CH₃I)_nI⁻ (n=0-2) are observed due to dissociative electron attachment of CH₃I molecule, similar to the case of CF₂Br₂ clusters.



However, in both molecular systems i.e. CF₂Br₂ and CH₃I clusters, negative ions are observed only at 532 nm laser pulses of gigawatt intensity conditions. In order to understand the negative ion formation at 532 nm, we can reconsider the three stage cluster ionisation mechanism which comprises of multiphoton ionisation ignited-inverse bremsstrahlung heating-electron impact ionisation. In the first step, constituent molecules of the cluster undergo multiphoton ionisation. This multiphoton ionisation process in the cluster is expected to be more facile in UV region as compared to visible and IR region. As a result of this facile ionisation, ionised cluster undergoes rapid expansion due to Coulombic repulsion. Rapid cluster expansion in UV region lowers the electron attachment probability to neutral atoms/ molecules. Therefore, no negative ion signal has been observed at 266 nm and 355 nm. On the contrary, in IR region, initial multiphoton ionisation is expected to be low as compared to UV region. Thus, cluster expands slowly and inner ionised electron

interacts with the laser field for longer time and energised via inverse bremsstrahlung process. The higher electron energy lowers the electron attachment cross-section to the neutral molecules drastically. As a result of that no negative ion signal has been observed in the time-of-flight mass spectrometer at 1064 nm. In visible wavelength i.e. at 532 nm since the photon energy is intermediate between UV and IR region, thus initial multiphoton ionisation in the cluster is optimised for collision between electron and the neutral atoms. Moreover, electron energy after electron-ion collision is not high enough to significantly reduce the collision cross-section. Thus, at 532 nm, an intermediate situation is produced which is favourable for generation of negative ion formation under our experimental conditions.

7.3.3 Effect of negative ion in cluster ionisation dynamics under gigawatt intense laser field

In section 7.3.2, we have explained how negative ions are formed in CF_2Br_2 , CH_3I clusters due to irradiation of 532 nm laser pulse of intensity $\sim 10^9 \text{ W/cm}^2$. However, it is worth discussing the effect of negative ions in the cluster ionisation dynamics in view of multiply charged atomic ion formation. Kosmidis and co-workers¹²⁰ have reported H^- and I^- as a result of interaction of methyl iodide clusters with pico-second laser pulses of intensity $\sim 10^{12} \text{ W/cm}^2$. According to these authors, the presence of negative ion within the positively charged cluster offers attractive electrostatic force. Subsequently, these negatively charged moieties temporally stabilize the multiply charged cluster before abrupt explosion. Based on this proposition, inner ionized electrons produced in $\text{CF}_2\text{Br}_2/\text{CH}_3\text{I}$ cluster would get more time to interact with the laser field because of presence of negative ions within the positively charged cluster. As a result, inner ionized quasi free electron would be energised more and lead to higher charge state formation in the ionized cluster. To understand the effect of negative ion formation in $\text{CF}_2\text{Br}_2/\text{CH}_3\text{I}$ cluster, Xe cluster

results are compared where possibility of negative ion formation is reasonably less based on electron affinity value. In xenon cluster, multiply charged ions were observed up to +10 due to interaction of 532 nm laser pulses (See figure 6.3) whereas in $\text{CF}_2\text{Br}_2/\text{CH}_3\text{I}$ clusters, multiply charged state of carbon, fluorine, bromine and iodine are limited up to +4, +4 +5 and +4 respectively under similar experimental conditions. Based on the ionisation potential of the highest observed charge state of these two cluster system, it can be concluded that the energization of the electron is also lesser in $\text{CF}_2\text{Br}_2/\text{CH}_3\text{I}$ cluster compared to Xe cluster. Therefore, the results of nanosecond studies show that negative ion formation does not influence the electron energization time scale in $\text{CF}_2\text{Br}_2/\text{CH}_3\text{I}$ cluster significantly and ionisation dynamics remains unaltered under gigawatt intense laser field.

7.4 Conclusions

Negative ion formation has been studied as a result of interaction of nanosecond laser pulses with CF_2Br_2 and CH_3I clusters. The experimental set-up was suitably modified for detection of negative ions. In the mass spectra, F^- , Br^- , I^- have been observed from CF_2Br_2 and CH_3I clusters along with negative ion signals of cluster fragments. Generation of negative ion under our experimental conditions is attributed to dissociative electron attachment of the neutral molecules present in the cluster. Moreover, based on the comparison of experimental results of CF_2Br_2 and CH_3I clusters with Xe clusters, it can be inferred that negative ion formation does not influence the electron energization time scale in cluster and ionisation dynamics remains unaltered under gigawatt intense laser field.

Chapter 8

Charge density measurement in atomic and molecular clusters under gigawatt intense laser field

8.1 Introduction

Laser-cluster interaction at medium to high laser intensity leads to generation of multiply charged energetic atomic ions. In general, time-of-flight mass spectrometer is used for determination of the charge state and measuring kinetic energy of these atomic ions. Although mass spectrometry is a very sensitive method for the detection of ions, it is difficult to comment on the efficiency of laser-cluster interaction at different wavelengths merely on the basis of the observation of charge state of multiply charged ions. It is possible that the total yield of ions (including multiply charged ions generated in the ionisation volume) at higher wavelength might be less than the total yield of singly charged ions generated at lower wavelength i.e. the multiply charged states are produced at the expense of the lower charge states. In order to understand this aspect and throw more light on the mechanism of laser-cluster interaction under gigawatt intense laser field, charge density of the interaction volume is required. The total charge density is the measure of the number of charge produced as a result of laser-cluster interaction per unit volume. Based on charge density measurements, one can get idea about the extent of ionisation by the laser pulse which will in turn help in determining the efficiency of laser-cluster interaction under given set of experimental conditions. For absolute charge determination, Faraday cup detector is used extensively because of its simplicity, low cost and ruggedness. Since the detector has no amplification system, the ion current can be

directly correlated to the number of charges. In our experiments, charge density has been measured using parallel plate which works on the similar principle of Faraday cup and details of the set up is described in the experimental section.

In the present work, charge density of C_2H_5Br , CH_3I and Xe clusters have been determined at different wavelengths using the modified set up. The charge density of a given system is compared with the observed charge state in the mass spectra. Further, charge densities of different cluster systems are compared to get a comprehensive idea of laser-cluster interaction under gigawatt intense laser field.

8.2 Experimental details

Details of the experiments have been described in Chapter 2 and only a description relevant to the charge density measurement is given here. For charge density measurement, ion optics of time-of-flight mass spectrometer has been modified. As explained earlier, repeller, extractor and accelerator electrodes are made up of fine grids for recording of mass spectra of atomic/ molecular clusters. During charge density measurement, the repeller and the extractor grids are replaced with solid stainless steel plates. Transmission loss of ions produced in laser-cluster interaction would be minimum in the plate configuration as compared to grid arrangement. Thus, the plate arrangement is helpful in collecting total charges produced in laser-cluster interaction. The modified electrical circuit has been shown in figure 8.1. From the circuit diagram it is very clear that the time-of-flight mass spectrometer becomes inoperable during the charge density experiments. However, it has been ensured that experimental parameters such as laser intensity, expansion conditions and wavelength are kept identical in the time-of-flight and charge density measurements so that the results could be correlated. Positive voltages were applied to the extractor plate in order to repel positive ions towards repeller plate.¹⁷⁶

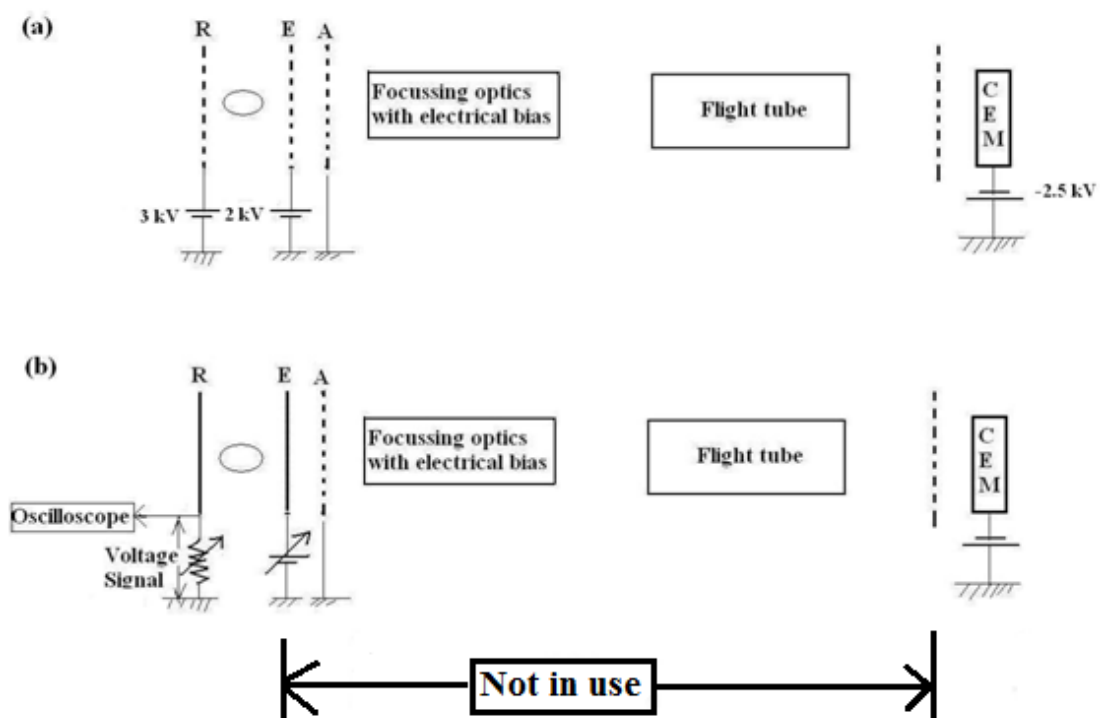


Figure 8.1: Electrical circuit of the ion optics for (a) time-of-flight mass spectrometry and (b) charge density experiments

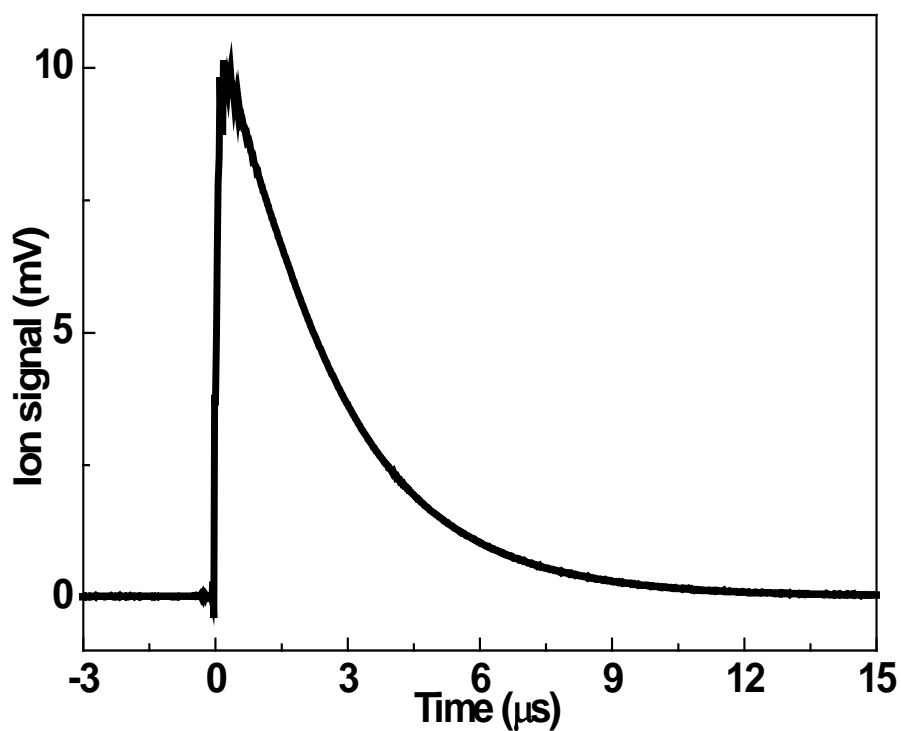


Figure 8.2: Typical oscilloscope trace for ion signal recorded at repeller plate across a 10 K Ω resistance, for a given applied voltage on extraction plate.

The ion current was measured across a suitable resistor (10 k Ω) connected to the repeller (collector) plate (Figure 8.1). Typical trace obtained in the oscilloscope is shown in figure 8.2.

The area under the curve = Volt (V) x time (t)

The charge produced in the interaction zone (Q) = Current (I) x time (t)

Again, Current (I) = Volt (V) / Resistance (R) (According to Ohm's law)

Thus, charge produced in the interaction zone

$$Q = [\text{Volt (V) x time (t)}] / \text{Resistance (R)}$$

Number of charges = Charge/ unit charge

In order to determine the charge density of the interaction zone, the obtained charge has to be divided with the volume of the interaction zone. For determination of the interaction volume, an aperture has been introduced between pulsed valve nozzle and interaction zone. The molecular beam, after passing through aperture, interacts with the focused laser beam (as shown in figure 8.3) and constitutes the interaction zone (shaded volume). Thus, the interaction volume can be considered as a cylindrical volume where aperture defines the height of the cylinder while focused spot size of the laser beam become the radius of the cylinder.

Volume of interaction zone (Cylindrical volume) = $\pi r^2 h$

where h and r denote diameter of aperture and laser spot radius respectively.

The diameter of the aperture is kept 6 mm during charge density measurement which denotes the height (h) of the cylindrical volume. Experimentally, the laser spot size at the interaction region is measured by putting a thin strip of copper foil and allowing the laser light to fall on it. The focused laser beam, drills a hole in the copper foil after ~200 shots. Five such holes were taken at different position of the copper

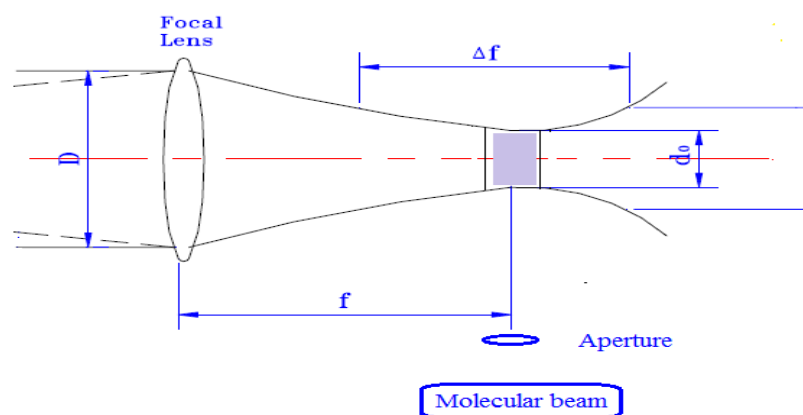


Figure 8.3: Laser-cluster interaction volume (shaded portion) to determine charge density for atomic/molecular clusters

foil at each wavelength and the average radius of the laser spot could be measured under Scanning Electron Microscope (SEM). The average radius of the laser spot at 266, 355, 532 and 1064 nm is found to be 30, 60, 85 and 158 μm respectively within $\pm 10\%$ error. In figure 8.4, a representative laser spot at 1064 nm is shown and similar spot has been observed at other wavelengths. The laser spot diameter also calculated using equation 2.2 (see in chapter 2). Theoretically calculated and experimentally measured values of laser spot diameter showed an identical trend i.e. increase in laser spot diameter with laser wavelength. However, the absolute value of laser spot diameter measured experimentally was higher than the theoretically calculated value. This is because calculation provides the diffraction-limited value of laser spot diameter, while experiments determined an average value (~ 200 laser shots) of laser spot diameter which is higher than the diffraction limited value. Experimentally, an ion signal was monitored by varying the position of lens and the laser spot diameter was measured at a point where ion signal was maximum. The differences in experimentally measured and theoretically calculated values of laser spot diameter do not alter our data interpretation significantly. Hence, charge density has been determined using an experimental value of laser spot diameter.

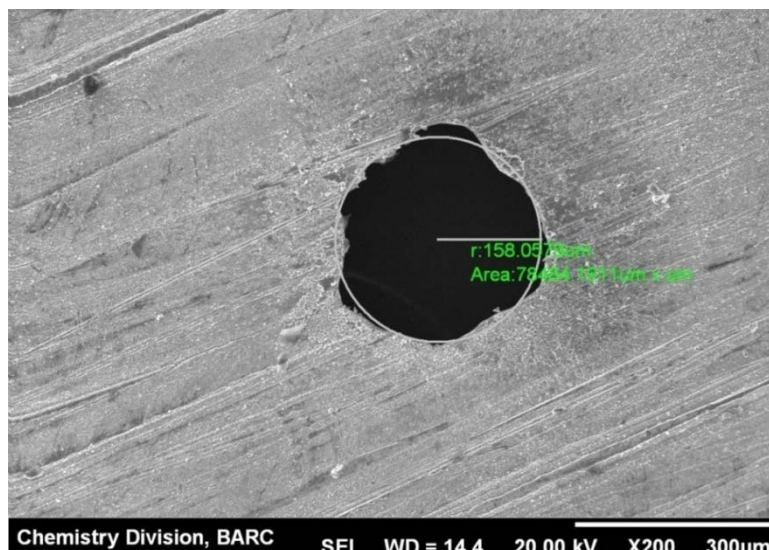


Figure 8.4: Scanning electron microscope image of the laser spot obtained at the interaction zone using 1064 nm laser pulses

8.3 Results and Discussion

8.3.1 Charge density measurements of C_2H_2Br , CH_3I and Xe clusters ionised at different wavelengths

Charge density measurement has been carried out in two molecular (C_2H_5Br and CH_3I clusters) and one atomic system (Xe clusters) at different wavelengths. The time-of-flight mass spectra at different wavelength have been already presented in chapter 4, 5 and 6. The charge density measurement has been carried out under similar experimental conditions so that this result can be compared with the earlier observed mass spectra.

In case of C_2H_5Br clusters, the ion signal observed for 532 nm ionisation on the repeller plate at different extraction voltage has been shown in figure 8.5. Similar traces were observed at 355 nm and 266 nm laser pulses. For a given wavelength, the charge density is initially found to increase and slowly attains saturation. The initial increase in charge density with increasing voltage indicates that ions are collected more efficiently. Application of sufficiently high extraction voltage helps to collect all the energetic multiply charged ions. The saturation region in the trace confirms

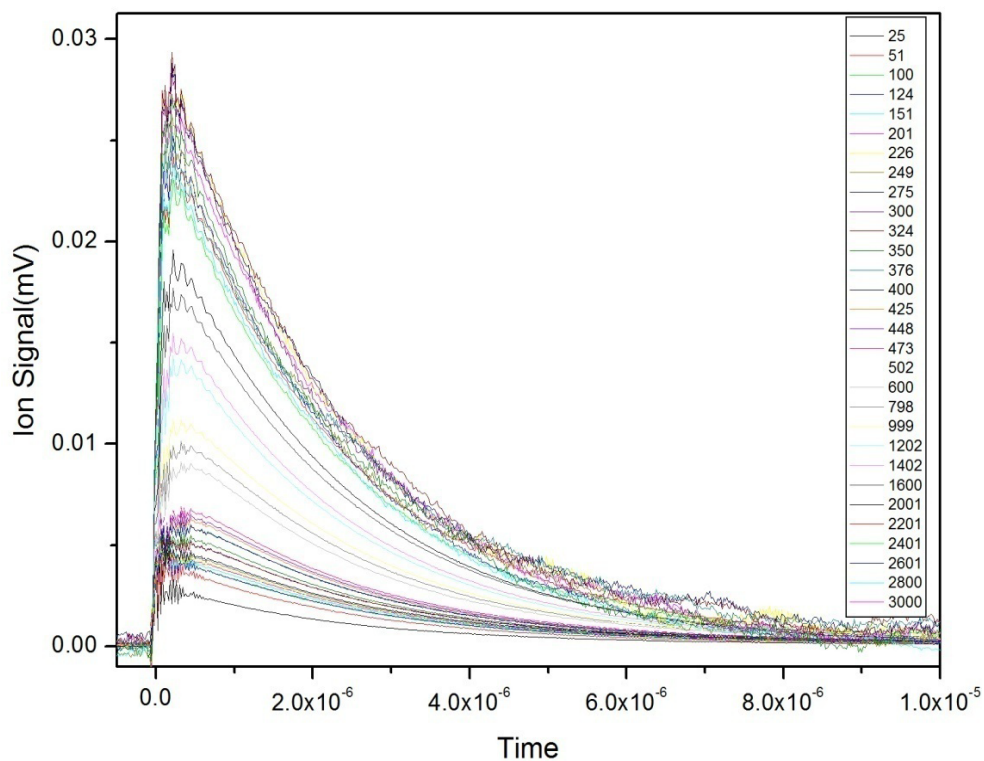


Figure 8.5: Ion signal at repeller plate as a function of extraction voltage for ethyl bromide clusters as a result of irradiation with laser pulses of 532 nm

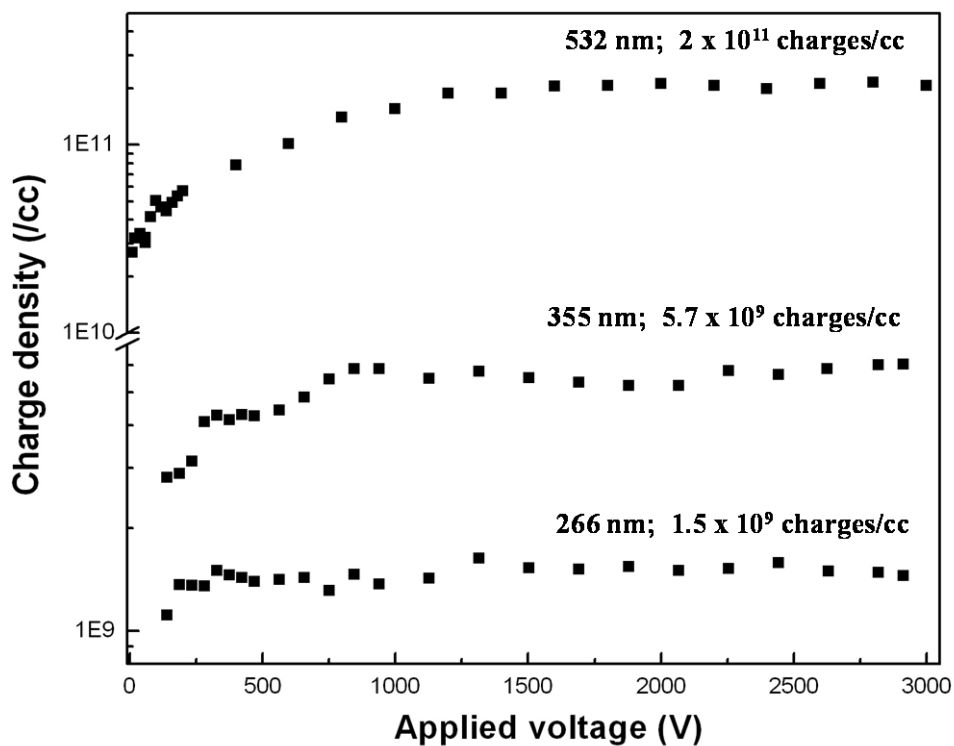


Figure 8.6: Charge density of ethyl bromide cluster as a function of applied voltage between parallel plates for ionisation at 532, 355 and 266 nm

collection of total ions produced in the laser-cluster interaction zone. Using the formula described in experimental section, charge density of the interaction zone at each extraction voltage has been calculated for different wavelengths and plotted in figure 8.6. From the charge density measurements, it can be concluded that with increase in wavelength there is an enhancement in the charge density of the interaction zone. Earlier, the highest observed charge state in the mass spectra of ethyl bromide clusters is +1, +2 and +5 at 266, 355 and 532 nm respectively. Thus, the charge state and the charge density measurements of ethyl bromide clusters show similar trend with increasing wavelength.

Similar studies have been carried out for $(\text{CH}_3\text{I})_n$ clusters at 266, 355, 532 and 1064 nm. The charge density of methyl iodide clusters with increasing extraction voltage at different wavelength is shown in figure 8.7.

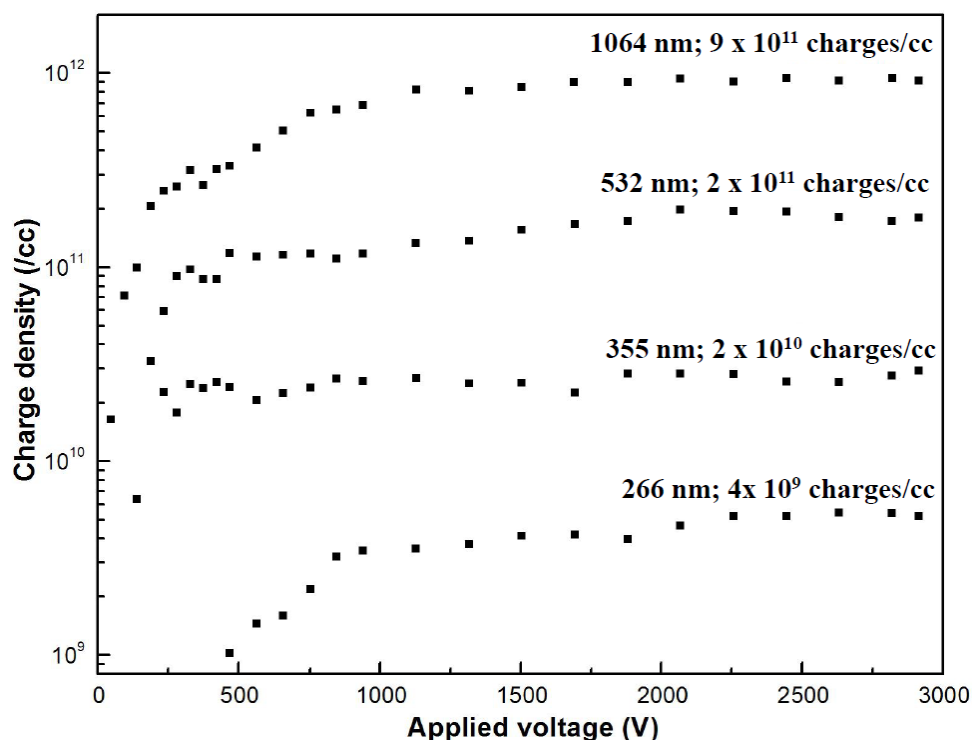


Figure 8.7: Charge density of methyl iodide cluster as a function of applied voltage between parallel plates for ionisation at 1064, 532, 355 and 266nm

Charge density of methyl iodide clusters is found to increase with laser wavelength. The highest observed charge state in the mass spectra is +1, +2, +4 and +11 at 266, 355, 532 and 1064 nm respectively. Thus, similar trend has been observed in case of mass spectra and charge density measurements.

In xenon clusters, the highest observed charge state at 266, 355, and 532 nm is +3, +6 and +10 respectively. Charge density of the interaction zone of xenon clusters measured as a function of extraction voltage, shows an enhancement of the charge density of the interaction zone with increase in laser wavelength. Thus, atomic and molecular clusters show similar trend in mass spectra and charge density measurements. It is worth mentioning here that no charge density measurement was shown at 1064 nm for ethyl bromide and xenon clusters because these cluster systems could not be ionized using 1064 nm.

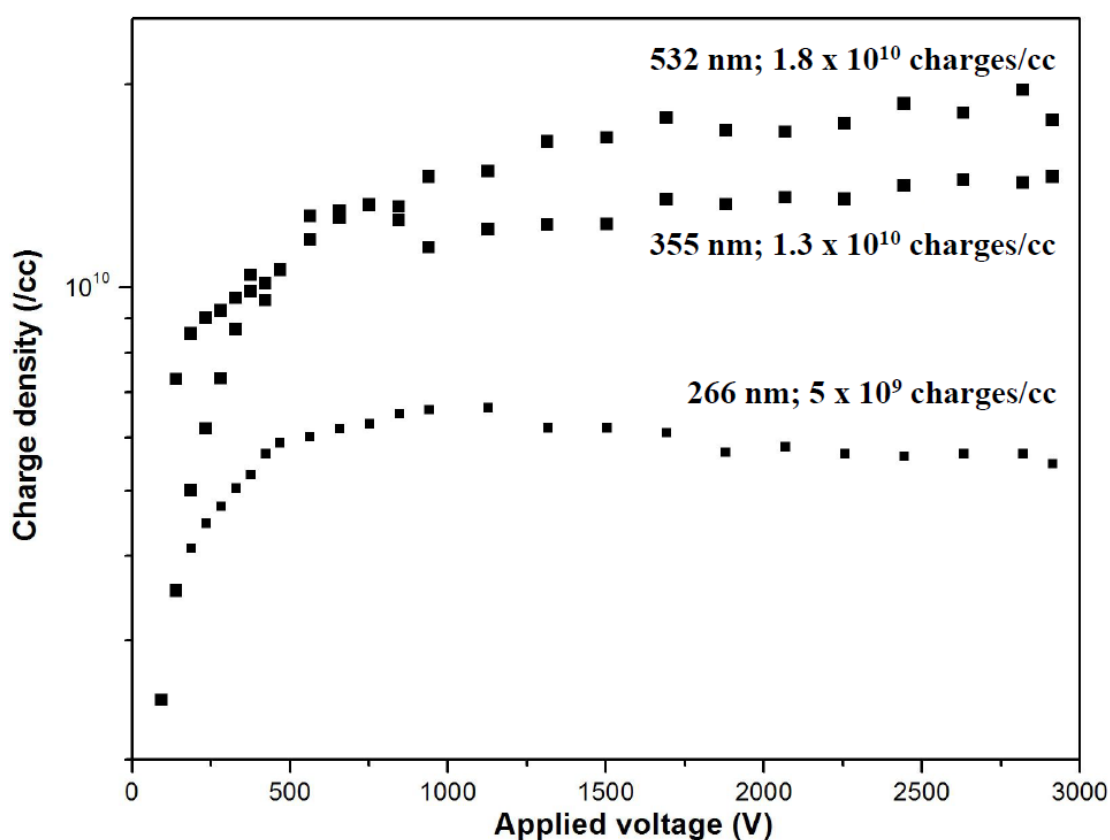


Figure 8.8: Charge density of xenon cluster as a function of applied voltage between parallel plates for ionisation at 532, 355 and 266 nm

8.3.2 Role of electron ionisation in generating charge density of interaction zone in atomic/molecular clusters

As discussed in section 8.1, the primary event in cluster ionisation is initiated through multiphoton ionisation under our experimental conditions. Subsequently, the trapped photoelectrons interact with the laser field and get energised via inverse bremsstrahlung process. These energized electrons cause further ionisation in the cluster leading to generation of multiply charged atomic ions. Thus, cluster ionisation process under gigawatt intense field is comprised of multiphoton ionisation (primary ionisation process) and electron impact ionisation (secondary ionisation process). In order to understand the role of these ionisation processes, charge density measurement of different atomic and molecular clusters is found to be useful.

For a particular atom or molecule, the number of photons required for ionisation would be less for shorter wavelength because of higher photon energy. Thus, the multiphoton ionisation probability would be more at shorter wavelength and should cause higher charge density in the interaction zone. However, we have observed lower charge density in all atomic/molecular clusters at shorter wavelength as compared to longer wavelength. This observation indicates that, if total ionisation is considered, the primary multiphoton ionisation is relatively less important ionisation channel under our experimental conditions. On the contrary, electron impact ionisation is expected to be more dominant at longer wavelength since electron energization will be more efficient at higher wavelength. The extraction of energy from the laser field increases quadratically with the laser wavelength (λ^2). We have also observed higher charge density at longer wavelength. Thus, based on the charge density measurement, it can be concluded that in case of clusters, the secondary ionisation process i.e. electron impact ionisation is a dominant and efficient ionisation

channel under gigawatt intense field. The charge produced due to electron impact ionisation is much more as compared to multiphoton ionisation. As a result, the total charge density of the interaction zone shows the trend of the electron impact ionisation rather than the multiphoton ionisation.

8.3.3 Comparative study of charge density measurement in atomic/molecular clusters

In this section, charge densities of different atomic and molecular clusters have been compared at different wavelengths along with the observed charge state in the time-of-flight mass spectrometer. The charge densities and corresponding charge states are presented in table 8.1. From the table, it can be concluded that charge density of a particular atomic/ molecular system, increases with laser wavelength. Moreover, their highest observed charge state also increases with laser wavelength. Thus, the charge state and charge density are complementary to each other. However, if we compare charge density of different atomic and molecular cluster at a particular wavelength then the correlation between the charge state in the mass spectra and the charge density becomes difficult. For example, consider the charge state and charge density of these three cluster systems at 532 nm. In C_2H_5Br and CH_3I clusters, the highest observed charge state is +5 and +4 respectively and the observed charge density $\sim 2 \times 10^{11}$ charges/cc. On the contrary, in Xe clusters, charge density of the interaction zone is found to be $\sim 1.8 \times 10^{10}$ charges/cc with the highest observed charge state +11. Thus, for different cluster system, based purely on the observed charge state it is very difficult to comment on the charge density of the interaction zone. In xenon clusters, the higher charge states are produced at the expense of the lower charge state. Thus overall charge density is low in xenon clusters as compared to C_2H_5Br/ CH_3I clusters however highest observed charge state in time-of-flight mass spectra is higher.

Table 8.1: Charge density of interaction zone for different atomic and molecular clusters at different wavelength is listed below. Corresponding highest observed charge state in mass spectra is also shown.

	266 nm	355 nm	532 nm	1064 nm
C₂H₅Br clusters	1.5 x 10 ⁹ Charges/cc	5.7 x 10 ⁹ Charges/cc	2 x 10 ¹¹ Charges/cc	-
Charge state	+1	+2	+5	
CH₃I clusters	4 x 10 ⁹ Charges/cc	2 x 10 ¹⁰ Charges/cc	2 x 10 ¹¹ Charges/cc	9 x 10 ¹¹ Charges/cc
Charge state	+1	+2	+4	+11
Xe clusters	5 x 10 ⁹ Charges/cc	1.3 x 10 ¹⁰ Charges/cc	1.8 x 10 ¹⁰ Charges/cc	-
Charge state	+3	+6	+10	

8.4 Conclusions

Charge density of the interaction zone has been measured for different atomic and molecular clusters under gigawatt intense laser field. For charge density measurement, the existing ion optics of time-of-flight mass spectrometer has been modified. The repeller and the extractor grids are replaced with thin metal plate for complete collection of ions. This arrangement makes the time-of-flight mass spectrometer inoperable however experiments are done under same experimental conditions so that the time-of-flight data can be compared with the charge density of interaction zone. For a particular atomic or molecular cluster system charge density of the interaction is found to increase with laser wavelength. In the mass spectrum, charge state of atomic ions as a result of laser-cluster interaction is found to increase with wavelength. Thus, it is concluded that with increases in laser wavelength, the efficiency of laser-cluster interaction increases leading to higher charge state in the mass spectra along with higher charge density. However, based on the charge state of

the atomic ions in the mass spectra it is difficult to comment on the charge density of the interaction zone. As shown in the results of interaction of xenon cluster with 532 nm laser pulses, the higher charge state (+11) corresponds to comparatively lower charge density (2×10^{10} charges/cc). Thus, charge density measurement is a complementary technique where absolute charge produced in the interaction zone can be determined which gives a better insight into the Coulomb explosion phenomena under gigawatt intense laser field.

Chapter 9

Conclusions and Future Scope of the Work

9.1 Conclusions

In the present thesis, interaction of atomic and molecular clusters with nanosecond long laser pulses resulting into gigawatt laser field has been studied using time-of-flight mass spectrometry technique. A cluster target is a unique combination of solid phase immersed in overall gas medium. Its solid like local density and gas like average density causes individual cluster to efficiently absorb laser energy forming highly charged atomic ions, molecular ions, energetic electrons etc. Thus, laser-cluster interaction has been studied extensively during the last two decades and opens new arena of research in cluster science. Earlier, studies have been mostly confined to femtosecond laser pulses with extremely high laser intensity. Limited literature is available on study of interaction of atomic and molecular clusters under gigawatt laser field. Thus, these studies will help to understand the ionisation dynamics and formation of highly charged species under such weak laser field.

Our observations are schematically shown in figure 9.1 to get a bird's eye view of laser-cluster interaction under gigawatt laser field. Generation of multiply charged atomic ions is the major channel due to efficient laser-cluster interaction and singly charged negative ion formation constitutes a minor channel under our experimental conditions. Thus, our efforts are mostly directed to elucidate the mechanism of positive ions formation with high charge state under gigawatt laser field. In order to understand the formation mechanism of multiply charged positive ions under gigawatt laser field, different parameters related to interaction have been systematically varied. Moreover, kinetic energy of multiply charged ions has been

measured along with the total ion yield at the interaction zone under given set of experimental conditions.

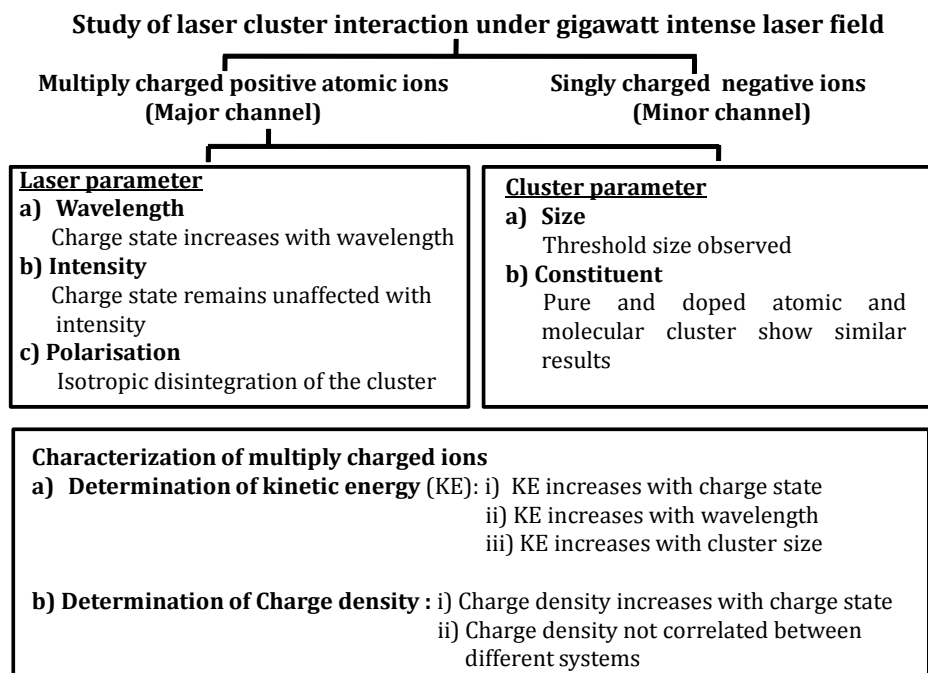


Figure 9.1: Schematic of laser-cluster interaction studies under gigawatt laser field

(i) Effect of laser parameters

Laser parameters like wavelength, intensity and polarisation were varied in different atomic and molecular clusters and effect of each parameter is described below-

(a) Wavelength: Laser wavelength plays a crucial role in determining the charge state of atomic ions in laser-cluster interaction under our experimental conditions. Irrespective of cluster constituents, it has been observed that charge state of atomic ions increases with laser wavelength. Thus, longer wavelength is able to generate higher charge state ions because of efficient electron heating mechanism as compared to shorter wavelength. However, a continuous increase in the wavelength will not enhance the charge state of atomic ions because of initial multiphoton ionisation step requirement. The first step of atomic ion formation is multiphoton ionisation process

and the multiphoton ionisation probability decreases with increase in number of photons required for ionisation of atom/molecule. In case of longer wavelength, the number of photons required for ionising an atom/molecule will be more which in turn lowers the ionisation probability and initial rate of ionisation in the cluster. This lower level of initial ionisation helps the cluster to undergo less Coulomb expansion and cluster survives for longer time in the laser field. As a result, the energization of quasi free electron will be higher and will generate higher charge states of atomic ions. In this way, longer wavelength is helpful in higher charge state formation. However, energy of the photon should be sufficient to cause initial multiphoton ionisation. Thus laser wavelength plays a decisive role in ionisation process of cluster under gigawatt laser field.

(b) Intensity: For a given laser wavelength, increase in laser intensity helps in increasing the ion yield of singly as well as multiply charged ions. However, no enhancement in the charge state of atomic ions could be observed with increase in laser intensity. An increase in the laser intensity helps in increasing total number of charge centers within the ionised cluster which causes early disintegration of the cluster. As a result, electrons confined in the cluster do not get sufficient time for energization which is vital for causing secondary ionisation. Thus, no enhancement in charge state has been attributed in the mass spectra with increase in laser intensity.

It was observed that the threshold laser intensity for observation of multiply charged species is inversely related to the cluster size. With increase in cluster size, the threshold intensity for observation of Coulomb explosion is found to decrease. This decrease in intensity occurs due to both multiphoton and electron impact ionisation. In multiphoton ionisation, increase in average cluster size enhances the ionisation probability thus leading to lower threshold laser intensity. In electron

impact ionisation, larger cluster size helps in retaining the inner ionised electron more efficiently which helps in enhanced heating of the electrons.

(c) Polarisation: Laser polarisation has been rotated from 0 – 360 degree (in steps of 45 degree) and mass spectra were recorded as a function of rotation angle in time-of-flight mass spectrometer. No change has been observed in the ion yield and kinetic energy of the multiply charged ions. Thus, laser polarisation does not affect the distribution of ions and Coulomb explosion of multiply charged ions is found to be isotropic in case of gigawatt intensity pulses.

(ii) Effect of cluster parameters

Cluster size and cluster constituents were varied during the experiments and effect of these parameters on generation of multiply charged atomic ions was studied which is described below-

(a) Cluster size: Cluster size plays an important role in nanosecond laser induced Coulomb explosion under gigawatt laser field. A threshold cluster size is observed in both atomic and molecular cluster for observation of multiply charged species. In case of molecular clusters, however, the threshold size of the cluster could not be estimated because of inapplicability of Hagen scaling laws. In atomic cluster i.e. Xe clusters, using the empirical formula, the threshold cluster size is estimated to be in the range of $17 < N < 50$. Thus, the threshold size helps in retaining the inner ionised quasi free electrons which in turn cause secondary multiple ionisations in the cluster. Above the threshold cluster size, further enhancement in the size helps in either increasing in the charge state of the atomic ions (in methyl iodide clusters) or increasing the kinetic energy of the multiply charged ions (in xenon clusters). Therefore, size determines the overall ionisation dynamics of the cluster under gigawatt laser field.

(b) Cluster constituent: Pure and doped clusters of different atoms and molecules

were irradiated with gigawatt laser pulses and the ionic outcome was studied. All atomic and molecular clusters studied in this work show similar trend at different laser wavelengths. The results suggest that similar mechanism operates for generation of multiply charged atomic ions. However, for initial multiphoton ionisation, presence of high lying Rydberg states help in facile ionisation of the cluster. Thus, the intermediate electronic states are required for ionisation using the low intensity laser pulse. Molecules having high ionisation potential were also tried. Because of higher photon requirement, initial multiphoton ionisation could not be observed in the mass spectrum. In order to ionise those molecular clusters, doped clusters were used where molecules with low ionisation potential are seeded into cluster. During the interaction of laser pulse with the doped cluster, molecules with low ionisation potential preferentially undergo multiphoton ionisation and create inner ionised quasi free electrons within the doped cluster. These electrons are then energised by the laser field and undergo indiscriminate collision with the neutral and ionic constituent of the doped cluster. As a result, molecule with high ionisation potential is forced to undergo secondary ionisation. Moreover, multiply charged atomic ions of the higher ionisation potential molecule were also observed in the mass spectrum. Thus, doped cluster method provides an indirect way to induce ionisation in high ionisation potential systems which is not ionisable under gigawatt laser field.

(iii) Characterisation of multiply charged ions

So far we have discussed how the laser and cluster parameters affect ionisation dynamics and multiple charge state formation in atomic and molecular clusters under gigawatt laser field. In this section we will summarise the results of characterisation of these multiply charged ions under different experimental conditions.

(a) Determination of kinetic energy: Kinetic energy of the multiply charged ions produced as result of Coulomb explosion has been measured for different atomic and molecular clusters using two methods, namely peak splitting and retarding potential method. Kinetic energy of the ions is a manifestation of the stored potential energy of the ions inside the cluster prior to Coulomb explosion. For a particular cluster system, kinetic energy of multiply charged ions increases with charge state under a given set of experimental conditions. This observation is quite obvious since Coulombic repulsive force will be more for higher charge state thus leading to higher kinetic energy. On the other hand, for a particular charge state, kinetic energy is found to increase with laser wavelength. This observation is also in accordance with the three stage cluster ionisation model (explained in section 3.3.3). According to this model, electron heating mechanism is more pronounced at higher wavelength which leads to more number of charge centers and thus higher kinetic energy is acquired by the same charge state at higher wavelength. Further, kinetic energy of different charge states has been studied as a function of cluster size. Kinetic energy is found to increase with cluster size. The larger cluster size helps in retaining the inner ionised electrons for longer duration which gives rise to more number of charge centers. As a result, kinetic energy of a particular charge state is found to increase with cluster size.

(b) Determination of charge density: In order to determine the total number of charges produced in the interaction zone, charge density measurement has been carried out for different experimental conditions and the results are compared with time-of-flight mass spectrometry results. For charge density measurement, ion optics of mass spectrometer has been modified slightly and measurements are done as a function of laser wavelength and cluster constituent. For a particular cluster system, charge density is found to increase with laser wavelength. This experimental finding

supports the time-of-flight mass spectrometry results. It also suggests that the secondary electron impact ionisation is more efficient as compared to multiphoton ionisation process. In the next set of experiments, charge density of different cluster system is compared at a particular wavelength. It was found that the charge density of the interaction zone does not correlate with the observed charge state in the time-of-flight mass spectrometer. Thus, charge density measurement is a complementary technique to time-of-flight mass spectrometer and determines the total charge produced as result of laser-cluster interaction in gas phase.

9.2 Future scope of the work

In the present thesis, laser-cluster interaction study has been carried out under gigawatt laser field. Extensive study has been done by varying different experimental parameters to understand laser-cluster interaction. In the following section, we will discuss some of the possible directions to pursue in order to improve our understanding of this complex phenomenon and also find some potential applications.

(a) Computer modelling:

The three stage cluster ionisation model has been used to explain the dynamics of laser-cluster interactions in atomic and molecular clusters in the present thesis. It must be mentioned that this model is very simple and qualitative in nature. The model grossly explains salient features of laser-cluster interaction under gigawatt laser field. However, in order to get a comprehensive description of the ionisation dynamics of the cluster under such low laser intensity conditions, simulation of the cluster ionisation process using self-consistent equation of motion in the electromagnetic wave of the laser is required. The code should include contribution of multiphoton and electron impact ionisation along with different laser and cluster parameters. Appropriate simulation of the experimental conditions will be able to predict the

spatial and temporal electron density in the cluster and extent of energy absorption via collisional ionisation. It is evident that a code of the kind which takes into account the effect of laser intensity and cluster size distributions etc is a daunting task. However, in the light of generation of multi keV multiply charged ions using laser intensity as low as $\sim 10^9$ W/cm², it will be worthwhile to invest efforts in such an endeavour.

(b) Measurement of electron energy:

In the three stage cluster ionisation model, two types of ionisation processes as i.e. multiphoton and electron impact ionisation have been described. Multiphoton ionisation process is the primary ionisation process under our experimental conditions. Laser power dependency study also confirms the photon dependency of any ionisation process. Using the number of photon requirement, multiphoton ionisation probability can be determined for given set of experimental parameters. In the second step, electron impact ionisation causes secondary ionisation giving rise to multiply charged ions and the cluster disintegrates due to Coulombic repulsion. The extent of electron impact ionisation depends on the electron impact ionisation cross-section of the atom/ ion and energy of electron. Thus, in order to get an idea of electron impact ionisation within the cluster, knowledge of electron energy is very essential. Therefore, there is need to measure the electron energy as a function of different experimental parameters which will help to model the phenomenon in a more accurate way under our experimental conditions. For such experiment, retarding potential analyser assembly will be useful along with sensitive electron detection system.

(c) Use of multiply charged ions for ion implantation/ion beam deposition:

In the present thesis, generation of energetic multiply charged atomic ions has been reported as a result of efficient laser-cluster interaction under gigawatt laser

field. Most of the efforts are directed to elucidate the mechanism of energy absorption from the laser field. Future studies can be carried out using these ions for ion implantation or ion beam deposition. In ion implantation technique, ions are accelerated in an electrical field and made to impact on the solid. As a result, the physical and chemical properties of the solid change and subsequently these properties are used for a particular application. The introduction of dopants in a semiconductor is the most common application of ion implantation. However, for ion implantation, typically the ion energy is in the range of 10-500 keV. Ion implantation has been carried out even with ion energy in the range of 1- 10 keV. Under our experimental conditions, ions are produced with keV energies (in xenon cluster). Thus, ion implantation study can be carried out without further acceleration of the ions. Moreover, low energy (hundreds of eV) multiply charged ions are produced from molecular clusters which are also useful for ion deposition on the surface. Thus, depending on the ion energy, these multiply charged ions can be useful for various applications.

(d) Possibility of higher harmonic generation:

For generation of coherent short wavelength, higher harmonic generation is one of the promising approach along with x-ray laser and free electron laser. Out of these, higher harmonic generation is most cost effective and most explored. The laser plasma produced due to interaction of high intense laser pulse with cluster acts as an efficient nonlinear medium for higher harmonic generation. The gas phase cluster target is superior for these studies as compared to solid target because the latter produces enough debris. Number of studies have been carried out under high intensity laser conditions which include effect of different laser parameters such as frequency, polarisation etc. on higher order harmonic generation. Similar studies can be designed

for cluster systems using gigawatt intense laser field. Since the laser conditions are mild, the detection system has to be more sensitive to detect the higher order harmonics. Successful accomplishment of this experiment will lead to generation of higher harmonics using simple, low cost nanosecond laser pulses with laser intensity as low as $\sim 10^9$ W/cm².

Thus, study of laser cluster interaction in gas phase has been carried out using gigawatt intense laser field. Different aspects of nanosecond laser induced Coulomb explosion mechanistic have been uncovered as a consequence of this work. Our studies enrich the understanding of laser-cluster interaction under such low intensity conditions and also provide an alternate way to produce energetic multiply charged ions which could have diverse applications.

References

1. Schurr, J.M. *Chem phys* **1976**, 15, 15.
2. Flytzanis, C.; Tang, C.L. *Phys. Rev. Lett.* **1980**, 45, 441.
3. Masalov, A. V.; Todirashku, S. S. *Opt. Commun.* **1980**, 32, 497.
4. Kwok, H. S.; Yablonovitch, E.; Bloembergen, N. *Phys. Rev. A.* **1981**, 23, 3094.
5. O' Connor, M. T.; Diebold, G. J. *Nature* **1983**, 301, 321.
6. Sreckovic, M.; Vedlin, B.; Backovic, N. *Opt. Laser Technol.* **1984**, 16, 145.
7. Bloembergen, N. *Mater Res Soc Symp Proc* **1986**, 51, 3.
8. Zimmermann, R.; Hartmann, M. *Phys. Status Solidi B* **1988**, 150, 365.
9. Burns, M. M.; Fournier, J. –M.; Golovchenko. J. A. *Science* **1990**, 249, 749.
10. Joshi, C.J.; Corkum, P.D. *Physics Today* **1995**, 48, 36.
11. Ditmire, T.; Zweiback, J.; Yanovsky, V.P.; Cowan, T. E.; Hays, G.; Wharton K. B. *Nature* **1999**, 398, 489.
12. Weisbuch, C.; Benisty, H. *Solid State Commun.* **2005**, 135, 627
13. Rist, S., Menotti, C., Morigi, G. *Phys. Rev. A* **2010**, 81,013404.
14. Van Vlack, C.; Kristensen, P.T.; Hughes, S. *Phys. Rev. B* **2012**, 85, 075303.
15. Szabo, A. *Phys. Rev. Lett.* **1970**, 25, 924.
16. Williamson, C.K.; Pastel, R.L.; Sausa, R. C. *Appl. Spectrosc.* **1996**, 50, 205.
17. Ewart, P.; Purdie, A. F. *J. Phys. B* **1976**, 9, L437.
18. Adoui, L.; Gobert, O.; Indelicato, P.; Lamour, E.; Meynadier, P.; Normand, D.; Perdrix, M.; Prigent, C.; Vernhet, D. *Nucl. Instrum. Meth. B* **2003**, 205, 341.
19. Donnelly, T.D.; Ditmire, T.; Neuman, K.; Perry, M.D.; Falcone, R.W. *Phys. Rev. Lett.* **1996**, 76, 2472.
20. Siegman, A. E. *Lasers* University Science Books, 1986.

21. Hitz, C. B.; Ewing, J. J.; Hecht, J. *Introduction to Laser Technology* Wiley-IEEE Press, 2012.
22. Castleman, Jr. A.W.; Keesee, R. G. *Science* **1988**, 241, 36.
23. Whelan, C.T.; Dreizler, R.M.; Maeck, J.H.; Walters, H.R. J. *New Directions in Atomic Physics* Springer, 1999.
24. Demtroder, W. *Atoms, Molecules and Photons* Springer, 2010.
25. Jortner, J. *Z. Phys. D Atom Mol Cl* **1992**, 24, 247.
26. Haberland, H. *Clusters of Atoms and Molecules* Berlin: Springer 1994.
27. Scoles, G. *Atomic and Molecular Beam Methods* Oxford University Press, New York, 1988.
28. Campargue, R. *Atomic and Molecular Beams - The State of the Art 2000* Springer, Berlin, 2001.
29. Hayes, J.M. *Chem. Rev.* **1987**, 87, 745.
30. Dietz, T. G.; Duncan, M. A.; Powers, D. E.; Smalley, R. E. *J. Chem. Phys.* **1981**, 74, 6511.
31. Palmer R.E. *Welcome to cluster world* New Scientist p.38, 1997.
32. Downard, K. *Mass Spectrometry: A Foundation Course* Royal Society of Chemistry, UK, 2004.
33. Karas, M.; Ingendoh, A.; Bahr, U.; Hillenkamp, F. *Biomed. Environ. Mass Spectrom.* **1989**, 18, 841.
34. Cotter, R.J. *Time-of-Flight Mass Spectrometry* American Chemical Society, Washington DC, 1994.
35. Guilhaus, M. *J. Mass Spectrom.* **1995**, 30, 1519.
36. Wiley, W.C.; McLaren, I.H. *Rev. Sci. Instrum.* **1955**, 26, 1150.
37. Mamyrin, B.A.; Shmikk, D.V. *Sov. Phys. JETP (Engl. transl.)* **1979**, 49, 762.

38. Bergmann, T.; Martin, T.P.; Schaber, H. *Rev. Sci. Instrum.*, **1989**, 60, 347.
39. DiMauro, L.F.; Freeman, R.R.; Kulander, K.C. *Multiphoton Processes* Am. Inst. Of Physics, New York, 2000.
40. Peticolas, W.L. *Ann. Rev. Phys. Chem.* **1967**, 18, 233.
41. Lin S.H. *Advances in Multiphoton Processes and Spectroscopy* vol. 1 World Scientific, Singapore, 1984.
42. McClain, W.M. *Acc. Chem. Res.* **1974**, 7, 129.
43. Goeppert-Mayer, M. *Ann. Phys.*, **1931**, 9, 273.
44. Xu, C.; Zipfel, W.; Shear, J.B.; Williams R.M.; Webb, W.W. *Proc. Natl. Acad. Sci.*, **1996**, 93, 10763.
45. Agostini, P.; Fabre, F.; Mainfray, G.; Petite, G.; Rahman, N. *Phys. Rev. Lett.* **1979**, 42, 1127.
46. Freeman, R. R.; Bucksbaum, P. H. *J. Phys. B: At. Mol. Opt. Phys.* **1991**, 24, 325.
47. Corkum, P. B.; Burnett, N. H.; Brunel, F. *Phys. Rev. Lett.* **1989**, 62, 1259.
48. Augst, S.; Strickland, D.; Meyerhofer, D.; Chin, S. L.; Eberly, J. H. *Phys. Rev. Lett.* **1989**, 63, 2212.
49. Ilkov, F. A.; Decker, J. E.; Chin, S. L.; *J. Phys. B* **1992**, 25, 4005.
50. Mevel, E.; Breger, P.; Trainham, R.; Petite, G.; Agostini, P.; Migus, A.; Chambaret, J. P.; Antonetti, A. A. *Phys. Rev. Lett.* **1993**, 70, 406.
51. Tolstikhin, O. I.; Morishita, T.; Madsen L. B. *Phys. Rev A* **2011**, 84, 053423
52. Keldysh, L.V. *Sov. Phys. JETP* **1965**, 20, 1037
53. Connerade, J.P. *Highly excited atoms* Cambridge University Press, 1998
54. Fennel, Th. Meiwes-Broer, K.-H. Tiggesbäumker, J. Reinhard, P.-G. Dinh, P. M. Surau, E. *Rev. Mod. Phys.* **2010**, 82, 1793

55. Sattler, K. D. *Handbook of nanophysics: clusters and Fullerenes* CRC Press, 2010.
56. Eliezer, S. *The interaction of high-power lasers with plasmas* Institute of Physics, 2002.
57. Chen, L. M.; Zhang, J.; Dong, Q. L.; Teng, H.; Liang, T. J.; Zhao, L. Z.; Wei, Z. *Y. Phys. Plasmas* **2001**, 8, 2925.
58. Yang, T. Y. B.; Kruer, W. L.; More, R. M.; Langdon, A. B. *Phys. Plasmas* **1995**, 2, 3145.
59. Krainov, V. P. *J. Phys. B: At. Mol. Opt. Phys.* **2000**, 33, 1585.
60. Castleman, A. W. Jr.; Keesee, R. G. *Ann. Rev. Phys. Chem.* **1986**, 37, 525.
61. Ditmire, T.; Tisch, J.W.G.; Springate, E.; Mason, M.B.; Hay, N.; Smith, R.A.; Marangos, J.; Hutchinson, M.H.R. *Nature* **1997**, 386, 54.
62. Castleman, A. W. Jr.; Poth, L.; Wisniewski, E. *Am. Sci.* **2002**, 90, 342.
63. Kumarappan, V.; Krishnamurthy, M.; Mathur, D. *Phys. Rev. A* **2003**, 67, 0632071.
64. Krainov, V. P.; Smirnov, M. B. *Phys. Rep.* **2002**, 370, 237.
65. Ford, J. V.; Zhong, Q Poth, L.; Castleman, A. W. Jr. *J. Chem. Phys.* **1999**, 110, 6257.
66. Ford, J. V.; Poth, L.; Zhong, Q.; Castleman, A. W. Jr. *Int. J. Mass Spectrom.* **1999**, 192, 327
67. Wabnitz, H.; Bittner, L.; de Castro, A. R. B.; Döhrmann, R.; Gürtler, P.; Laarmann, T.; Laasch, W.; Schulz, J.; Swiderski, A.; von Haefen, K.; Möller, T.; Faatz, B.; Fateev, A.; Feldhaus, J.; Gerth, C.; Hahn, U.; Saldin, E.; Schneidmiller, E.; Sytchev, K.; Tiedtke, K.; Treusch, R.; Yurkov, M. *Nature*, **2002**, 420, 482.
68. Auguste, T.; Monot, P.; Mainfray, G.; Manus, C. *J. Phys. B: At. Mol. Opt. Phys.* **1992**, 25, 4181.

69. Sharma, P.; Vatsa, R. K.; Kulshreshtha, S. K.; Jha, J.; Mathur, D.; Krishnamurthy, M. *J. Chem. Phys.* **2006**, 125, 034304.
70. Sharma, P.; Vatsa, R. K. *Rapid Commun. Mass Spectrom.* **2007**, 21, 2663.
71. Sharma, P.; Vatsa, R. K. *Euro. Phys. Lett.* **2008**, 84, 43003.
72. Gibson, J. K. *J. Chem. Phys.* **1994**, 98, 11321.
73. Johnston, R. L. *Atomic & Molecular Clusters* CRC Press, 2002.
74. Li, W.; Liu, J.; Wang, W.; Chen, Q.; Zhang, H.; Tian, Y.; Zhang, Z.; Qi, R.; Wang, C.; Leng, Y.; Li, R.; Xu Z.; *Phys. Plasmas* **2009**, 16, 113106.
75. Majumder, C.; Jayakumar, O.D.; Vatsa, R.K.; Kulshreshtha, S.K.; Mittal, J.P. *Chem. Phys. Lett.* **1999**, 304, 51.
76. Majumder, C.; Jayakumar, O.D.; Vatsa, R.K.; Kulshreshtha, S.K. *Ind. J. Chem.* **2001**, 40A, 577.
77. Hagena, O.F. *Z. Phys. D Atoms, Mol. Cl* **1987**, 4, 291.
78. Silfvast, W.T. *Laser Fundamentals* Cambridge University Press, Cambridge, 1998.
79. Andrews, D.L. *Applied Laser Spectroscopy: Techniques, Instrumentation and Applications* VCH, New York, 1992.
80. Webster, J. G. *The measurement, instrumentation, and sensors handbook* CRC Press, 1999.
81. Dahl, D.A. *Simion version 8.0.4-2008-01-0* Idaho National Laboratory.
82. Wiza, J.L. *Nucl. Instr. and Meth.* **1979**, 162, 587.
83. Whetten, R.L.; Fu, K.J.; Grant, E.R. *J. Chem. Phys.*, **1983**, 79, 2626.
84. Mann, D. E.; Thrush, B. A. *J. Chem. Phys.* **1960**, 33, 1732.
85. Walton, J. C. *J. Chem. Soc. Faraday Trans. I* **1972**, 68, 1559.
86. Krajnovich, D.; Zhang, Z.; Butler, L.; Lee, Y. T. *J. Phys. Chem.* **1984**, 88, 4561.

87. Gosnell, T. R.; Taylor, A. J.; Lyman, J. L. *J. Chem. Phys.* **1991**, 94, 5949.
88. Vatsa, R. K.; Kumar, A.; Naik, P.D.; Rama Rao K.V.S.; Mittal J.P. *Chem. Phys. Lett.* **1993**, 207, 75.
89. Van Hoeymissen, J.; Uten, W.; Peeters, J. *Chem. Phys. Lett.* **1994**, 226, 159.
90. Cameron, M. R.; Johns, S. A.; Metha, G. F.; Kable, S. H. *Phys. Chem. Chem. Phys.* **2000**, 2, 2539.
91. Park, M. S.; Kim, T. K.; Lee, S.; Jung, K.; Volpp H.; Wolfrum, J. *J. Phys. Chem. A* **2001**, 105, 5606.
92. Hsu, C.Y.; Huang, H. Y.; Lin, K. C. *J. Chem. Phys.* **2005**, 123, 134312.
93. Lide, D.R.; Kehiaian, H.V. *CRC Handbook of Thermophysical and Thermochemical Data* CRC Press, Boca Raton: FL, 1994.
94. Gillotay, D.; Simon, P. C. *J. Atmos. Chem.* **1989**, 8, 41.
95. Bulcourt, N.; Booth, J.; Hudson, E. A.; Luque, J.; Mok, D. K. W.; Lee, E. P.; Chau, F.; Dyke, J. M. *J. Chem. Phys.* **2004**, 120, 9499.
96. Sapers, S. P.; Vaida, V.; Naaman, R. *J. Chem. Phys.* **1988**, 88, 3638.
97. Syage, J. A.; Steadman, J. *Chem. Phys. Lett.* **1990**, 166, 159.
98. Choi, Y. K.; Koo, Y. M.; Jung, K. W. *J. Photochem Photobiol A* **1999**, 127, 1.
99. Fan, Y. B.; Randall, K. L.; Donaldson, D. J. *J. Chem. Phys.* **1993**, 98, 4700.
100. Vidma, K. V.; Baklanov, A. V.; Khvorostov, E. B.; Ishchenko, V. N.; Kochubei, S. A.; Eppink, A. T. J. B.; Chestakov, D. A.; Parker, D. H. *J. Chem. Phys.* **2005**, 122, 204301.
101. Lokhman, V. N.; Ogurok, D. D.; Ryabov, E. A. *Chem. Phys.* **2007**, 333, 85.
102. Karras, G.; Danakas, S.; Kosmidis, C. *J. Phys. Chem. A* **2011**, 115, 4186.
103. Ito, F.; Ohmura, H.; Nakanaga, T. *Chem. Phys. Lett.* **2006**, 420, 157.

104. Das, S.; Badani, P. M.; Sharma, P.; Vatsa, R. K.; Das, D.; Majumder, A.; Das, A. K. *Rapid Commun. Mass Spectrom.* **2011**, 25, 1028.
105. D.R. Lide (Ed.), *CRC Handbook of Chemistry and Physics* CRC Press: New York, 2004.
106. Mulser, P.; Bauer, D. *High Power Laser-Matter Interaction* Springer, 2010.
107. Ditmire, T.; Donnelly, T.; Rubenchik, A. M.; Falcone, R. W.; Perry, M. D. *Phys. Rev. A.* **1996**, 53, 3379.
108. Wang, W.; Li, H.; Niu, D.; Wen, L.; Zhang, N. *Chem. Phys.* **2008**, 352, 111.
109. Zhang, N.; Wang, W.; Cang, H.; Wang, H.; Li, H. *Chem. Phys. Lett.* **2009**, 469, 14.
110. Zhao, W.; Wanga, W.; Qua, P.; Hou, K.; Li, H. *Chem. Phys. Lett.* **2012**, 543, 55.
111. Jha, J.; Mathur, D.; Krishnamurthy, M. *Appl. Phys. Lett.* **2006**, 88, 041107.
112. Nakashima, N.; Shimizu, S.; Yatsuhashi, T.; Sakabe, S.; Izawa, Y. J. *Photochem. Photobiol. C: Photochem. Rev.* **2000**, 1, 131.
113. Dobosz, S.; Schmidt, M.; Perdrix, M.; Meynadier, P.; Gobert, O.; Normand, D. *JETP Lett.* **1998**, 68, 485.
114. Jortner, J.; Last, I. *ChemPhysChem* **2002**, 3, 845.
115. Thomas, H.; Bostedt, C.; Hoener, M.; Eremina, E.; Wabnitz, H.; Laarmann, T.; Plönjes, E.; Treusch, R.; de Castro, A. R. B.; Möller, T. *J. Phys. B: At. Mol. Opt. Phys* **2009**, 42, 134018.
116. Kumarappan, V.; Krishnamurthy, M.; Mathur, D. *Phys. Rev. Lett.* **2001**, 87, 085005
117. Saalman, U.; Siedschlag, Ch.; Rost, J. M. *J. Phys. B: At. Mol. Phys.* **2006**, 39, R39.

118. Kou, J.; Zhakhovskii, V.; Sakabe, S.; Nishihara, K.; Shimizu, S.; Kawato, S.; Hashida, M.; Shimizu, K.; Bulanov, S.; Izawa, Y.; Kato, Y.; Nakashima, N. *J. Chem. Phys.* **2000**, 112, 5012.
119. Siozos, P.; Kaziannis, S.; Kosmidis, C. *Int. J. Mass Spectrom.* **2003**, 225, 249.
120. Karras, G.; Kosmidis, C. *Int. J. Mass Spectrom.* **2010**, 290, 133.
121. Giuliani, A.; Motte-Tollet, F.; Delwiche, J.; Mason, N. J.; Jones, N. C.; Gingell, J. M.; Walker, I. C.; Hubin-Franskin, M.-J. *J. Chem. Phys.* **2000**, 112, 6285.
122. Mathur, D.; Rajgara, F. A. *J. Chem. Phys.* **2010**, 133, 061101.
123. Mathur, D.; Rajgara, F. A.; Holkundkar, A. R.; Gupta, N. K. *Phys. Rev. A* **2010**, 82, 025201.
124. Kreisler, D.; Echt, O.; Knapp, M.; Recknagel, E.; Leiter, K.; Märk, T. D.; Sáenz, J. J.; Soler, J. M. *Phys. Rev. Lett.* **1986**, 56, 1551.
125. Scheier, P.; Mark, T. D. *Chem. Phys. Lett.* **1987**, 136, 423.
126. Echt, O.; Sattler, K.; Recknagel, E. *Phys. Lett. A* **1982**, 90, 185.
127. Poth, L.; Castleman, A. W. Jr. *J. Phys. Chem. A* **1998**, 102, 4075.
128. Luo, X.; Niu, D.; Kong, X.; Wen, L.; Liang, F.; Pei, K.; Wang, B.; Li, H. *Chem. Phys.* **2005**, 310, 17.
129. Wen, L.; Li, H.; Luo, X.; Niu, D.; Xiao, X.; Wang, B.; Liang, F.; Hou, K.; Shao, S. *Chem. Phys.* **2006**, 322, 360.
130. He, J.; Liu, C.; Li, F.; Sa, R.; Wu, K. *Chem. Phys. Lett.* **2008**, 457, 163.
131. Miyazaki, M.; Fujii, A.; Ebata, T.; Mikami, N. *Chem. Phys. Lett.* **2004**, 399, 412.
132. Symes, D. R.; Hohenberger, M.; Henig, A.; Ditmire, T. *Phys. Rev. Lett.* **2007**, 98, 123401.
133. Sakabe, S.; Nishihara, K.; Nakashima, N.; Kou, J.; Shimizu, S.; Zhakhovskii, V.; Amitani, H.; Sato, F. *Phys. Plasmas* **2001**, 8, 2517.

134. Karras, G.; Kosmidis, C. *Phys. Chem. Chem. Phys.* **2012**, 14, 12147.
135. Karras, G.; Kosmidis, C. *Chem. Phys. Lett.* **2010**, 499, 31.
136. Last, I.; Levy, Y.; Jortner, J. *J. Chem. Phys.* **2005**, 123, 154301.
137. Jha, J.; Mathur, D.; Krishnamurthy, M.J. *Phys. B: At. Mol. Opt. Phys.* 2005, 38, L291.
138. Nishi, N.; Shinohara, H. *Z. Phys. D - Atoms, Molecules and Clusters* **1989**, 12, 269.
139. Springate, E.; Hay, N.; Tisch, J.W.G.; Mason, M.B.; Ditmire, T.; Hutchinson, M.H.R.; Marangos, J.P. *Phys. Rev. A* **2000**, 61, 063201.
140. Ditmire, T.; Tisch, J.W.G.; Springate, E.; Mason, M.B.; Hay, N.; Marangos, J.P.; Hutchinson, M.H.R. *Phys. Rev. Lett.* **1997**, 78, 2732.
141. Snyder, E.M.; Buzza, S.A.; Castleman, A.W. Jr. *Phys. Rev. Lett.* **1996**, 77, 3347.
142. Schulz, J.; Wabnitz, H.; Laarmann, T.; Gürtler, P.; Laasch, W.; Swiderski, A.; Möller, T.; de Castro, A.R.B. *Nuc. Instr. Meth Phys Res A* **2003**, 507, 572.
143. Ziaja, B.; Wabnitz, H.; Wang, F.; Weckert, E.; Moller, T. *Phys. Rev. Lett.* **2009**, 102, 205002.
144. Namba, S.; Takiyama, K.; Hasegawa, N.; Kishimoto, M.; Nishikino, M.; Kawachi, T.; Sukegawa, K.; Yamatani, H.; Tanaka, M.; Ochi, Y.; Nagashima, K. *J. Phys. Conf. Ser.* **2008**, 112, 042057.
145. Lezius, M.; Dobosz, S.; Normand, D.; Schmidt, M. *Phys. Rev. Lett.* **1998**, 80, 261.
146. Ishikawa, K.; Blenski, T. *Phys. Rev. A* **2000**, 62, 063204.
147. Kumarappan, V.; Krishnamurthy, M.; Mathur, D. *Phys. Rev. A* **2003**, 67, 043204.
148. Kumarappan, V.; Krishnamurthy, M.; Mathur, D. *Phys. Rev. A* **2002**, 66, 033203.

149. Luo, X.; Li, H.; Niu, D.; Wen, L.; Liang, F.; Wang, B.; Xiao, X. *Phys. Rev. A* **2005**, 72, 013201.
150. Dorchies, F.; Blasco, F.; Caillaud, T.; Stevefelt, J.; Stenz, C.; Boldarev, A.S.; Gasilov, V.A. *Phys. Rev. A* **2003**, 68, 023201.
151. Badani, P.M.; Das, S.; Mundlapati, V.R.; Sharma, P.; Vatsa, R.K. *AIP Advances* **2011**, 1, 042164.
152. Islam, M.R.; Saalman, U.; Rost, J.M. *Phys. Rev. A* **2006**, 73, 041201.
153. Gantefor, G.; Broker, G.; Holub-Krappe, E.; Ding, A. *J. Chem. Phys* **1989**, 91, 7972.
154. Moustazis, S. D.; Balcou, Ph.; Chambaret, J.-P.; Hulin, D.; Grillon, G.; Rousseau, J.-Ph.; Schmidt, M. *AIP Conf. Proc.* **2002**, 639, 197.
155. Ter-Avetisyan, S.; Schnurer, M.; Busch, S.; Nickles, P. V. *J. Phys. B: At. Mol. Opt. Phys.* **2004**, 37, 3633.
156. Nakamura, T.; Fukuda, Y.; Yogo, A.; Tampo, M.; Kando, M.; Hayashi, Y.; Kameshima, T.; Pirozhkov, A.S.; Esirkepov, T. Zh.; Pikuz, T.A.; Faenov, A.Y.; Daido, H.; Bulanov, S.V. *Phys. Lett. A* **2009**, 373, 2584.
157. Faenov, A. Ya.; Fukuda, Y.; Pikuz, T. A.; Kando, M.; Kotaki, H.; Homma, T.; Kawase, K.; Kameshima, T.; Daito, I.; Hayashi, Y.; Sakaki, H.; Bolton, P.; Pirozhkov, A.; Yogo, A.; Tampo, M.; Nakamura, T.; Mori, M.; Ogura, K.; Kawachi, T.; Daido, H.; Tajima, T.; Bulanov, S. V. *J. Korean. Phys. Soc.* **2010**, 56, 279.
158. Rajeev, R.; Madhu Trivikram, T.; Rishad, K. P. M.; Narayanan, V.; Krishnamurthy, M. *New J.Phys.* **2013**, 15, 043036.
159. Finch, C. D.; Parthasarathy, R.; Akpati, H. C.; Nordlander, P.; Dunning, F. B. *J. Chem. Phys* **1997**, 106, 9594.

160. Kalamarides, A.; Marawar, R. W.; Ling, X.; Walter, C. W.; Lindsay, B. G.; Smith, K. A. Dunning, F. B. *J. Chem. Phys* **1990**, 92, 1672.
161. Sunagawa, T.; Shimamori, H. *J. Chem. Phys* **1997**, 107, 7876.
162. Underwood-Lemons, T.; Gergel, T. J.; Moore, J. H. *J. Chem. Phys* **1995**, 102, 119.
163. Langer, J.; Matt, S.; Meinke, M.; Tegeder, P.; Stamatovic, A.; Illenberger, E. *J. Chem. Phys* **2000**, 113, 11063.
164. Zumdahl, S.S. *Introductory Chemistry, 5th Ed* Boston: Houghton Mifflin Co, 2003.
165. Christophorou, L. G. *Chem. Rev.* **1976**, 76, 409.
166. E.; Alge, N. G.; Adams, D. Smith. *J. Phys. B: At. Mol. Phys.* **1984**, 17, 3827.
167. Hildebrandt, G. F.; Kellert, F. G.; Dunning, F. B.; Smith, K. A.; Stebbings, R. F. *J. Chem. Phys* **1978**, 68, 1349.
168. Stockdale, J. A.; Davis, F. J.; Compton, R. N.; Klots, C. E. *J. Chem. Phys* **1974**, 60, 4279.
170. Alajajian, S. H.; Bernius, M. T.; Chutjian, A. *J. Phys. B: At. Mol. Phys.* **1988**, 21, 4021.
171. Christodoulides, A. A.; Shultes, E.; Schumacher, R.; Schindler, R. N.; Z. *Naturforsch* **1974**, 29a, 389.
172. Shimamori, H.; Tatsumi, Y.; Ogawa, Y.; Sunagawa, T. *Chem Phys. Lett.* **1992**, 194, 223.
173. Nagesha, K.; Marathe, V.R.; Krishnakumar, E. *Int. J. Mass. Spectrom.* **1995**, 145, 89.
174. Krishnakumar, E.; Nagesha, K. *Rapid Commun. Mass Spectrom.* **1995**, 9, 336

175. Weber, J.M.; Fabrikant, I.I.; Leber, E.; Ruf, M.-W.; Hotop, H. *Eur. Phys. J. D* **2000**, 11, 247.
176. Majumder, A.; Mago, V. K.; Ray, A. K.; Kathar, P. T.; Das, A. K. *Appl. Phys. B* **2005**, 81, 669.